Title

Evaluation of ASCE 41 Guidelines for Performance-Based Seismic Assessment of Steel Moment-Frame and Concrete Shear Wall Buildings

Author

Hernandez-Bassal, Laura Liliana

Publication Date

2023

Peer reviewed|Thesis/dissertation

Evaluation of ASCE 41 Guidelines for Performance-Based Seismic Assessment of Steel Moment-Frame and Concrete Shear Wall Buildings

By

LAURA LILIANA HERNÁNDEZ-BASSAL

DISSERTATION

Submitted in partial satisfaction of the requirements for the degree of

DOCTOR OF PHILOSOPHY

in

Civil and Environmental Engineering

in the

OFFICE OF GRADUATE STUDIES

of the

UNIVERSITY OF CALIFORNIA

DAVIS

Approved:

Sashi K. Kunnath, Chair

Amit Kanvinde

John E. Bolander

Committee in Charge

2023

Abstract

Performance-based seismic evaluation and retrofit of existing buildings documented in ASCE 41, a professionally recognized standard, contain guidelines and provisions that extend over several analysis procedures. The consistency between the linear and nonlinear analysis procedures outlined in the standard was investigated through the detailed assessment of four existing steel moment frame and concrete shear wall buildings in California. The buildings were instrumented by the California Strong Motion Instrumentation Program, which allowed for the calibration of the structural simulation models against recorded data from past earthquakes. The primary ASCE 41 based assessments of the calibrated models were followed by a comprehensive incremental dynamic analysis (IDA) of each building based on FEMA P-695 to evaluate the collapse probability inherent in the ASCE 41 Collapse Prevention performance level. Finally, a correlation between a system-based drift demand parameter and Immediate Occupancy (IO), Life Safety (LS), and Collapse Prevention (CP) was established for the four buildings.

This dissertation addresses some of the core issues in ASCE 41 through comprehensive case studies of 3-story and 6-story steel moment frame buildings, and 3-story and 5-story reinforced concrete shear wall buildings. First, options for modeling of the primary structural components are explored, followed by a system-based calibration of the model against displacement and acceleration time histories in past earthquakes recorded at the site. For the steel buildings, a major focus was on obtaining the nonstructural stiffness contribution at low intensities, and understanding how the contribution of nonstructural components diminishes during strong shaking. For the concrete buildings, extensive effort was devoted to modeling options for flexural-controlled versus shear-controlled walls.

The ASCE 41 assessments demonstrated inconsistency between the four analysis procedures. The linear static and linear dynamic procedures produce similar component demands, drifts, and performance levels but were shown to be conservative compared to the nonlinear procedures. The nonlinear static and nonlinear dynamic procedures differed significantly in component-demands and drift patterns, and the static procedure underestimated the demands in the upper stories of the six-story steel building. These basic assessments were followed by incremental dynamic analyses and collapse probability fragility curves were developed based on an assumed collapse condition at 6% story drift. Results from the simulation studies indicate that the current component-based Life Safety and Collapse Prevention performance levels are conservative and a quantified comparison is presented using a drift-based approach. Findings from this research work indicate the need to modify the current acceptance criteria for each performance level to include a system-based demand criteria. The dissertation concludes with recommendations for future research focused on developing methodologies to augment acceptance criteria as well as the need for improved guidelines for shear-controlled walls and ground motion scaling for hazard-consistent assessments.

Acknowledgements

The research presented in this dissertation was made possible by the financial support from the California Department of Conservation, California Geological Survey (Strong Motion Instrumentation Program) under Contract 1019-013 and Contract 1020-005. Additional support was provided by the University of California, Davis, through the Dissertation Year Fellowship, Miguel Velez Fellowship, and Graduate Research Award. External financial support was also received through the ASCE O.H. Ammann Research Fellowship, the American Concrete Institute Presidents' Fellowship, and the SEAOCC Graduate Student Scholarship. These organizations are gratefully acknowledged for their generous support. Any opinions, findings, conclusions, or recommendations expressed in this dissertation are those of the author and do not necessarily represent the views of these organizations.

I am immensely grateful for the continuous support and guidance from my research advisor, Professor Sashi Kunnath, who fully supported my research endeavors throughout my years at UC Davis. His commitment to teaching and mentoring his PhD students is extraordinary and I feel lucky to have been one of his last students. I am especially thankful for his encouragement, flexibility, and support as I decided to become a mother during my PhD and balance research and motherhood.

I thank my dissertation committee members at UC Davis, Amit Kanvinde and John Bolander, for reviewing my dissertation and providing feedback on my work. As the research evolved, I was also fortunate to hold discussions and receive feedback from the following practicing engineers and professors, who I thank for their time and support: Insung Kim and Jim Malley (Degenkolb), Afshar Jalalian (Rutherford + Chekene), Dimitrios Lignos (École

Polytechnique Féderale de Lausanne), Kevin Moore (Simpson Gumpertz & Heger), and Jose Restrepo (University of California, San Diego).

I am thankful for having had like-minded colleagues at UC Davis who I worked with and learned from, including Ahmad Hassan, Ahmed Aljasar, Renmin Pretell, Jin Zhou, Han Yang, Hexiang Wang, and Qiwei Zhang. I will always cherish our conversations about courses, research, and life.

During my time at UC Davis, I grew as a researcher but also as an individual, thanks to Professor Colleen Bronner. I learned from her what it means to be an inclusive teacher, to care about students, and to purposefully seek out ways to support their learning and well-being. Through her leadership and dedication, I became inspired to advocate for diversity, equity, inclusion and justice in engineering and beyond.

To my husband Patrick, what a journey have we been through, a wonderful one that is. It has been an honor to have done my PhD at the same time as yours. You have been an excellent companion in this journey and I have learned so much from you. Side by side, we did it! I look forward to the many more adventures we shall embark on together. To my daughter Arabella, you are my light and my world. Mi niña, gracias por acompañarme todos los días de tu vida hasta ahora. Verte dormir mientras que trabajaba durante tus siestas, o por la noche, me daba paz y alegría, porque al despertarte tenía el privilegio de compartir momentos especiales contigo.

Mami, gracias por tu amor incondicional y por apoyarme en todo momento. Papi, gracias por iluminar mi camino desde el cielo.

Diosito, gracias por guiarme, iluminarme, y acompañarme en todo momento.

Table of Contents

List of Figures

List of Tables

1 Introduction

The development of ASCE 41 (ASCE 2017) and other ongoing efforts directed towards the enhancement of performance-based codes represent a significant advancement in the practice of earthquake engineering. While the guidelines in ASCE 41 deal primarily with existing buildings, the ability to define performance goals have led many practitioners to use the methodology for the design of new buildings. The blueprint for future performance-based codes is inherent in the ASCE 41 methodology. However, calibration and validation of the modeling parameters and acceptance criteria to real building performance is clearly needed for practicing engineers to gain confidence in the proposed methodologies. The use of strong motion data obtained from instrumented buildings experiencing strong ground shaking is an essential part of this process.

1.1 Previous Work

There have been numerous studies examining the methodologies and provisions in ASCE 41: Maison et al. (2009) evaluated the characterization of collapse through application of the ASCE 41 methodology on a four-story moment frame building that was tested to collapse on a shaking table; Lagaros and Fragiadakis (2011) compared the ASCE 41 pushover methodology to the capacity spectrum method and the N2 method proposed in the Eurocode; Birely et al. (2014) highlighted the inadequacies in ASCE 41 for modeling flexural walls; Kutter et al. (2016) examined the modeling methods for rocking of shallow foundations. There have also been studies investigating particular types of structural and protective systems (unreinforced masonry, base-isolation, etc.) and non-structural elements such as infill walls. However, at the commencement of

this dissertation work, there were no detailed studies examining the basis of the acceptance criteria in ASCE 41, which is used to assign a performance level to a building.

ASCE 41 permits as many as four analytical procedures to estimate seismic demands: Linear Static Procedure (LSP), Linear Dynamic Procedure (LDP), Nonlinear Static Procedure (NSP), and Nonlinear Dynamic Procedure (NDP). This implies that the evaluation of a regular low to mid-rise building using any of the methods should reach essentially the same assessment on the performance level [i.e., Immediate Occupancy (IO), Life Safety (LS), or Collapse Prevention (CP)] of the system. Recently, Harris and Speicher (2018) carried out a detailed ASCE 41-based assessment of six modern steel frames varying in height from four to sixteen stories designed to the provisions of ASCE 7 (ASCE 2017). Their study identified numerous inconsistencies in the different evaluation procedures: for example, LDP consistently resulted in lower demand-to-capacity ratios (DCRs) than LSP and likewise NSP consistently resulted in lower DCRs than NDP – though it is recognized that nonlinear responses are sensitive to model and analysis parameters.

Recently, the Applied Technology Council (ATC) and the Engineering Laboratory of the National Institute of Standards and Technology (NIST) published the findings of a collaborative project (NIST GCR 22-917-50 2022) where six instrumented reinforced concrete structures were assessed with the objective of benchmarking evaluation procedures in ASCE 41. One major conclusion was that the current component based acceptance criteria overestimates the damage in the observed structures, and it is suggested that ASCE 41 adapts the use of acceptance criteria based on global building performance in addition to local component criteria.

Given the serious concerns initially raised in the study by Harris and Speicher, this study re-evaluates the ASCE 41 acceptance criteria using models of existing buildings that have been

calibrated to instrumented data. Utilizing strong motion data obtained from instrumented buildings experiencing strong earthquake ground shaking is critical to the development of performance-based procedures since it facilitates model calibration. Hence, the calibration of computer models to observed/recorded response is crucial to the task of performing simulation studies and related evaluation tasks since errors resulting from incorrect system modeling can compromise overall research findings. The availability of strong motion data greatly enhances our ability to validate analytical procedures and eliminate to a great extent errors arising from assumptions and simplifications in system modeling.

1.2 Objectives and Scope of Research

The primary objective of the research is to evaluate the consistency between the different analysis methods permitted in ASCE 41. A regular building that meets the criteria for linear and nonlinear static analysis can be assessed by any of the four procedures: LSP, LDP, NSP or NDP. The question is whether all four methods will provide the same assessment of the building in terms of the acceptance criteria for the respective methods. For example, it would be problematic if one procedure deemed a building to satisfy the acceptance criteria for Life Safety whereas another procedure concludes that Life Safety criteria have not been met.

Additionally, as per the current ASCE 41 provisions, a building is deemed not to meet a performance objective if even a single primary component fails to meet the corresponding acceptance criteria. While such a restriction appears logical for a critical load-bearing column, the requirement can be lowered if the members failing the criteria by a small degree are not system-critical. The study by Harris and Speicher (2018) clearly questions the validity of requiring all components in a redundant system to meet specified acceptance criteria corresponding to target

performance objectives. Hence, this study will attempt to develop a new system-level acceptance criteria to augment the current component-based acceptance criteria.

The above key concerns are investigated in this dissertation through numerical studies wherein a set of regular steel moment frame and reinforced concrete shear wall buildings are assessed using all four analysis procedures. The goals of the project are achieved through completion of the following tasks:

- First, relevant building and strong motion data are collected, compiled and reviewed. Both steel moment frame and reinforced concrete shear wall buildings with varying heights are identified based on preliminary information such as the complexity of plan configuration to avoid selecting buildings that do not pass the criteria for linear and static procedures.
- Computer models are developed for each of the target structures from structural drawings and available material property information. The open source software, OpenSees, and the commercial software, Perform3D, are used in the simulations for the steel and concrete buildings, respectively. The simulation models are validated to ensure that the each building has been adequately modeled in terms of mass and stiffness so that the observed fundamental period of the building (as ascertained from frequency analysis of the acceleration time traces of the instrumented building response) can be reproduced with reasonable accuracy. Due consideration is given to modeling of nonstructural elements in the case of steel buildings. Likewise, comparisons of time-history traces of displacement and acceleration at recorded floor levels are carried out to also ensure reliability of the member models and assumed dynamic properties.
- The calibrated models are then used in detailed simulations to address the issues previously listed as the focus of this proposed effort. The simulations include linear and nonlinear,

static and dynamic analyses. This is followed by a comprehensive evaluation of displacements, inter-story drift, member plastic rotations (for nonlinear analyses), panel zone distortions (for steel buildings) and distribution of section yielding (again for nonlinear analyses).

- The results of the simulations are examined to determine consistency in the predicted assessment of the target buildings using the four ASCE 41 procedures.
- Finally, the effectiveness or lack thereof of the component-based acceptance criteria is critically evaluated, through a FEMA-P695 based Incremental Dynamic Analysis (IDA) for each of the buildings.

While focusing on the main research objectives highlighted above, there are several other important related issues that have also been evaluated in this dissertation. These include the investigation of: the effect of panel zone modeling on performance-based assessments, damping in buildings under low-intensity versus strong ground motions, ground motion scaling for 2D buildings, ground motion scaling for 3D buildings with significantly different periods in each direction, the linear dynamic procedure (LDP) when using the response spectrum method versus a suite of recorded ground motions, the effect of ground motion variability in the ASCE 41 assessments, and modeling choices in flexure vs shear-controlled reinforced concrete walls.

2 Selected Buildings and Model Calibration

An exhaustive and systematic search of the Center for Engineering Strong Motion database (https://www.strongmotioncenter.org) was carried out to identify potential buildings for this study. Several steel and reinforced concrete moment frame and shear wall buildings were considered as possible targets for the proposed research. Eventually, a decision was made to focus on steel moment frame buildings and reinforced concrete (RC) shear wall buildings, since these building types are commonly found in seismic regions in the United States. The two steel moment-frame structures and the two RC shear-wall buildings listed in Table 2-1 were selected for the assessment studies needed to achieve the goals of the proposed research. Data from multiple earthquakes were available for all buildings, but only the ground motions listed in the table were used in the model validation study.

Table 2-1: Buildings considered in the study

Building Information	**CSMIP Station**	**Records To Be Used**
Steel Buildings San Bernardino 3-Story Office Building	23516	Landers 1992; San Bernardino 2009
Burbank 6-story Commercial Building	24370	Whittier 1987; Sierra Madre 1991
RC Shear Wall Buildings Taft 3-story School Building	35409	Maricopa 2010
Santa Rosa 5-story Commercial Building	68387	South Napa 2014

2.1 Steel Building 1

The first structure selected for assessment is a 3-story office building designed in 1958 and composed of moment frames along the perimeter of the plan serving as the lateral load resisting system in both directions. The gravity system is a wood truss-joist system supported on steel columns that spans in the north-south direction. Figure 2-1 shows the plan view of the building and the elevation of the typical perimeter frame used in the assessment.

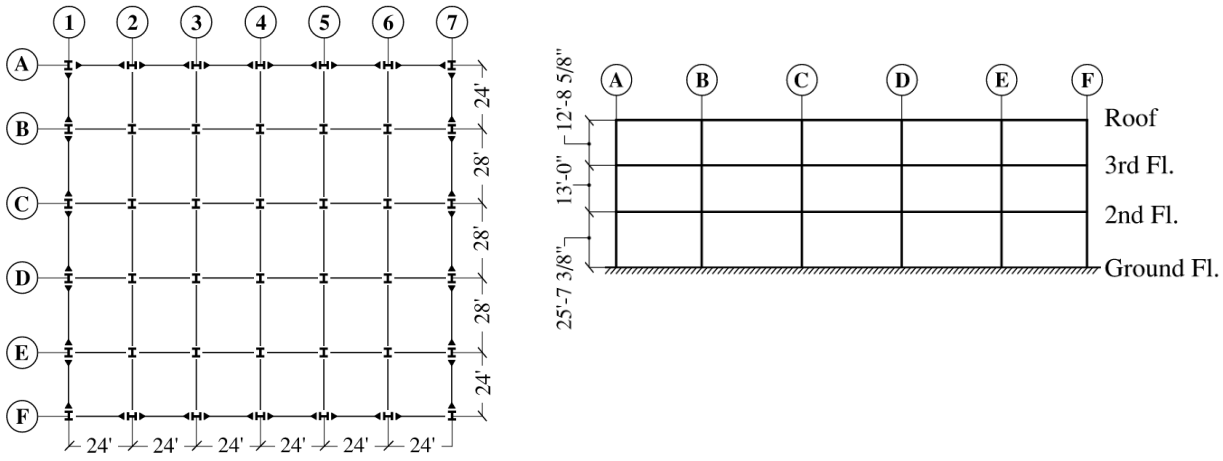

Figure 2-1: Plan view of building and elevation of typical perimeter frame

This building was instrumented with a total of 13 accelerometers as follows: there are 3 accelerometers located at the ground level and the second floor, 4 accelerometers at the third floor level, and 3 accelerometers at the roof as can be seen in Figure 2-2. The instrumentation of this structure allows for the measurement of the following motions:

1. Ground Floor (foundation): one vertical and one horizontal in each of the two directions

2. Second Floor: three horizontal – one in the N-S direction and two in the E-W direction
3. Third Floor: four horizontal – one in the N-S direction and three in the E-W direction
4. Roof: three horizontal – one in the N-S direction and two in the E-W direction

As previous indicated, this station has recorded data from numerous earthquakes. However, as indicated in Table 2-1, only the motions from the 1992 Landers earthquake and the 2009 San Bernardino earthquake were considered in the model calibration since they represent the largest seismic intensities imposed on the structure.

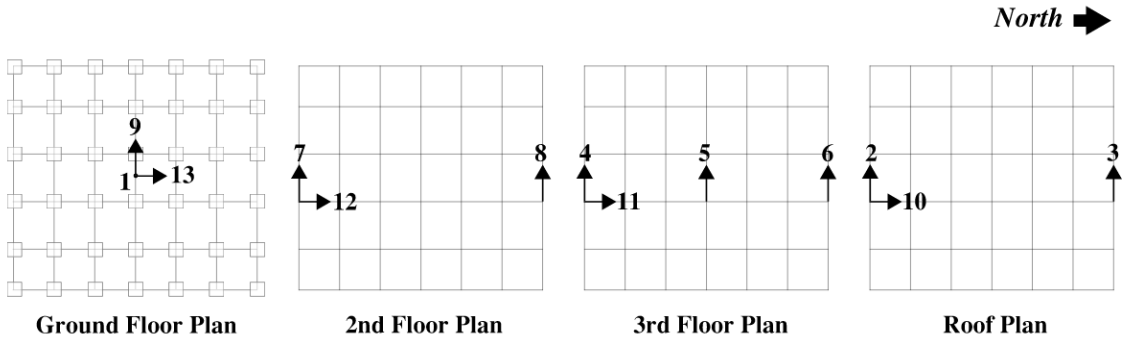

Figure 2-2: Layout of accelerometers in the building

2.1.1 Building Modeling

Given the general symmetry of the building plan and the fact that torsional motions were not evident in the profile of the recorded floor displacement histories, the analyses were carried out on a two-dimensional model (Figure 2-3) of the perimeter moment frame along Line-1 in the east-west direction. The building has embedded column bases connected to spread footings and grade beams and therefore the base was assumed to be fully restrained – an assumption that was shown to be reasonable for such a base connection (Falborski et al. 2020). The diaphragms were assumed

to be rigid in plane and hence all nodes on a floor level were constrained to have the same lateral displacement.

For steel moment frames, panel zones have been shown to significantly influence the behavior of the frame system. Additionally, in the ASCE 41 evaluation, panel zones are considered to be primary components that need to be evaluated in the performance assessment. For the two-dimensional OpenSees models, panel zones were added at the intersection of the beams and columns, where a moment connection exists. The panel zones were modeled with a set of elastic beam-column elements, with a trilinear-equivalent rotational spring on the upper right corner that captures the shear distortion through the use of the Hysteretic material model.

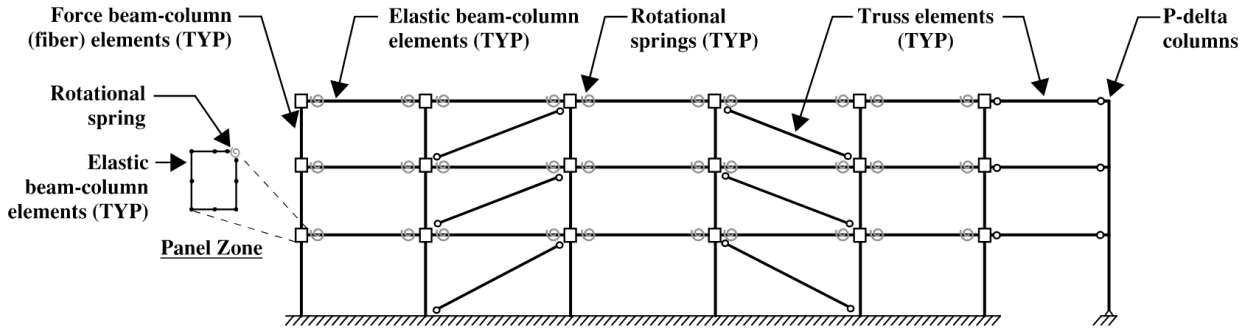

Figure 2-3: OpenSees model of typical perimeter frame

Beams are modeled using elastic beam-column elements with inelastic springs (constructed with zero-length elements) at the ends as shown in Figure 2-3. All inelastic action (for nonlinear procedures) is lumped into these concentrated springs whose cyclic response is represented using the Modified Ibarra-Medina-Krawinkler deterioration model (Ibarra et al. 2005). In order to capture the axial load-moment interaction, columns are modeled as force-based elements with five Lobatto integration points and the Updated Voce-Chaboche (Hartloper et al. 2021) material model was used to represent the inelastic cyclic behavior of steel. An additional leaning column is

attached to the moment frame using rigid links with pinned connections at each end to account for P-Delta effects and contributing gravity loads from the interior frames are applied at each level. A set of diagonal braces were also added at each level to represent the stiffness contribution of non-structural elements – the process by which the brace stiffness was determined is described in the next section.

Calibration of Non-Structural Stiffness

The model was calibrated assuming elastic behavior when the structure was subjected to the ground motions referenced. This assumption is valid as (1) there is no period variation in any of the ground motions and (2) there was no evident structural damage in the structure itself following the seismic events. Once the structural model was created, an eigenvalue analysis was carried out on the bare frame structure without the diagonal braces and the fundamental period of the structure was estimated as 0.70 sec. However, the model only represented the bare frame of the structure, not accounting for composite beam-slab effects nor the stiffness of nonstructural components. Therefore, additional studies were completed to accurately model the total stiffness of the system. A Fast Fourier Transform (FFT) was carried out using the acceleration time histories at each level and Transfer Functions (relative to the base) were obtained for both the Landers and San Bernardino earthquakes. The resulting plots for the Landers recordings are shown in Figure 2-4 where a predominant frequency is evident at approximately 1.8 Hz (corresponding to a period of 0.56 sec).

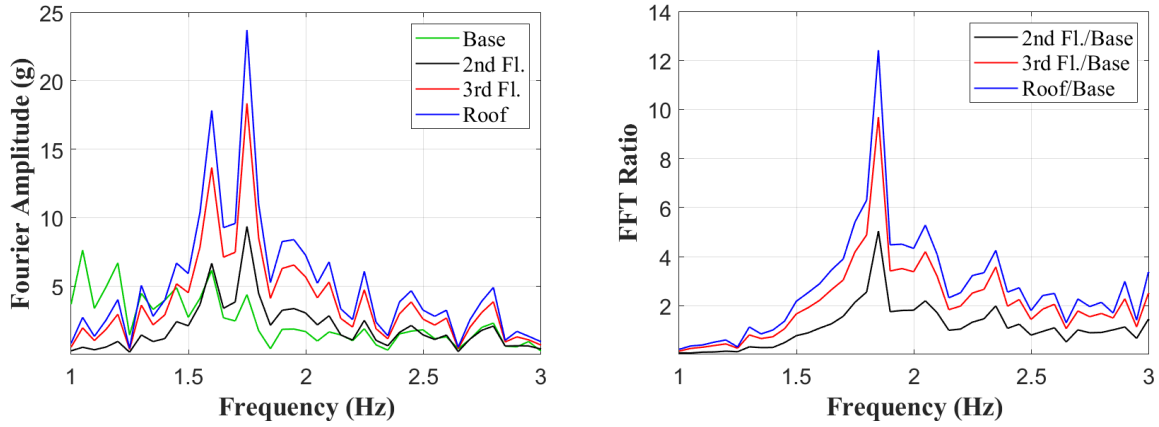

Figure 2-4: Fourier transform and transfer functions from acceleration histories recorded during Landers earthquake

In search for a more accurate procedure to determine the stiffness of the structure, the methodology proposed by Falborski et al. (2020) was implemented. At any time instant during the dynamic response of the structure, the shear in any story *K* can be estimated from:

$$V_k^{story}(t) = V_K^{NS}(t) + V_K^{STR}(t) + C_K \cdot \dot{\Delta}_K(t) = \sum_{i=K}^{N} m_i \ \ddot{u}_i(t) \tag{2-1}$$

In the above equation, $V_K^{story}(t)$ is the instantaneous shear in story *K* at time *t*, $V_K^{NS}(t)$ and $V_K^{STR}(t)$ are the story shears from the non-structural and structural components, respectively, $C_K \cdot \dot{\Delta}_K(t)$ is the story force due to damping, and $\sum_{i=K}^{N} m_i \ \ddot{u}_i(t)$ is the sum of the inertia forces above story *K*. Using the recorded time histories, the time instants at which the interstory velocities are zero are determined for each story *K*. At these instants, the damping force is eliminated in Equation (2-1). The lateral displacements at each floor corresponding to these time instants are determined and applied statically to the model. The resulting shears will be 'structural' story shears at each level. The total shear is determined by summing the inertia forces above that level, hence

the non-structural contribution can be established. At each time instant when the interstory velocity is zero, the nonstructural story shear can be plotted vs. the corresponding interstory drift at story *K*. Linear regression can be used to fit the data points and the resulting slope represents the nonstructural story stiffness. The estimated story stiffnesses are shown for a typical floor in Figure 2-5 for the San Bernardino recordings.

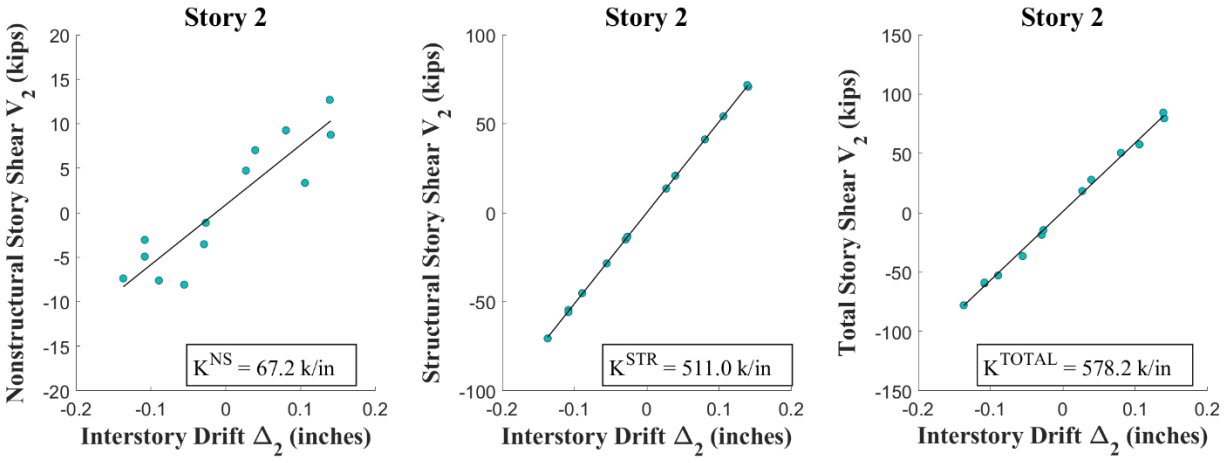

Figure 2-5: Estimating non-structural stiffness for a typical story

In order to add the nonstructural stiffness, truss elements were introduced in two bays at each floor as shown previously in Figure 2-3. The properties of the braces were adjusted until the total story stiffness matched the calculated values shown in Table 2-2. This was accomplished iteratively by updating the areas of the braces, applying static lateral loading to the model and determining the total story stiffness. The addition of the braces to the model as well as incorporating the additional stiffness of the joist floor system altered the fundamental period of the frame to 0.54 sec, reasonably consistent with the estimated building period in the east-west direction from the FFT analysis. In the absence of the braces, the building period increases to 0.63 sec.

Table 2-2: **Estimated components of story stiffness**

Story	*Stiffness (k/in)*			
	K^{NS}	K^{STR}	K^{TOTAL}	K^{NS}/K^{TOTAL}
1	51.9	551.1	603.0	0.09
2	67.2	511.0	578.2	0.12
3	102.9	340.3	443.2	0.23

While the estimation of nonstructural stiffness is useful during the calibration of the building model, it should also be acknowledged that the relative contribution of non-structural components to the overall building response diminish as the deformations increase. Consequently, the assessment of buildings at extreme limit states associated with Life Safety (LS) and Collapse Prevention (CP) can be performed in the absence of non-structural components assuming their contribution to the system response to be negligible. In a simulation model, when using an advanced software such as OpenSees, it is possible to set up limiting deformations at which a component can be removed from the model. This would be the most appropriate approach to incorporating non-structural components in a simulation model that is expected to deform well into the inelastic range.

Calibration of Damping

The concept behind Equation (2-1) can also be used to calibrate damping. In this case, the time instants at which the interstory drifts are zero are considered. Therefore, the total damping force in any story at these time instants will be equal to the sum of the inertia forces above that story. However, the damping coefficients will correspond to the lateral degree-of-freedom of the floor and additional calibration will be needed to establish Rayleigh coefficients associated with the mass and stiffness matrices of the system. In Appendix A.1, this procedure was implemented and the results presented. However, for the final calibration of this model, a simpler approach was

followed: the roof acceleration response spectrum was compared to that obtained with the actual recorded motions, to obtain an approximate damping ratio. Results are presented in Figure 2-6, which shows that a damping of 10% (assigned to both the 1st and 2nd mode) produced a reasonable match. However, in the ASCE 41 evaluations presented in the next chapter, which examine responses at the design event, a value of 3% of critical damping was used in both modes since the contribution of nonstructural components is expected to be negligible at these deformation demands.

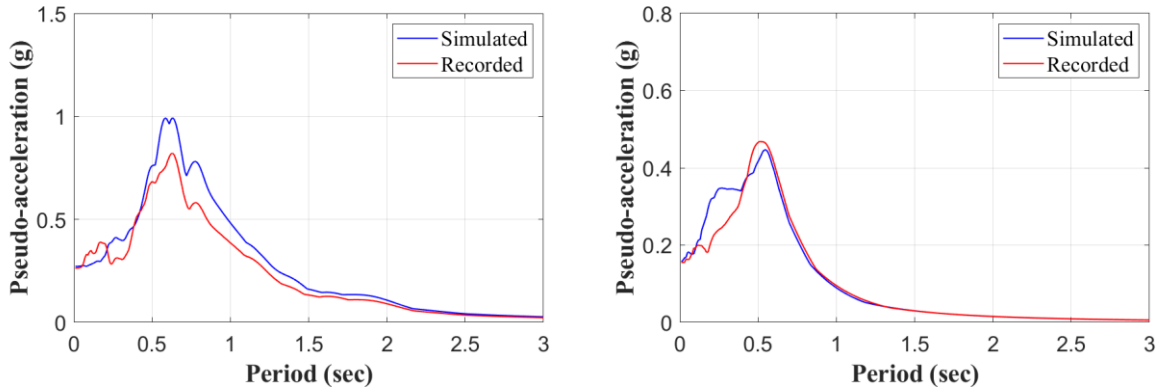

(a) (b)

Figure 2-6: Comparison of acceleration spectra using data from the roof response: (a) Landers; (b) San Bernardino

2.1.2 Model Validation

When examining the time series for the Landers earthquake, unusual long-period content was observed throughout the record, particularly in the floor displacement histories (see roof history shown in Figure 2-7). Therefore, a high-pass filter was applied with a corner frequency of 0.5 Hz using an 8th order zero phase delay Butterworth filter. Figure 2-7 shows the base acceleration as well as the relative roof displacement before and after filtering.

The model was calibrated using a two-dimensional model described in Section 2.1.1. The simulated and recorded roof displacement histories during the Landers and San Bernardino shaking are shown in Figure 2-8. The peak displacements during the Landers earthquake are slightly over-estimated – this is attributed to the fact that the 10% damping used in the simulation was lower than the observed damping (see Figure 2-6). The magnitude of the response during the San Bernardino earthquake was negligible during the first 25 seconds, hence roof displacement history is shown beyond this point.

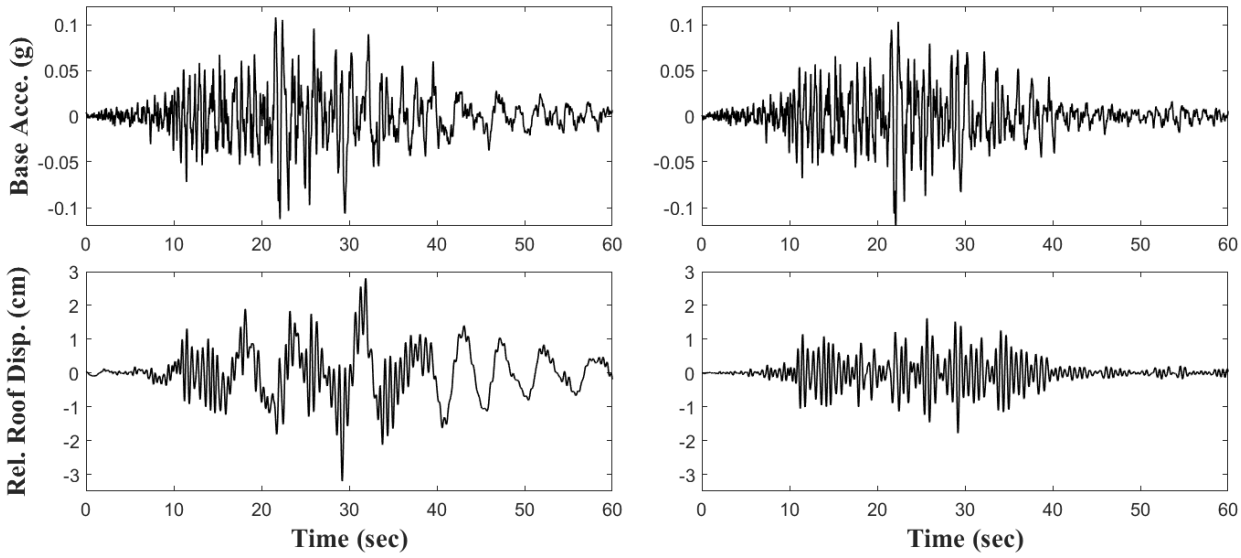

Figure 2-7: Unfiltered (left) and filtered (right) time histories

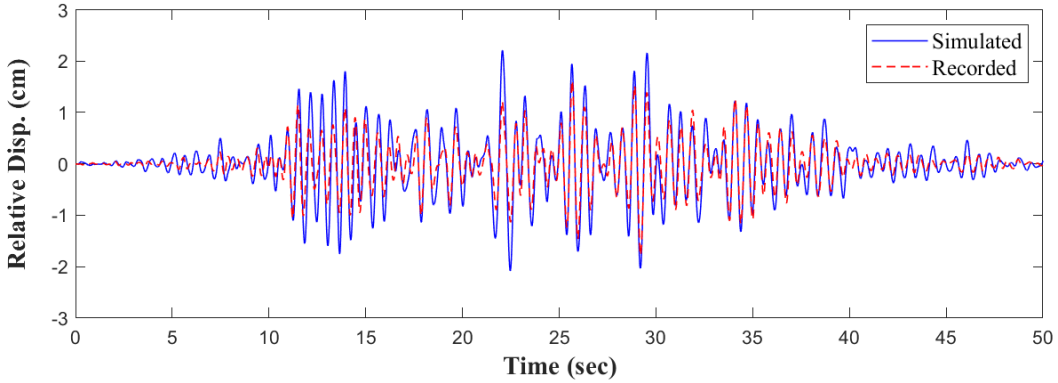

(a)

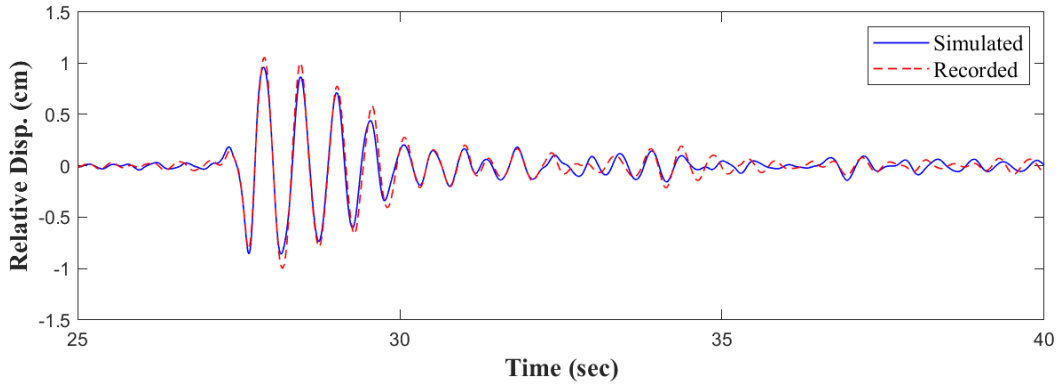

(b)

Figure 2-8: Comparison of recorded vs. simulated roof displacement histories: (a) Landers; (b) San Bernardino

2.2 Steel Building 2

The second structure selected for assessment is a 6-story commercial building designed in 1976 and located in Burbank, California. The structure has moment frames along the perimeter of the building serving as the lateral load resisting system in both directions. The gravity system is composed of concrete on metal deck spanning in the east-west direction, supported by wide flange steel beams. Figure 2-9 shows the plan view of the building and the elevation of the perimeter frame used in the assessment.

The building has been instrumented by the California Strong Motion Instrumentation Program with thirteen accelerometers: four at the ground level to record base accelerations in all three orthogonal directions, and three each at the 2nd, 3rd, and 7th floor (roof) – as shown in Figure 2-10. Instrumented data from several earthquakes are available for this building. However, of the available data, two recorded motions with the highest ground peak accelerations (PGA) were selected to calibrate the simulation model: Whittier (1987) and Sierra Madre (1991). The

Northridge ground motion which had a higher peak acceleration was not used since there were missing recordings at the 3rd floor.

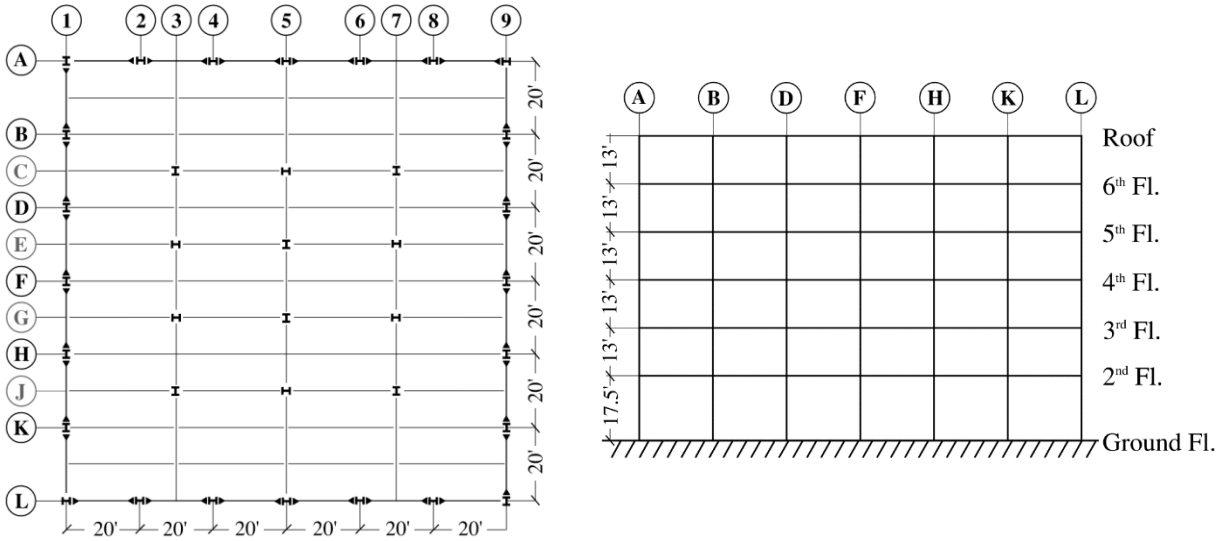

Figure 2-9: Plan view of building and elevation of perimeter frame

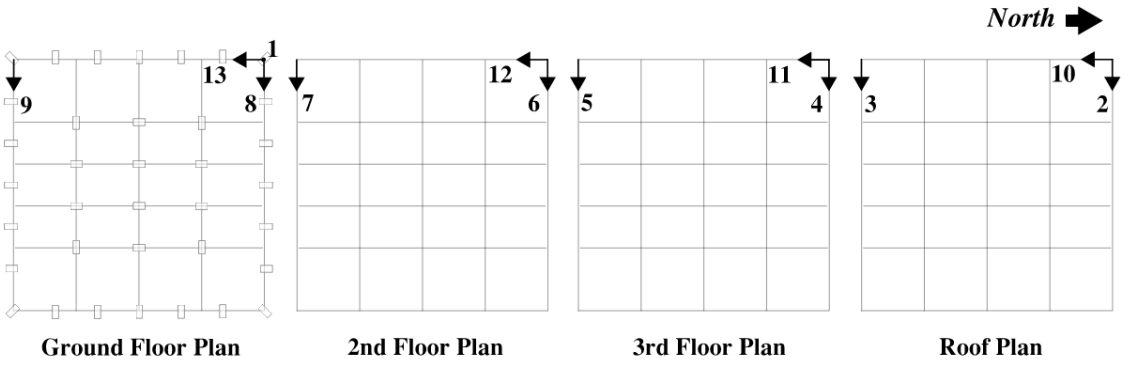

Figure 2-10: Locations of installed sensors

Ground Motion Interpolation

During the validation process in the next section, it is of interest to compare the recorded versus the simulated building behavior at all floors. However, only four floors were instrumented in the direction of interest. In order to obtain the time histories at the uninstrumented floors, both the

mode-based and the piece-wise cubic polynomial interpolation (PWCPI) procedures were considered (Goel 2008). Using the mode-based approach, the interpolated third story showed a significantly higher drift than the other floors, and differed from the drift captured by the simulation. For a building of this height, it is strange to see a large participation from the higher modes. Therefore, the PWCPI procedure results, which provided a satisfactory match to the simulated results, were implemented for the remainder of the calibration process.

2.2.1 Building Modeling

Given that there is no evidence of torsional motions from the time histories for this symmetric building, the assessment was conducted using a two-dimensional model of the south perimeter moment frame in the east-west direction. The OpenSees model, shown in Figure 2-11 follows the same modeling approach and assumptions described for Building 23516 in Section 2.1. The model includes panel zones, braces to represent non-structural components, and a leaning P-delta column on which gravity loads from the interior frames are applied.

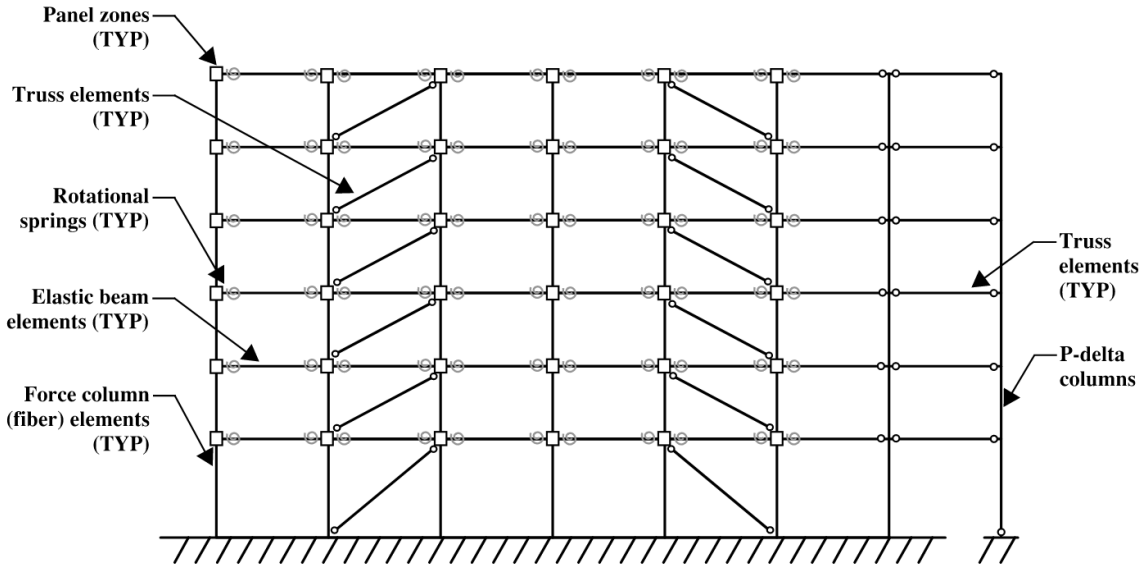

Figure 2-11: Elevation view of OpenSees model

Calibration of Non-Structural Stiffness

The model was calibrated assuming the structure remained elastic when subjected to the recorded ground motions. This is a valid assumption when examining the peak drifts during the response to each earthquake as well as the transfer functions of the recordings. A preliminary eigenvalue analysis of the bare frame without panel zones indicated that the fundamental period was approximately 1.6 sec. The effective moment of inertia of the beams was increased in order to account for composite action of the concrete slab on metal deck, decreasing the period to 1.52 sec but the addition of panel zones to the model increased the period back to 1.6 sec. Finally, braces were introduced at all levels in the 2nd and 5th bays to incorporate the nonstructural stiffness, further decreasing the period to 1.25 sec. The procedure to estimate the contribution of the nonstructural components is similar to the methodology outlined for the 3-story building in Section 2.1.2. Data from both the Whittier and Sierra Madre earthquakes were used in the calibration. Estimates of the non-structural stiffness for three floors using recordings from the Sierra Madre earthquake are displayed in Figure 2-12.

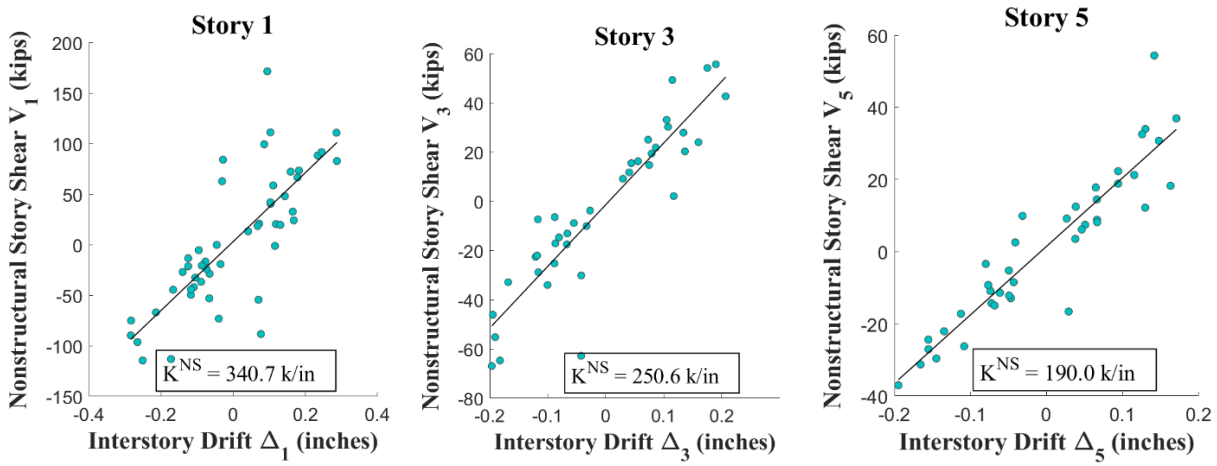

Figure 2-12: Estimates of nonstructural stiffness for three floors using instrumented data from the Sierra Madre earthquake

The breakdown of the stiffness contributions from the bare frame (structural stiffness), the nonstructural components and the total story stiffness are listed in Table 2-3 for the Sierra Madre earthquake.

Calibration of Damping

The damping in this model was calibrated by comparing the simulated and recorded pseudo-acceleration spectra for two earthquakes. An adequate match for all identified periods was not possible for both records as evident from Figure 2-13. Hence, the damping that better matched the time history acceleration and displacement response for both the Whittier and the Sierra Madre earthquakes was selected. The final damping was modeled using Rayleigh damping with coefficients corresponding to 3% of critical damping in the 1st and 2nd modes.

Table 2-3: **Estimated components of story stiffness**

Story	***Stiffness (k/in)***			
	K^{NS}	K^{STR}	K^{TOTAL}	K^{NS}/K^{TOTAL}
1	340.7	452.2	793.0	0.43
2	221.6	734.5	956.1	0.23
3	250.6	608.5	859.1	0.29
4	236.7	501.1	737.8	0.32
5	190.0	423.6	613.6	0.31
6	16.2	390.5	406.7	0.04

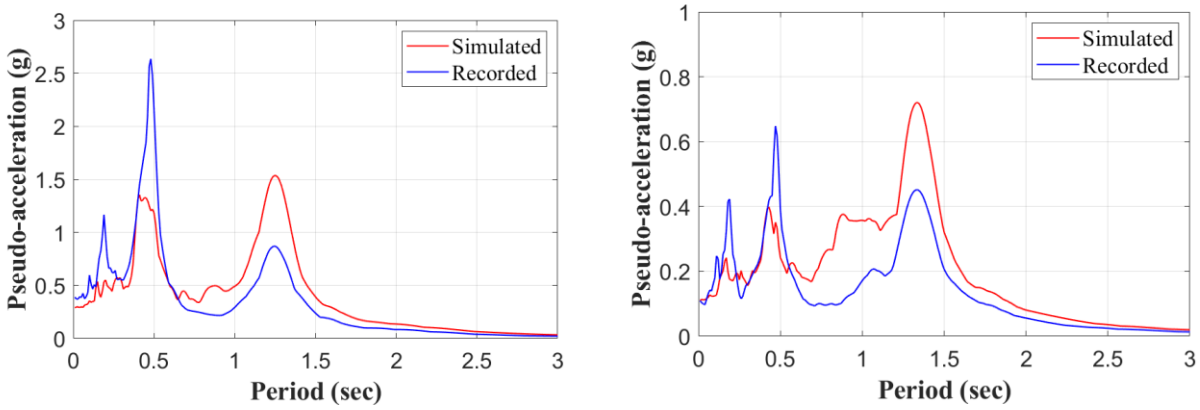

(a) (b)

Figure 2-13: Comparison of acceleration spectra using data from the roof response: (a) Whittier (b) Sierra Madre

2.2.2 Model Validation

The calibrated elastic model as outlined in Sections 2.2.2 and 2.2.3 was subjected to both the Whittier and Sierra Madre earthquakes. The comparison of the simulated and recorded displacement time histories at the roof level is shown in Figure 2-14. Both simulations indicate that the actual damping in the building was slightly lower than assumed in the model but the overall response reasonably reproduces the observed behavior – both in terms of building period and the recorded peak displacements.

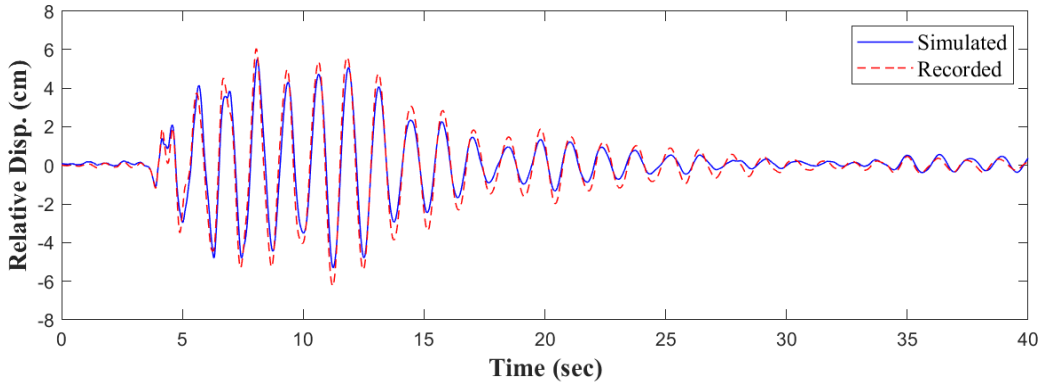

(a)

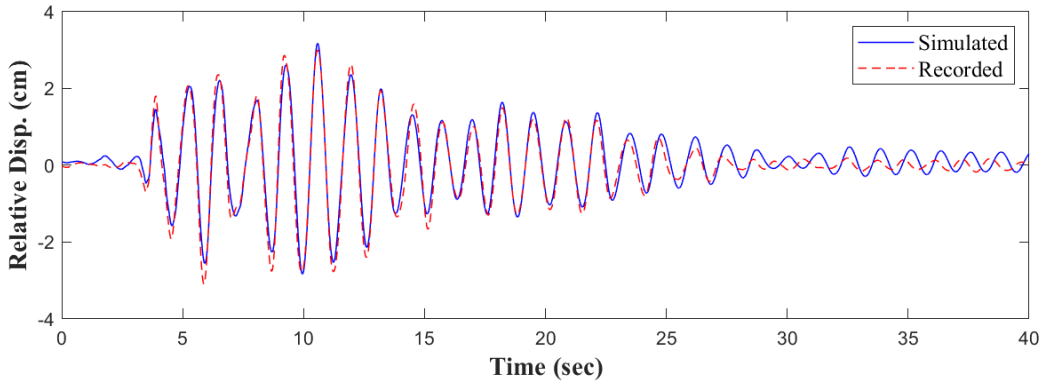

(b)

Figure 2-14: Comparison of recorded vs. simulated roof displacement histories: (a) Whittier; (b) Sierra Madre

2.3 Concrete Building 1

The first structure selected for the assessment is a 3-story school building designed in 1948 and located in Taft, California. The gravity system is composed of reinforced concrete slabs, supported on pan joists, and beams, supported by walls and columns. The lateral force resisting system includes concrete slab diaphragms and shear walls. There are four principal L-shaped walls at the corners with embedded columns at the gridlines, and two additional rectangular walls in the longitudinal direction. The building wall framing conserves symmetry.

Figure 2-15 shows the typical floor plan view. The building has been instrumented by the California Strong Motion Instrumentation Program (CSMIP Station 35409) with thirteen accelerometers: six at the ground level to record base accelerations in all three orthogonal directions, three each at the 2nd floor, and four at the roof of the building – as shown in Figure 2-16. There are a total of six recorded earthquakes measured at this site. However, only the 2010 Maricopa Earthquake sensor recordings will be used for the calibration since this is the earthquake with the largest ground peak acceleration.

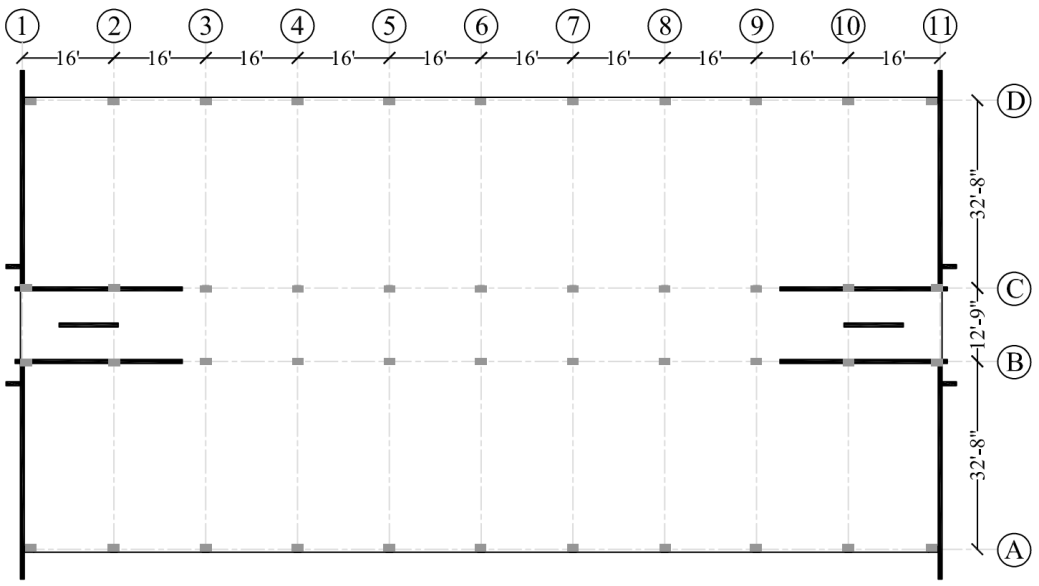

Figure 2-15 : Plan view of building at typical floor

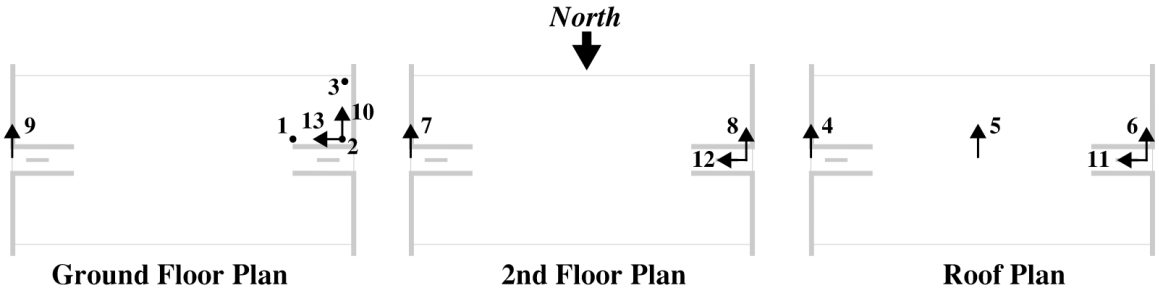

Figure 2-16: Layout of accelerometers in the building

2.3.1 Building Modeling

ASCE 41 does not provide specific guidelines on modeling a shear wall element. Many options exist for modeling a concrete wall: the simplest approach is to model the wall as a beam-column element with inelastic behavior lumped into a concentrated spring with aggregated shear; the next level of refinement would be a beam-column element with distributed properties where selected integration points are discretized into fibers representing cover concrete, core concrete and reinforcing steel. RC walls have also been modeled using multi-spring macro-models consisting

of a set of springs distributed in a manner that captures the strain distribution across the section of the wall as well as the migration of the neutral axis under lateral cyclic loading.

In order to understand the capabilities of the available 2D models in different software programs, two computational platforms were considered: OpenSees (McKenna 2021) and Perform-3D (CSI 2021). Validation studies were carried out on two shear wall specimens. The first wall considered is specimen **RW2** (Figure 2-17a), part of the set of walls tested by Thomsen and Wallace (1995). This is a relatively slender wall with a height to width ratio of 3.0, in which inelastic deformations are expected to be dominated by flexure, and subjected to a constant axial load of $0.07f_c'A_g$ throughout the test. The second wall is specimen **RW-A15-P10-S78** (Figure 2-17b), tested by Tran and Wallace (2012). This wall has a height to width ratio of 1.5 and nonlinear shear deformations are expected to contribute to the overall response. A constant axial load of $0.064f_c'A_g$ was maintained at the top of the wall. Both wall elevations are shown in Figure 2-17.

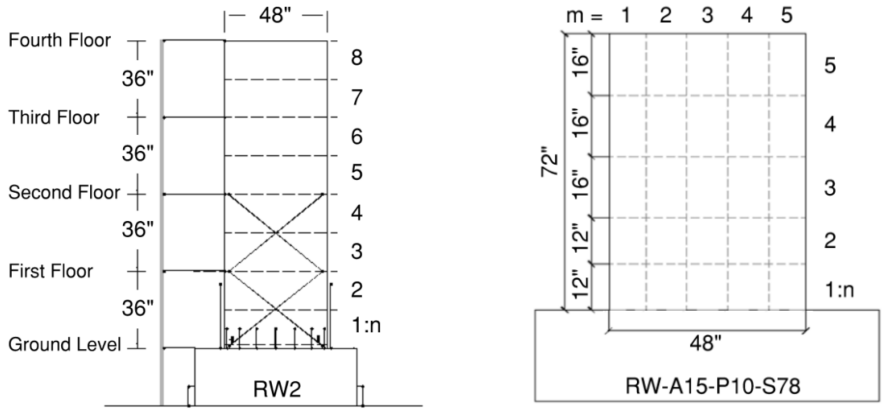

(a) (b)

Figure 2-17: Elevation of wall specimens: (a) Specimen 1 (Thomsen & Wallace 1995); (b) Specimen 2 (Tran & Wallace 2012)

The two walls were modeled in OpenSees using three different modeling options: a beam-column element with fiber-section discretization, the Multiple Vertical Line Element Model (MVLEM), and the Cyclic Shear-Flexural Interaction Multiple Vertical Line Element (SFI-MVLEM). They were modeled in Perform-3D using the Shear Wall element with Inelastic section – for Specimen 1, an elastic shear material was used whereas an inelastic shear material was used for Specimen 2. Note that MVLEM and SFI-MVLEM are derivatives of the original element introduced by Japanese researchers (Kabayasawa et al. 1983) and later enhanced by others (Orakcal et al. 2004; Massone et al. 2006; Kolozvari et al. 2015).

Figure 2-18 compares the numerically simulated response for Specimen 1 versus the measured cyclic response for all four modeling choices. In general, all models produce a good match. Both the MVLEM and SFI-MVLEM models capture the initial stiffness well, whereas the beam-column with fiber-section and Perform-3D models slightly overestimate it though they do a better job in predicting the strength in each cycle. Since the material models in Perform-3D are multilinear, the resulting force-deformation response is also multilinear.

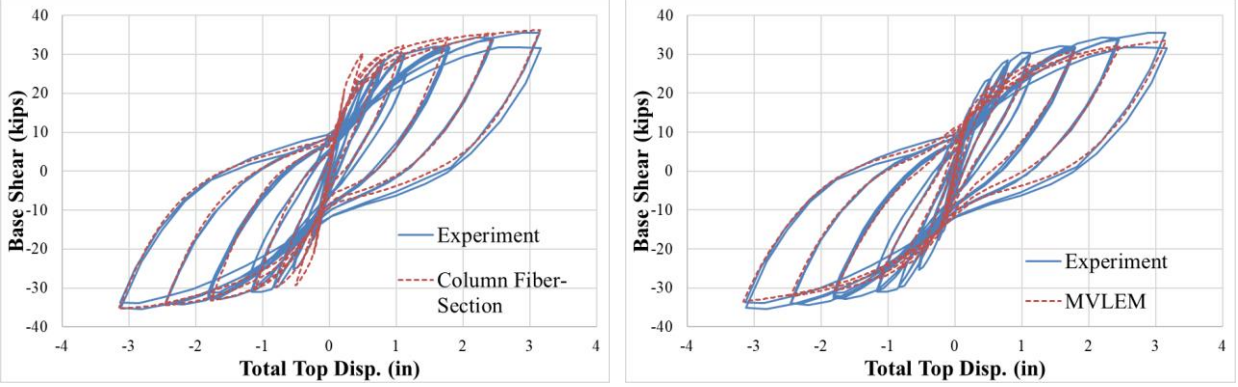

(a) (b)

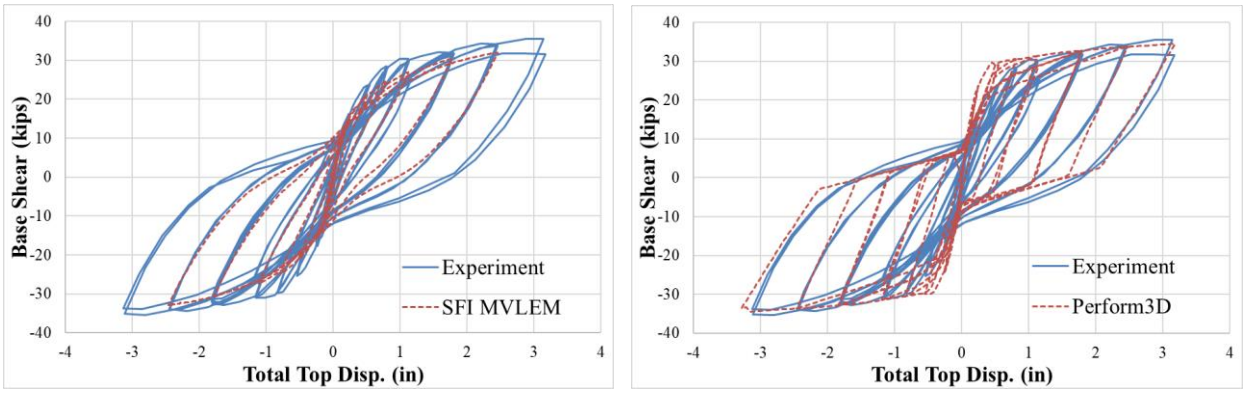

(c) (d)

Figure 2-18: Validation of modeling approaches using results from Specimen 1: (a) OpenSees with beam-column element and fiber section; (b) OpenSees MVLEM; (c) OpenSees SFI-MVLEM; (d) Perform-3D

Figure 2-19 shows the results for Specimen 2. It is evident that the SFI-MVLEM model produces the best results. The beam-column element with fiber-section (and aggregated shear spring) and the MVLEM model are unable to accurately capture the pinched response observed in the experiment. In Perform-3D, it is unclear as to how shear is coupled with flexure. The manual simply indicates that the shear wall is a "compound" element with either elastic or inelastic shear material. Despite numerous attempts to tune the inelastic shear material properties, it was difficult to obtain a suitable response for this experimental wall.

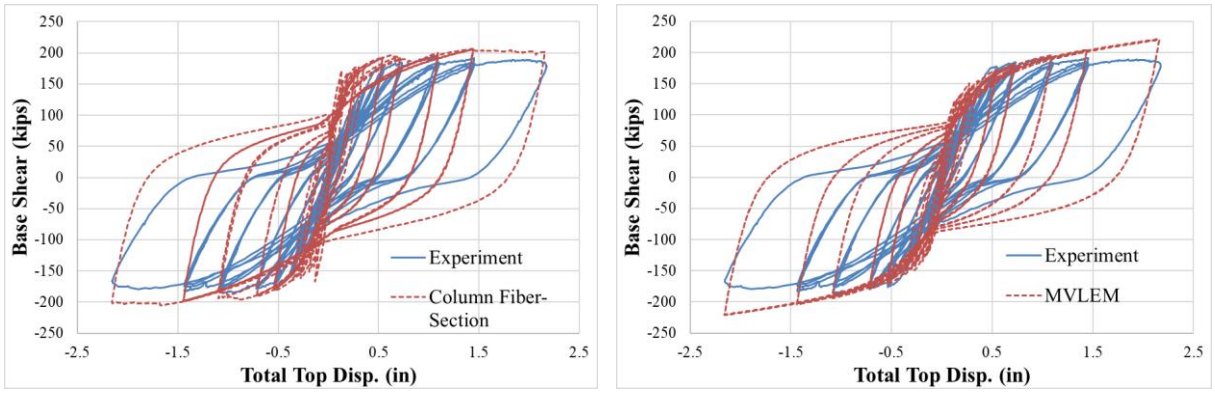

(a) (b)

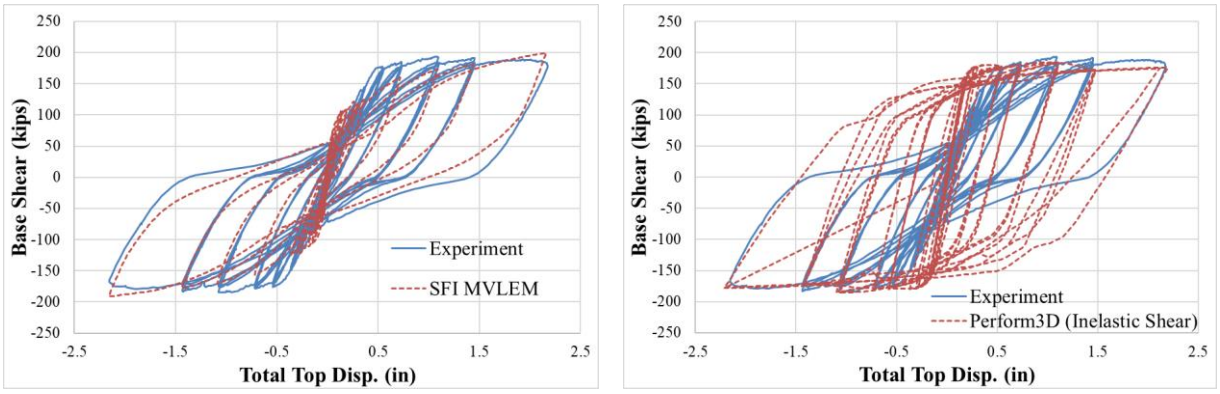

(c) (d)

Figure 2-19: Validation of modeling approaches using results from Specimen 2: (a) OpenSees with beam-column element and fiber section; (b) OpenSees MVLEM; (c) OpenSees SFI-MVLEM; (d) Perform-3D

One of the two concrete buildings considered in this study includes L-shaped walls. Hence, in order to understand the behavior of non-rectangular walls and the modeling capabilities of Perform3D, two experimental L-shaped wall specimens, from a series of wall tests completed by Han et al. (2019), were modeled in Perform3D. Two specimens were selected for the validation study: specimen LW1 with a wall height of 1200 mm and specimen LW9 with a height of 2000 mm; all other geometric and reinforcement properties were the same. The models were subjected to cyclic lateral loading and the simulated response was compared to the experimental data, as shown in Figure 2-20.

After initial modeling of wall LW1, the Perform3D results showed that the wall segment perpendicular to the loading was incorrectly resisting a large part of the load and therefore artificially increasing the shear capacity of the L-shaped wall. Decreasing the wall out-of-plane stiffness, from 40% to 10% of the elastic modulus *E*, readjusted the results so that the simulated response better matched the experimental wall response under the cyclic lateral loading. An out-of-plane stiffness value of 0.1E was therefore applied to the walls of the three-story building.

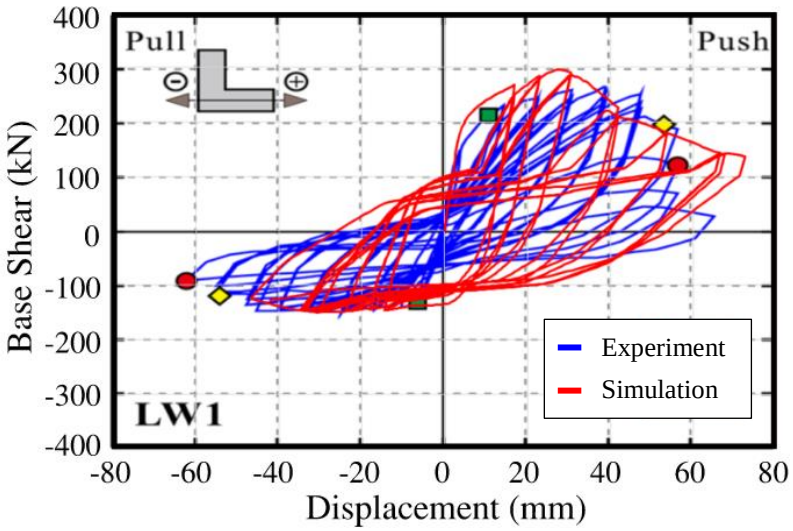

(a)

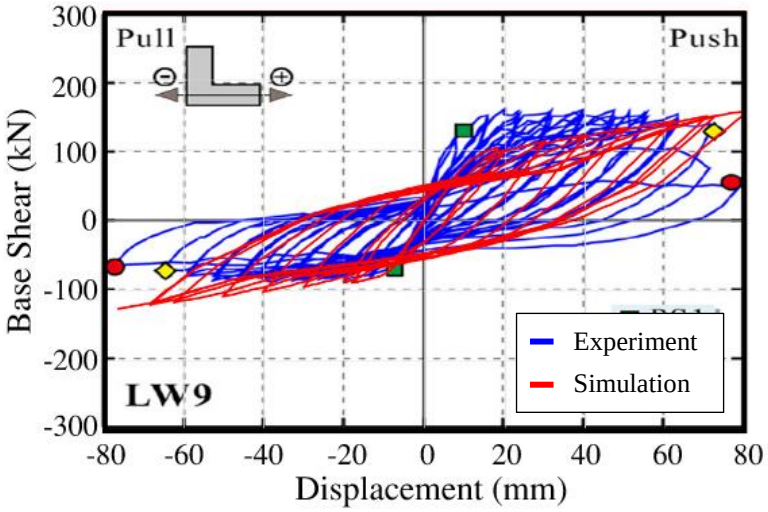

(b)

Figure 2-20. Simulation vs experimental results of cyclic loading (figures modified from Han et al., 2019); (a) LW1 wall; (b) LW9 wall

Three-dimensional (3D) Perform-3D Model

Given that the main lateral load resisting system is composed of L-shaped walls, it was necessary to create a three-dimensional building model, in order to capture any potential torsional modes as well as to account for non-symmetric response following inelastic action. Therefore, the analyses

were carried out using the commercial software Perform-3D (CSI 2021). Figure 2-21 shows the 3D and transverse and longitudinal elevation views of the model.

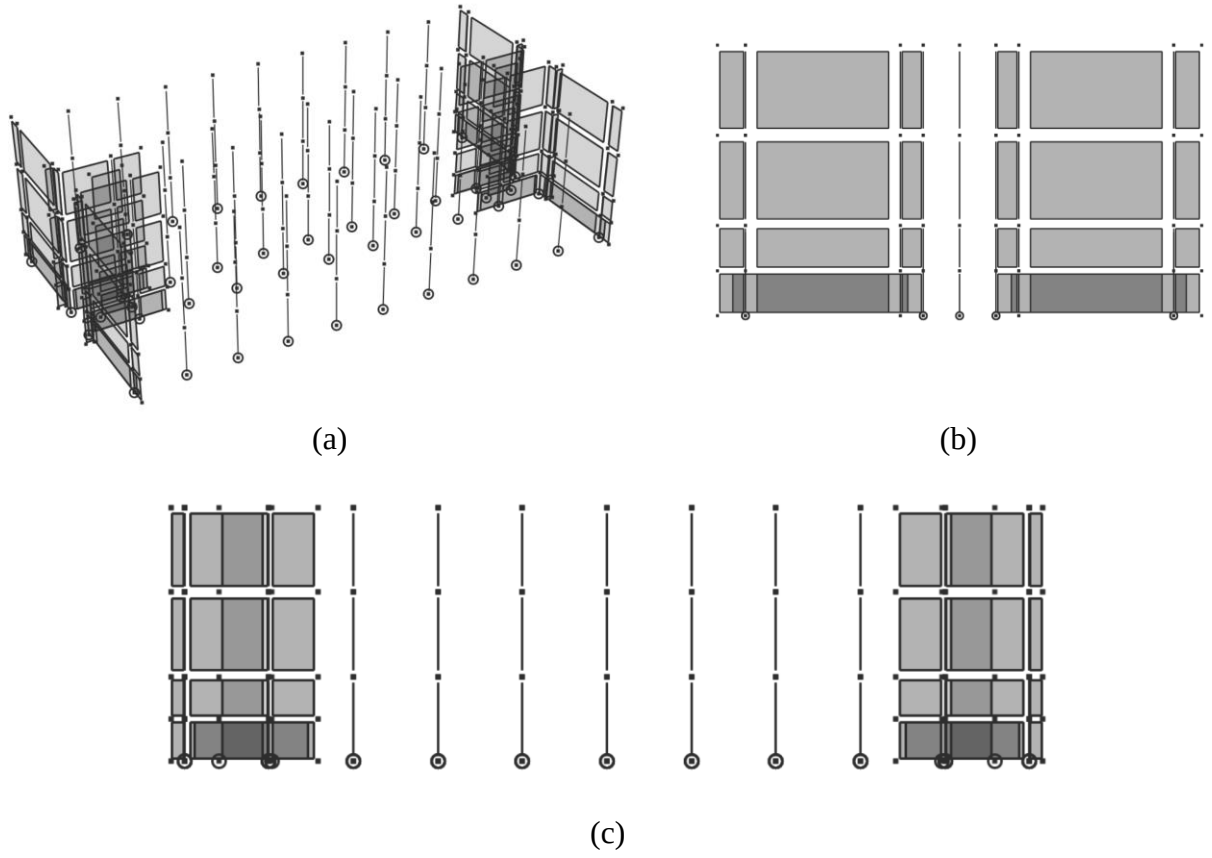

Figure 2-21. Perform3D model: (a) 3D view, (b) N-S elevation (transverse), (c) E-W elevation (longitudinal)

The walls were modeled in Perform3D using the *Shear Wall, Inelastic Section,* and the columns using the *Column, Inelastic Fiber Section*. The wall elements at the first story were divided into two elements along the height, to ensure a proper hinge length, with the upper stories walls modeled the full height. The unconfined and confined concrete were modeled using the *Inelastic 1D Concrete Material*, and were assigned to the walls and columns respectively. The rebar was modeled using the *Inelastic Steel Material, Non-Buckling*. For both concrete and steel materials, strength loss was considered. The parameters used follow the stress-strain relationship

shown in Figure 2-22 and are listed in Table 2-4. Cyclic degradation for the three materials was specified with the following energy factors: 1, 0.4, 0.4, 0.1, 0.1 at points Y, U, L, R, and X respectively, as recommended by Lowes et. al (2018). The shear material was specified as elastic with a shear modulus equal to 0.4 times the elastic modulus.

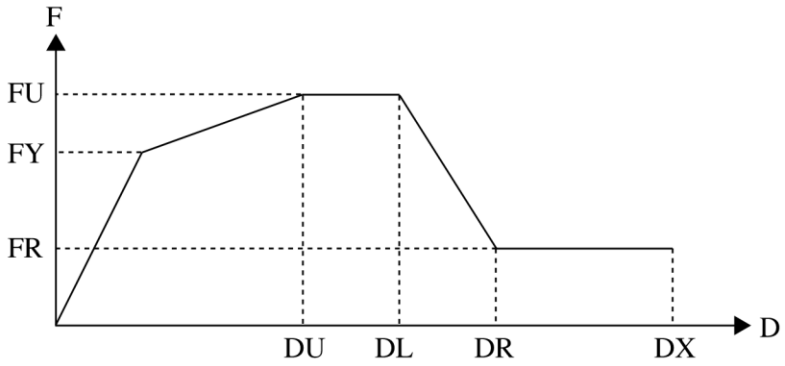

Figure 2-22. Perform-3D: Parameters for concrete stress-strain relationships

Table 2-4. Stress-strain properties

Properties	Unconfined Concrete	Confined Concrete	Steel Rebar
E (ksi)	3491	3694	29000
FY (ksi)	2.25	2.52	41.25
FU (ksi)	3.75	4.2	51.5625
DU	0.0025	0.0035	0.045
DL	0.003	0.004	0.07
DR	0.01	0.035	0.1
DX	0.2	0.2	0.2
FR/FU	0.1	0.2	0.2

2.3.2 Model Validation

An eigenvalue analysis was carried out on the model and the first and second mode periods were estimated to be 0.1936 sec and 0.143 sec in the longitudinal and transverse directions, respectively.

A value of 7.5% damping in the two modes were assigned. The structure was then subjected to the Maricopa EQ in each direction independently. The corresponding ground motions recorded at sensors 13 and 10 were applied to the longitudinal and transverse directions, respectively. Figure 2-23 compares the observed versus simulated roof displacement histories.

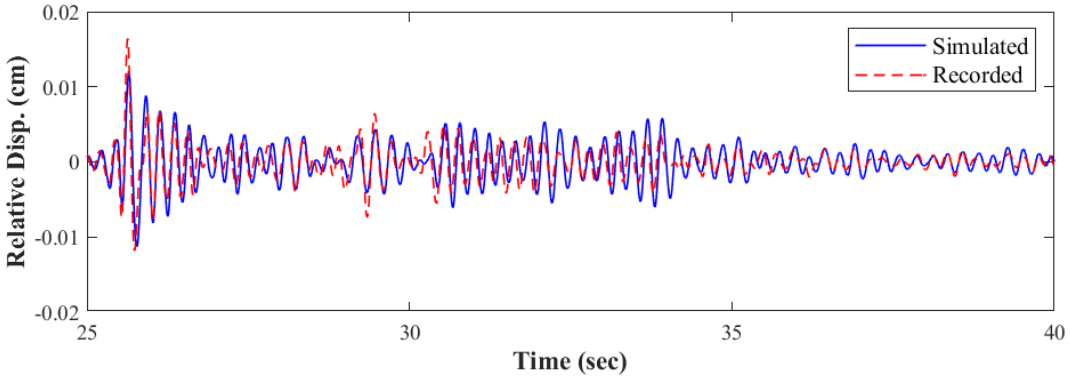

(a)

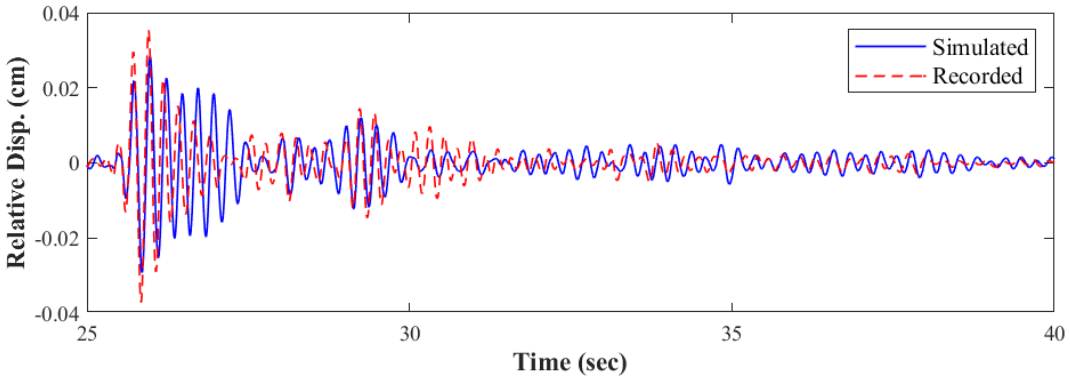

(b)

Figure 2-23. Comparison of Maricopa EQ recorded vs. simulated roof displacement histories: (a) Transverse; (b) Longitudinal direction

2.4 Concrete Building 2

The second concrete structure selected is a 5-story commercial building designed in 1967 and is located in Santa Rosa, California. The gravity system consists of reinforced concrete slabs, supported by girders running in the longitudinal directions, and supported by columns and walls.

The lateral force resisting system is composed of concrete slab diaphragms and shear walls. The north and south shear walls in the longitudinal direction are symmetric. However, the east and west transverse walls differ due to the first-story opening in the west wall, causing a shear wall transfer and a thicker first-story west wall. The wall elevations and a typical floor plan view are shown in Figure 2-24 and Figure 2-25, respectively. The locations of the sensors are shown in Figure 2-26.

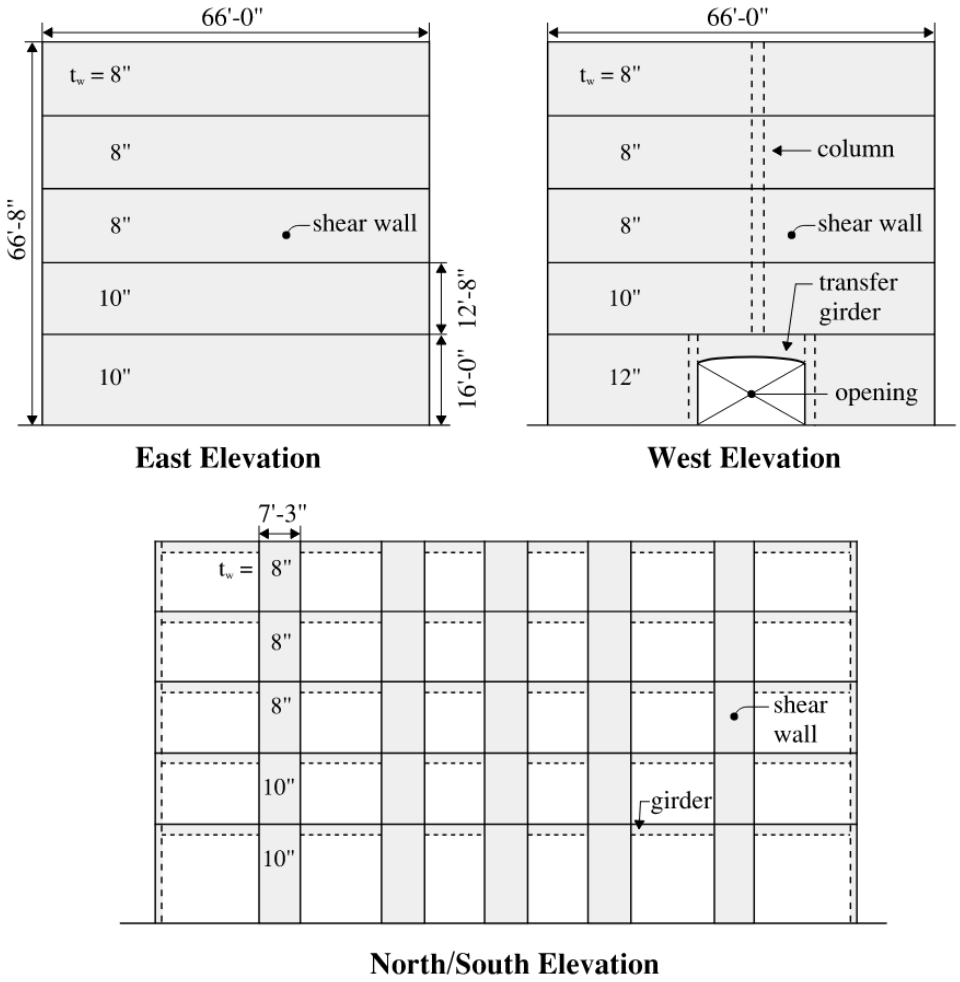

Figure 2-24. Elevation views of shear walls

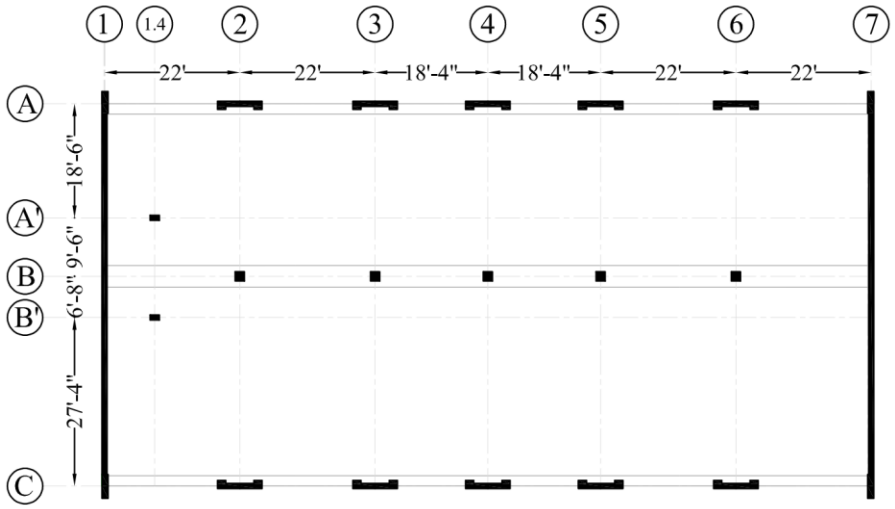

Figure 2-25. Plan view of building at typical floor

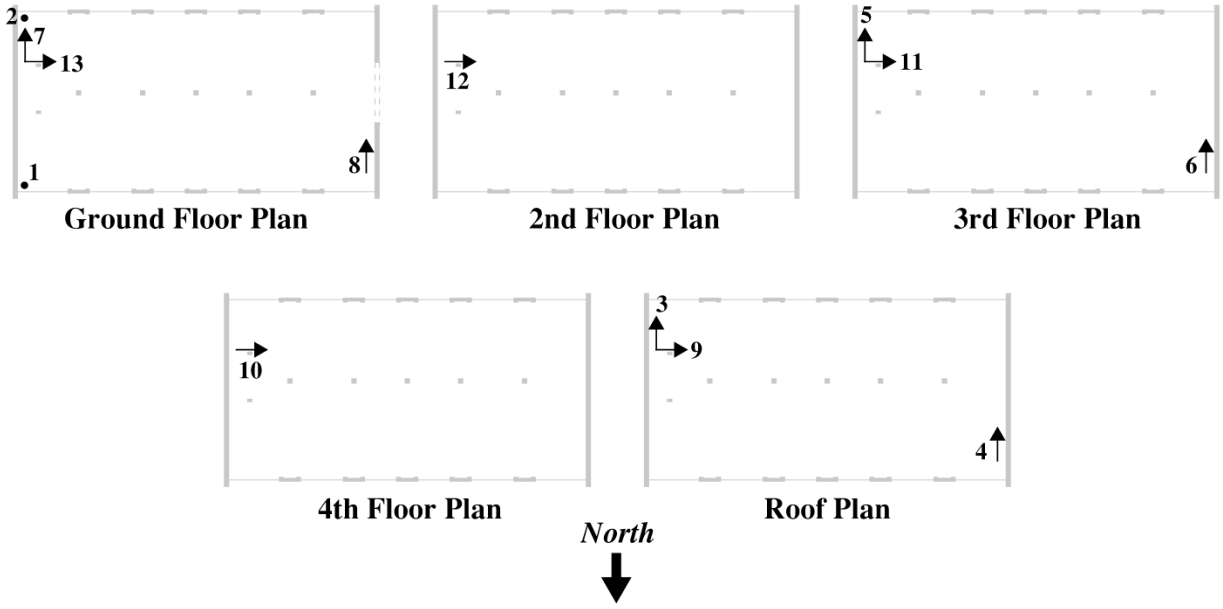

Figure 2-26. Locations of installed sensors

2.4.1 Building Modeling

A 3D model of the building structure was created in Perform3D. Figure 2-27 shows a 3D view of the plan, where the walls, columns, and longitudinal beams are visible. There is a horizontal rigid floor constraint applied at each level, and all base nodes are fixed.

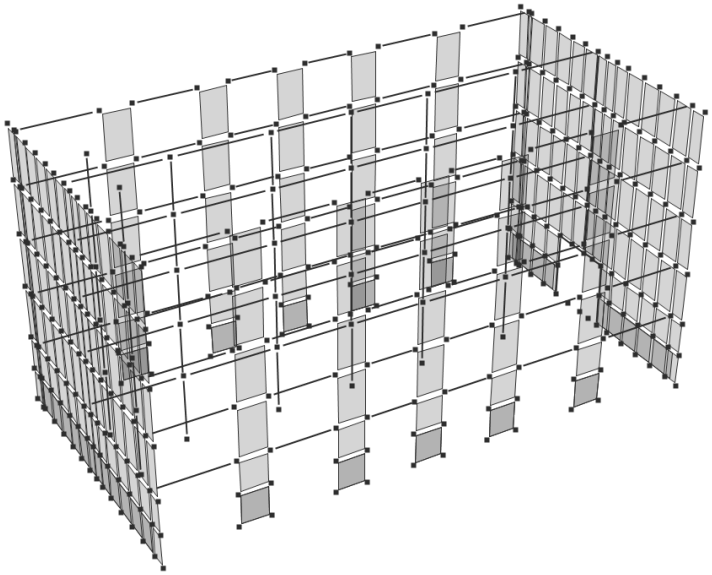

Figure 2-27. 3D view of Perform3D model

In general, the elements used and material behavior assigned are similar to that of the three-story building. However, because of the aspect ratio of the transverse walls, the corresponding shear material was modeled using an inelastic trilinear relationship, as shown in

Figure 2-28. The ultimate stress FU was computed to be 0.34 for the transverse walls, by calculating the shear strength following ACI 318 (2014) and dividing the result by the web area. The final material stress-strain properties of all elements are listed in Table 2-5, while the inelastic shear properties for the transverse walls are listed in Table 2-6.

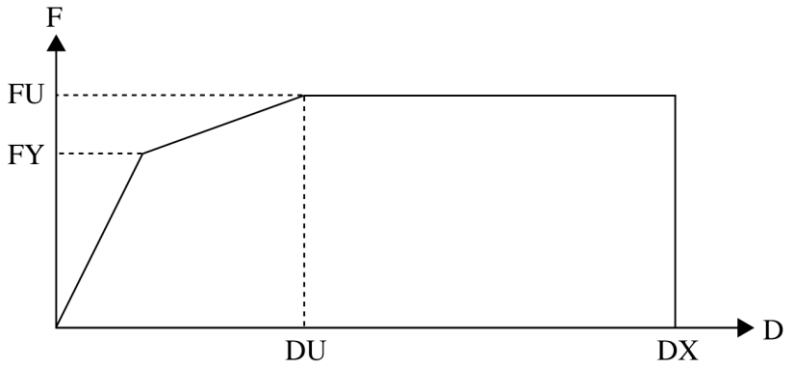

Figure 2-28. Perform3D inelastic shear material relationship

Table 2-5. Strength-strain material parameters

Properties	Unconfined Concrete	Confined Concrete	Steel Rebar
E (ksi)	4189	4433	29000
FY (ksi)	3.24	3.63	50
FU (ksi)	5.4	6.05	62.5
DU	0.0025	0.0035	0.045
DL	0.003	0.004	0.07
DR	0.01	0.035	0.1
DX	0.2	0.2	0.2
FR/FU	0.1	0.2	0.2

Table 2-6. Strength-strain concrete shear parameters (for transverse walls)

Properties	Inelastic Concrete Shear Material
G (ksi)	1529
FY (ksi)	0.26
FU (ksi)	0.34
DU	0.004
DX	0.1

2.4.2 Model Validation

An eigenvalue analysis was completed and the first and second mode periods were estimated to be 0.86 sec and 0.17 sec in the longitudinal and transverse directions, respectively. A value of 7.5% damping in the two modes were assigned. The structure was then subjected to the South Napa EQ in each direction, concurrently. The corresponding ground motions recorded at sensors 13 and 7

were applied to the longitudinal and transverse directions, respectively. Figure 2-29 compares the simulated response using the final calibrated model with the recorded response in each horizontal direction. In the transverse direction, the period and the relative displacement at the roof level match reasonably well. However, in the longitudinal direction, the modeled structure is stiffer than recorded response. It is important to note that the calibration produced a better match when the ground motion component was applied in each direction and the calibration was completed in the same direction, independently. However, for this 3D model, it was essential to apply the ground motions concurrently to represent the true building response under actual ground shaking, and therefore the calibration was completed for the model with both ground motions applied simultaneously. Also, for this building, a goal was to investigate the behavior and modeling of the squat walls for possible shear-controlled behavior. From this perspective, the calibration in the transverse direction was satisfactory.

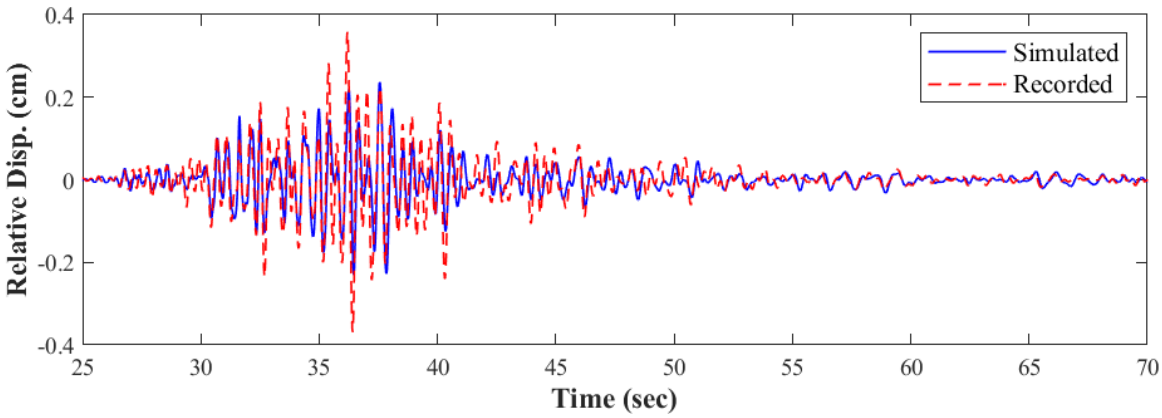

(a)

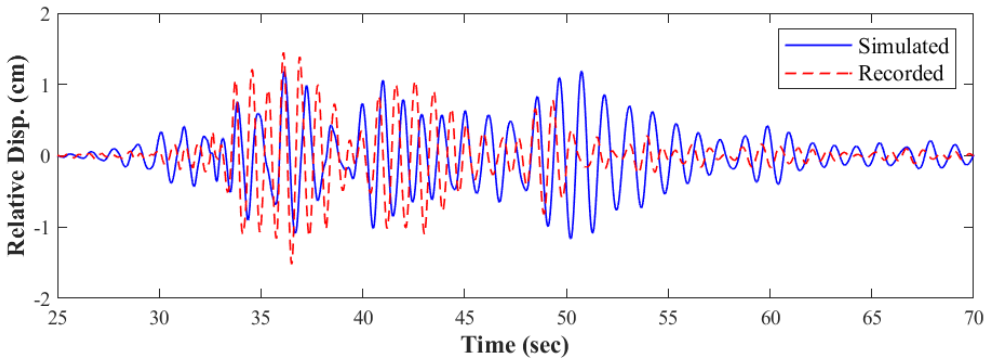

(b)

Figure 2-29. Comparison of South Napa EQ recorded vs. simulated roof displacement histories: (a) Transverse; (b) Longitudinal direction

2.5 Discussion

In order to realistically evaluate the issues mentioned in Chapter 1, it was essential to begin with realistic computer models of the existing buildings. Hence, calibrating the models to observed data was a critical aspect of the proposed evaluation. It was also important to follow the model parameters defined by ASCE 41-17, since the objective of this project was to complete a critical evaluation of the guidelines in the document. The calibration was carried out at both a system and component level. Generally, the response in the recorded data in all buildings showed a constant fundamental period and there was no evidence of yielding/damage, nor was there any documentation of observed damage when the earthquakes occurred. Therefore, the system-level calibration was completed for an elastic response, where the variables adjusted were the mass, nonstructural stiffness, and damping. In order to establish confidence in each model beyond the elastic range, some components (such as the panel zones for the steel buildings, or the shear walls for the concrete buildings) were calibrated to experimental tests so that the component inelastic behavior could be captured as accurately as possible.

For the steel buildings, the beams, columns, and panel zones were modeled to adequately capture the nonlinear behavior of each component. These components were respectively modeled in OpenSees using elastic beam-column elements with inelastic springs at member ends, force-based elements for columns, and a set of elastic beam-column elements with rotational springs. Additionally, at the system level, the effort focused on accurately modeling the structural and nonstructural story stiffness, as well as damping. For the concrete buildings whose responses were controlled by shear walls, a comparative study of modeling approaches was completed for two reinforced concrete wall specimens. The walls were modeled using a total of four distinct modeling schemes in OpenSees and Perform3D. The results show that for the flexure-controlled specimen, the MVLEM and SFI-MVLEM models in OpenSees better captured the initial stiffness and the OpenSees beam-column with fiber-section and Perform-3D shear wall models better predicted the strength, albeit all models produced a reasonable match of the overall cyclic force-deformation response. In the shear-controlled specimen, the SFI-MVLEM produced the best results, capturing the stiffness, strength and pinched response under cyclic loading.

Four existing buildings located in California were selected from the Center for Engineering Strong Motion database, two of which are steel moment frame buildings constructed in 1958 and 1976, respectively, and two reinforced concrete shear wall buildings built in 1948 and 1967, respectively. Two-dimensional models of the exterior moment frames in the steel buildings were created in OpenSees, and three-dimensional models of the concrete buildings were created in Perform3D. The models were validated through comparisons of simulated versus observed time-history of displacement and acceleration at recorded floor levels. Only the results for the roof relative displacement were presented in this chapter. In the case of the steel buildings, the calibrated models produced reasonable estimates of the recorded responses. For the concrete

buildings, both components of the recorded ground motion were applied. The simulated response of the building with L-shaped walls was generally comparable to the recorded response. However, the simulated displacement histories for the 5-story building were unable to reproduce the recorded response, particularly in the longitudinal direction. This can potentially be attributed to the significant difference in the modal periods of the building in each direction.

3 ASCE 41-Based Assessment of Buildings

Seismic performance assessments following the guidelines in ASCE 41-17 were completed by analyzing the validated computer models of the buildings presented in the previous chapter. All four analysis procedures prescribed in ASCE 41 were carried out for each building: the linear static (LSP), linear dynamic (LDP), nonlinear static (NSP), and nonlinear dynamic procedures (NDP). The objective of these analyses are to compare the results between each of the four procedures, in terms on demands as well as designation of the following performance levels: Immediate Occupancy (IO), Life Safety (LS), and Collapse Prevention (CP).

3.1 Assessment of 3-Story Steel Building

The calibrated two-dimensional OpenSees model of the 3-story steel building, presented in Section 2.1, was assessed using all four analysis procedures recommended in ASCE 41. Since the assessment criteria is performed for every component in the system, the notation shown in Figure 3-1 will be used when summarizing the results of the performance assessment. Note that only two typical component notations are shown in the figure – the remaining components will be represented in a similar fashion with different color codes for each column line or bay.

The seismicity considered in the assessment of this building is based on the BSE-2E hazard level, which represents a 5% probability of occurrence in 50 years. The resulting response spectrum for the site based on ASCE 41 provisions is shown in Figure 3-2 with the following parameters: S_{XS} = 1.9 g; S_{X1} =1.25 g; T_o = 0.13 sec and T_s = 0.66 sec.

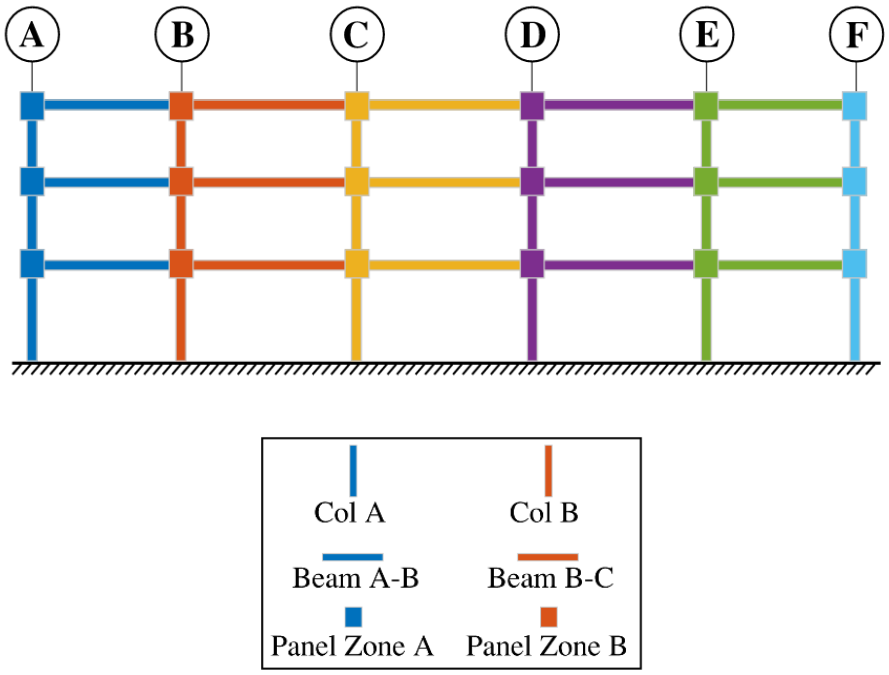

Figure 3-1: Component notation

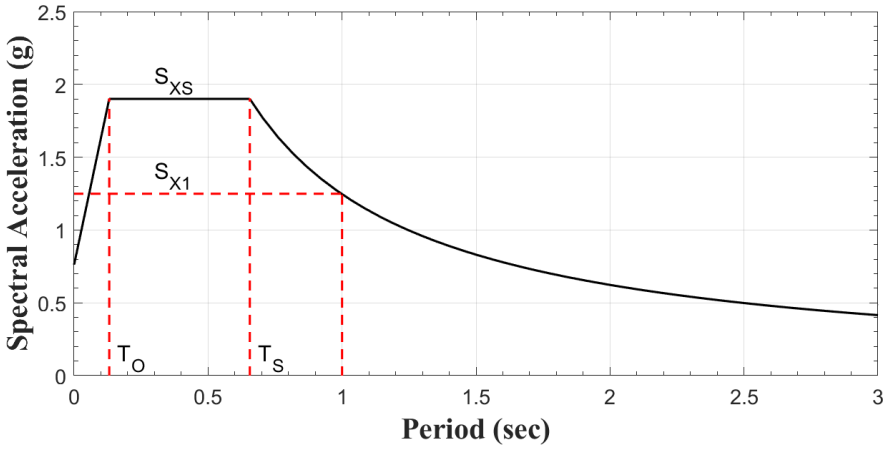

Figure 3-2: Target Response Spectrum

3.1.1 Linear Procedures

The applicability of linear analysis procedures in ASCE 41 is based on four configurations of irregularity defined as follows: (a) *In-Plane Discontinuity Irregularity* if there is a seismic-force-

resisting element in one story but does not continue, or is offset within the plane of the element, in the story immediately below; (b) *Out-of-Plane Discontinuity Irregularity* if there is any primary element of the seismic-force-resisting system where an element in one story is offset out of plane relative to that element in an adjacent story; (c) *Weak Story Irregularity* if the ratio of the average shear DCR for elements in any story to that of an adjacent story in the same direction exceeds 125%; and (d) *Torsional Strength Irregularity* if the diaphragm above the story under consideration is not flexible and, for a given direction, the ratio of the critical element DCR for primary elements on one side of the center of resistance of a story to the critical element DCR on the other side of the center of resistance of the story exceeds 1.5.

None of the above conditions was found to be applicable to the 3-story structure under consideration and hence linear procedures were allowable for the performance-based assesment of the building. For the Linear Static Procedure (LSP), an equivalent static load, representative of the seismic hazard outlined in the previous section, is applied over the height of the building. First, the pseudo lateral force V is calculated by using the following expression provided in ASCE 41:

$$V = C_1 C_2 C_m S_a W \tag{3-1}$$

The modification factors that account for inelastic behavior C_1 and hysterisis characteristics C_2 were both determined to be 1.0, whereas the effective mass factor C_m = 0.9. The spectral acceleration S_a at the fundamental period of the building was obtained from Figure 3-2. The effective seismic weight of the building is 2058 kips and half this value was used to estimate the total lateral load on each perimeter frame. Gravity loads and load combinations were applied as specified in Section 7.2.2 of ASCE 41. Note that ASCE 41 stipulates that mathematical models for use with linear analysis procedures shall include the stiffness and resistance of only the primary components unless the total initial lateral stiffness of secondary components in a building exceeds

25% of the total initial lateral stiffness of primary components. Consequently, the brace elements representing the nonstructural components were removed during the analysis.

All elements were deformation-controlled, hence the maximum moment demands in each element were obtained due to the applied lateral forces and the corresponding demand-to-capacity ratios (DCRs are plotted in Figure 3-3a).

For the Linear Dynamic Procedure (LDP), the assessment was based on the response spectrum method. Considering the first three modes was sufficient to capture at least 90% of the participating mass of the frame. The equivalent static lateral load vector was then determined from:

$$\{p\} = [m]\{\Phi\}\Gamma\ S_a \tag{3-2}$$

where [m] is the lumped mass matrix, $\{\Phi\}$ is the mode shape vector, Γ is the modal participation factor, and S_a is the spectral acceleration at the fundamental period of the frame, obtained from the target response spectrum (Figure 3-2). Peak responses are recorded for each set of lateral loads obtained from Equation (3-2) and the modal demands are combined using the square root sum of squares (SRSS). The DCRs are shown in Figure 3-3b alongside the LSP results.

It is seen that both linear procedures produce very similar DCR values – several beams exceed Life Safety (LS) performance level at the lower two levels whereas the columns exhibited much better performance just exceeding Immediate Occupany (IO) limits at the first floor level. Panel zones exceeded IO performance level at the first story level. The predicted story drifts are comparable for both the static and dynamic methods.

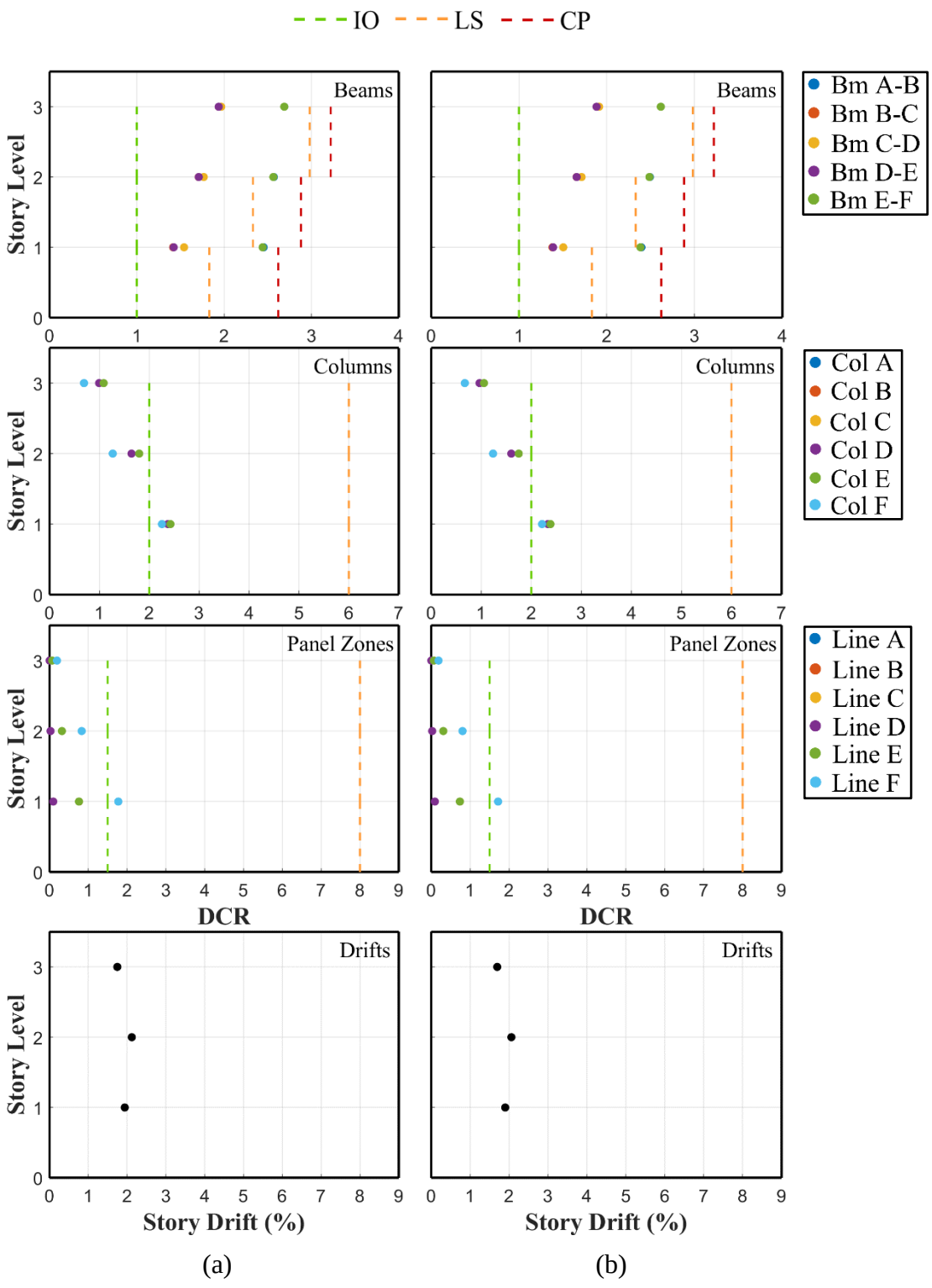

Figure 3-3: Demand-to-capacity ratios for beams/columns/panel zones and resulting interstory drifts from (a) Linear Static and (b) Linear Dynamic Procedures

3.1.2 Nonlinear Procedures

As described previously, nonlinear action in the beams is represented by concentrated springs while columns are modeled using distributed plasticity elements with fiber sections to capture axial force-moment interaction effects. The response of each nonlinear spring is based on the Modified Ibarra-Medina-Krawinkler (I-M-K) model proposed in Ibarra et al. (2005). The transformation of the I-M-K model into the ASCE 41 backbone envelope for use in nonlinear procedures is displayed in Figure 3-4. All parameters shown in Fig. 3-4 are described in the online documentation for OpenSees Version 3.2.2 (2021).

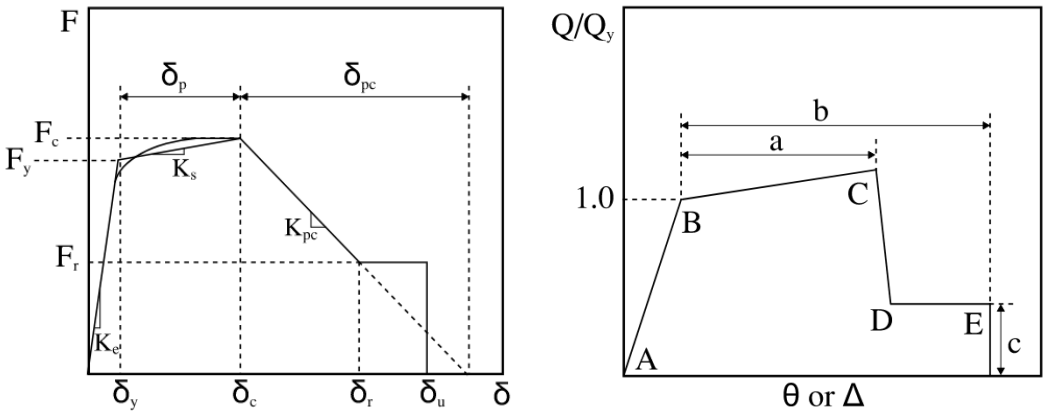

Figure 3-4: Modified Ibarra-Medina-Krawinkler model (left) and transformed backbone parameters (right) used in nonlinear procedures

Nonlinear Static Procedure

For the Nonlinear Static Procedure (NSP), the target displacement δ_t is calculated using:

$$\delta_t = C_0 C_1 C_2 S_a \frac{T_e^2}{4\pi^2} g \tag{3-3}$$

The modification factors that account for the multi to single degree-of-freedom transformation, inelastic behavior, and hysteretic characteristics, respectively, were determined to be: C_0 = 1.3, C_1 = 1.034 and C_2 = 1.002. The effective fundamental period, and consequently the target

displacement, were estimated through an iterative process to establish a converged effective period. The final computed target displacement was 11.28” (corresponding to a roof drift of 2.3 %) and an initial to effective stiffness ratio of 1.24. The inelastic demands in the beams, columns and panel zones at the target displacement are estimated following a pushover analysis of the simulation model using OpenSees. The ductility demands are compared to the ASCE 41 acceptance criteria in Figure 3-9a. Both beams and columns are seen to satisfy Immediate Occupancy whereas panel zones fail the IO criteria.

Nonlinear Dynamic Procedure

The nonlinear dynamic procedure (NDP) involves the selection of ground motions for the performance-based assessment. In order to select ground motions that are representative of the seismic hazard, the site deaggregation, which controls the target spectrum, was examined through the USGS Unified Hazard Tool (2017). After inputting site data such as location, site class, approximate spectral period, and seismic hazard probability, the deaggregation displayed in Figure 3-5 was obtained.

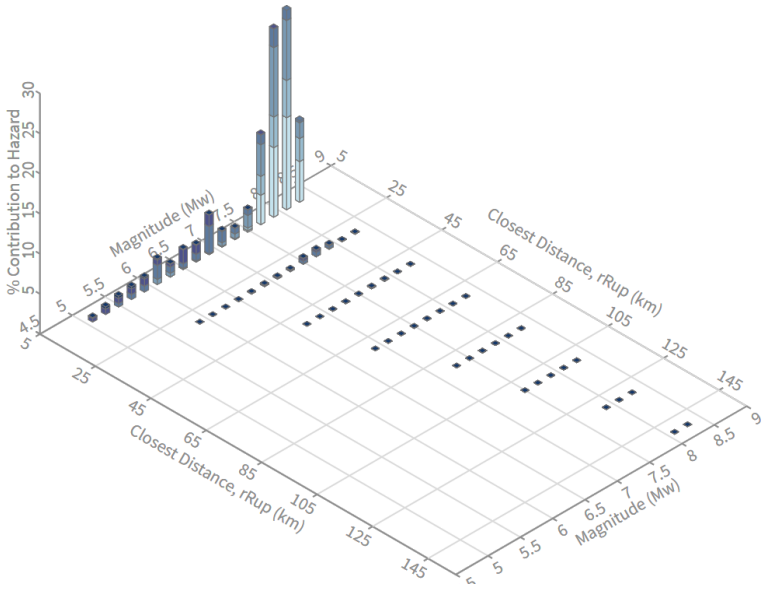

Figure 3-5: Site Deaggregation (USGS)

As evident from the figure, the dominant (mode) moment magnitude is around 8.0 with the closest distance to the rupture surface being around 6 to 8 km. Table 3-1 highlights the contribution of each causative fault to the total deaggregation. It is seen that 45.8% of the contribution comes from the San Jacinto fault while 32.2% arises from the San Andreas fault, totaling 78%. The rest of the data with smaller contributions is not shown in the table. This breakdown will be used in the selection of ground motions for the hazard level at this site. Note that both the San Jacinto and San Andreas faults are strike-slip.

Table 3-1: Deaggregation contributors (USGS, 2017)

Source Set	**rRup**	**M_w**	**%**	**% Sum**
UC33brAvg_FM31 (System)				
San Jacinto (San Bernardino) [4]	0.54	8.01	22.92	38.9
San Andreas (San Bernardino N) [5]	11.27	7.73	11.07	
San Andreas (San Bernardino S) [0]	11.4	6.95	2.79	
San Andreas (North Branch Mill Creek) [0]	10.96	7.97	2.14	
UC33brAvg_FM32 (System)				
San Jacinto (San Bernardino) [4]	0.54	8.01	22.86	39.0
San Andreas (San Bernardino N) [5]	11.27	7.74	11.11	
San Andreas (San Bernardino S) [0]	11.4	6.96	2.81	
San Andreas (North Branch Mill Creek) [0]	10.96	7.98	2.23	

M_w = Moment magnitude, rRup =Distance from rupture surface

It is challenging to find recorded ground motions that satisfy all of the characteristics identified during the deaggregation. Given the objective of the study, priority was placed on selecting ground motions with spectral shape that are similar to the target spectrum within the periods of interest, followed by consideration of near-fault characteristics. A total of 51 ground motions were downloaded from the PEER NGA-West2 ground motion database (Ancheta et al. 2013) with the following filters: fault type: strike slip; magnitude: 6 to 8; distance to rupture: 0 to

12 km; and shear wave velocity Vs30: 180 to 360 m/s. Ground motions with spectral shapes significantly different from the target spectrum were discarded. The final 11 sets of ground motion (pairs) were scaled such that the average maximum direction spectra (RotD100) was at or above 90% of the target response spectrum in the period range $0.2T_1$ – $1.5T_1$. Figure 3-6 shows the RotD100 spectra of the final selection as well as the RotD100 mean, and 90% and 100% of the target response spectrum.

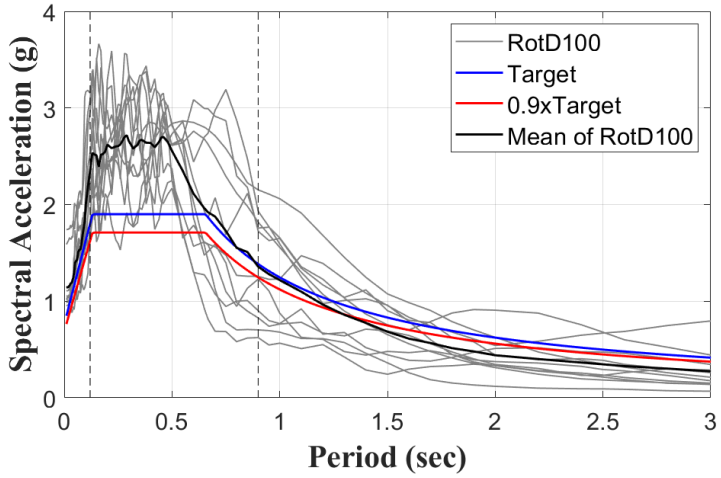

Figure 3-6: Scaled maximum direction spectra of selected ground motions

Given that the site is classified as near-fault, the horizontal components of each selected set were rotated to the fault-normal and fault-parallel directions of the causative fault. The fault closest to the site is the San Jacinto fault, hence this fault angle was used as the reference for rotating the ground motions. Figure 3-7 shows a sample rotation for one set of ground motions, where the original components downloaded were rotated 180° and 270° with respect to the true north azimuth.

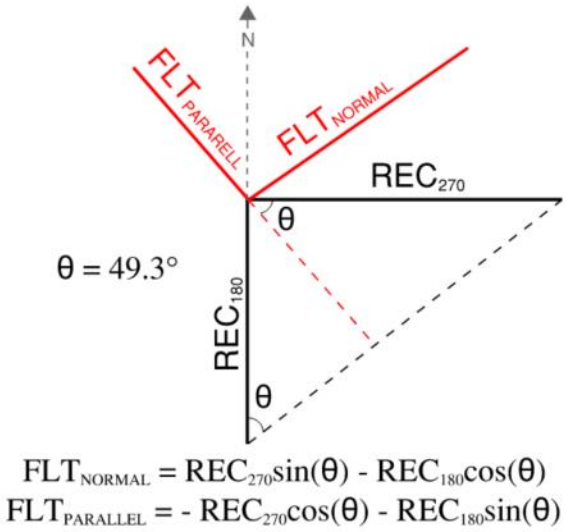

Figure 3-7: Rotating ground motion components to fault normal and parallel

All other sets were also rotated with respect to both their original orientation and the fault angle. ASCE 41-17 does not provide specific guidance on ground motion selection for 2D analysis. Therefore, the following procedure was implemented: for each ground motion set already rotated in the fault parallel and normal orientations, the base motions and their spectra in each direction were compared; the motion with a larger evident pulse in the time history or a larger spectral value within the target period range was selected. A additional scale factor of 1.1 was necessary to ensure that the actually applied ground motions had a mean spectra that was equal to or above 90% of the target spetrum in the required period range. Figure 3-8 shows the final ground motion spectra and Table 3-2 summarizes essential details of the selected records.

Nonlinear simulations of the calibrated numerical model were carried out using OpenSees for each of the eleven ground motions, and mean values of the plastic rotations in the beams and columns at each end of the element as well as the panel zone distortions were determined. Results are presented in Figure 3 9b alongside the estimates from NSP.

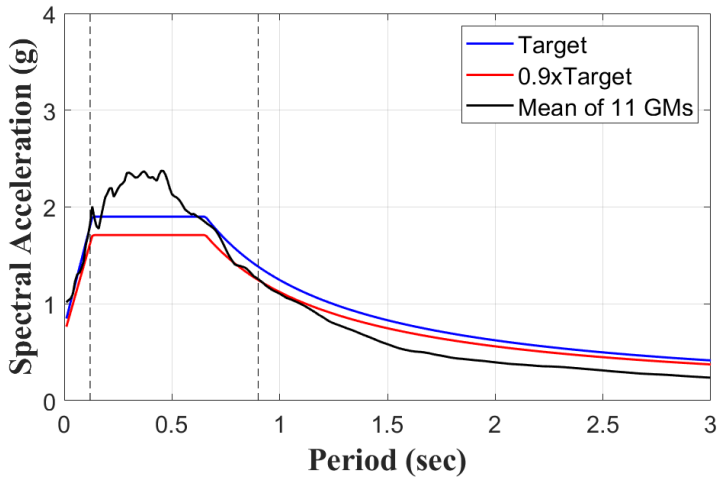

Figure 3-8: Mean spectra of the selected rotated ground motion components and comparison to target spectrum at site

Using the average demands from all 11 ground motions as per ASCE 41, all beams and columns satisfy the Immediate Occupancy Limit (IO) and most panel zones fail the IO limit, but all satisfy the Life Safety (LS)/Collapse Prevention (CP) limit, for both NSP and NDP. Therefore the system can be classified as satisfying the LS performance level. However, if the maximum demand from any of the ground motions is considered, beams and panel zones exceed the CP limit, while the columns exceed the IO limit.

Two interesting observations arise from these findings: first, the assessment using linear procedures resulted in a more conservative assessment of the building performance since both linear methods concluded that the system would fail Life Safety limits whereas both nonlinear procedures indicate that the building will satisfy acceptance criteria for this limit state; and next, the choice of ground motions may play an important role in the assessment when using NDP because the maximum demands from one or more earthquakes may be significantly larger than the mean demand estimate. An additional observation from the nonlinear procedures is that the drift

profiles are different for the two methods – the static procedure indicates maximum demands at the 1st story level whereas the dynamic procedure results in peak demands at the 3rd story level.

Table 3-2: Details of selected ground motions

GM #	Record #	Earthquake Name	Year	Station Name	M	R_{rup} (km)
1	6	Imperial Valley-02	1940	El Centro Array #9	6.95	6.1
2	30	Parkfield	1966	Cholame-Shandon Array #5	6.19	9.6
3	95	Managua_-Nicaragua-01	1972	Managua_ ESSO	6.24	4.1
4	162	Imperial Valley-06	1979	Calexico Fire Station	6.53	10.5
5	165	Imperial Valley-06	1979	Chihuahua	6.53	7.3
6	185	Imperial Valley-06	1979	Holtville Post Office	6.53	7.5
7	558	Chalfant Valley-02	1986	Zack Brothers Ranch	6.19	7.6
8	725	Superstition Hills-02	1987	Poe Road (temp)	6.54	11.2
9	4098	Parkfield-02_ CA	2004	Parkfield - Cholame 1E	6.00	3.0
10	4102	Parkfield-02_ CA	2004	Parkfield - Cholame 3W	6.00	3.6
11	4108	Parkfield-02_ CA	2004	Parkfield - Fault Zone 3	6.00	2.7

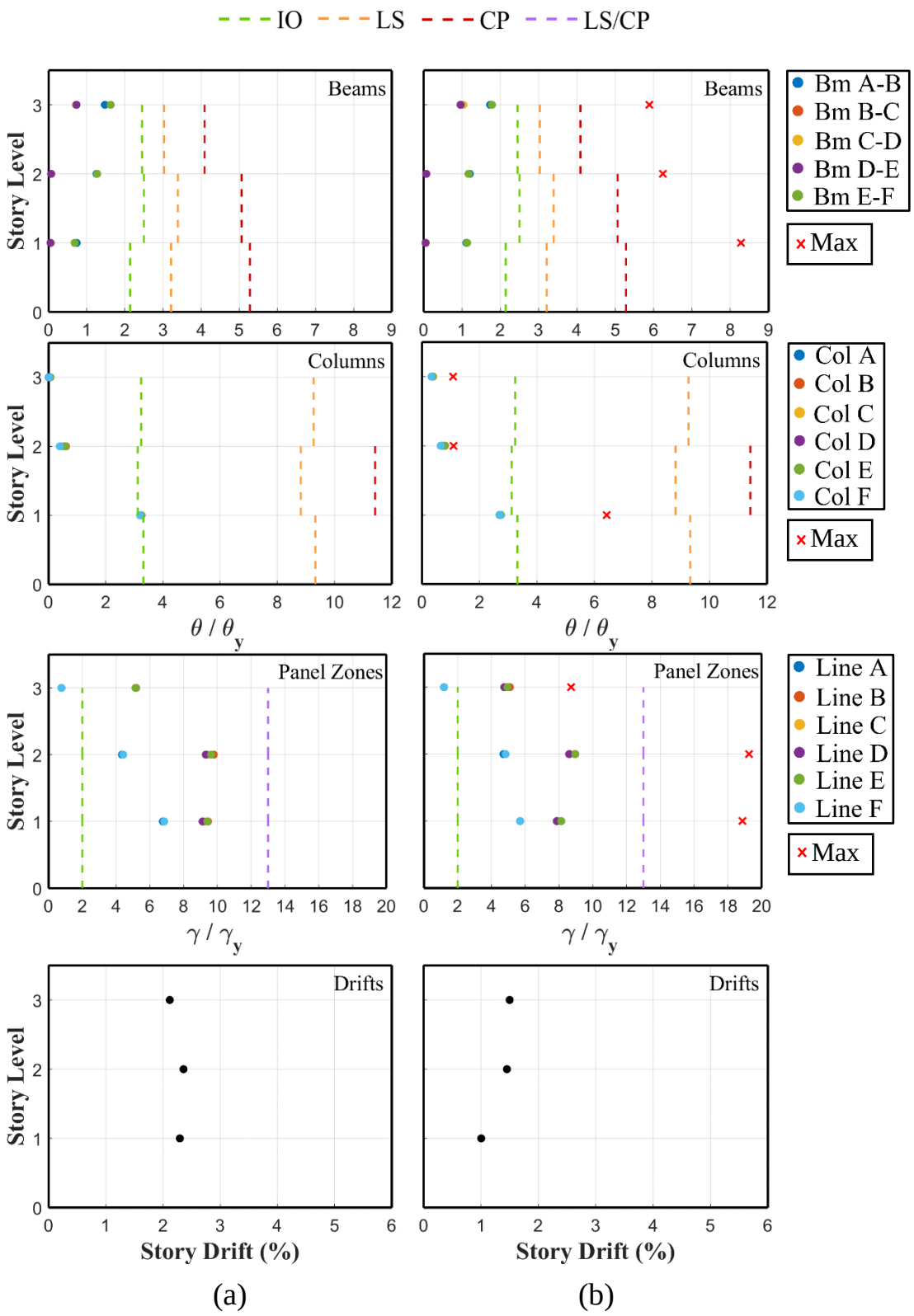

Figure 3-9: Inelastic demands in beams/columns/panel zones and interstory drifts from (a) Nonlinear Static Procedure and (b) Nonlinear Dynamic Procedure

3.2 Assessment of 6-Story Steel Building

The calibrated two-dimensional OpenSees model of the 6-story steel building, presented in Section 2.2, was assessed using all four analysis procedures recommended in ASCE 41. Since the assessment criteria is performed for every component in the system, the notation shown in Figure 3-10 will be used in presenting the results of the performance assessment. The response spectrum for the site corresponding to the BSE-2E hazard level is shown in Figure 3-2 with the following key parameters: S_{XS} = 1.55 g; S_{X1} =0.96 g; T_o = 0.12 sec and T_s = 0.62 sec.

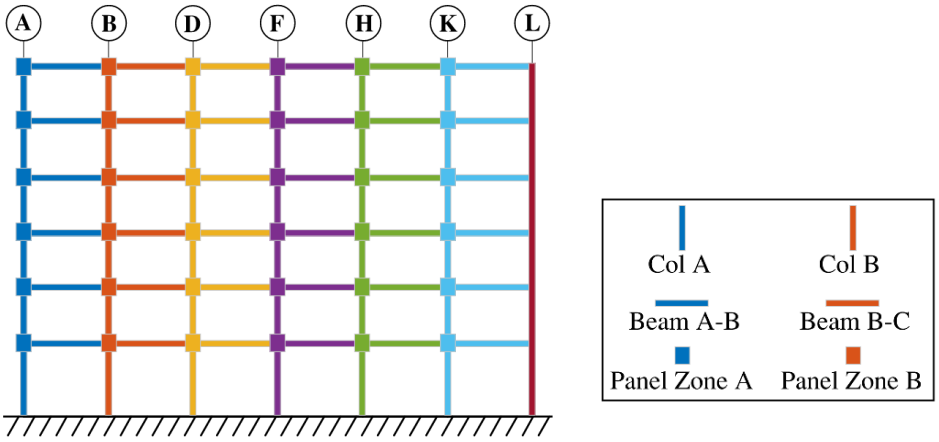

Figure 3-10: Component notation

3.2.1 Linear Procedures

The applicability of linear analysis procedures in ASCE 41, as described previously in Section 3.1.1, for the assessment of the building was first checked. Any irregularities arising from considerations of in-plane discontinuity, out-of-plane discontinuity, weak-story irregularity and torsional strength irregularity were evaluated and found not to be applicable for the building.

For the Linear Static Procedure (LSP), the values used for the modification factors C_1 and C_2 were 1.0 and the parameter C_m was determined to be 0.9 for the 6-story frame. The spectral acceleration S_a obtained from the response spectrum shown in Figure 3-2 was 0.6314 g. The effective seismic weight of the building is 8262 kips and half this value was used to estimate the total lateral load on the perimeter frame.

For the Linear Dynamic Procedure (LDP), the response spectrum method was once again used for the building assessment. It should be noted that the LDP analysis was also carried out using SAP2000 for the 2D frame, producing similar results.

The resulting demand-to-capacity ratios for LSP and LDP are shown in Figure 3-11a and Figure 3-11b, respectively. As observed from the plotted results, both linear procedures produce similar DCR values as well as interstory drifts. Several beams on the lower floors are seen to exceed Collapse Prevention (CP) limits. LSP results in a slightly more conservative assessment than the LDP procedure. In terms of the performance of columns, both procedures produce almost similar DCR values across the building height. In the case of panel zones, an assessment using LSP indicates that LS limits are exceeded on the first floor whereas LDP results are less conservative with panel zones passing LS limits.

Overall, as per component-based ASCE 41 acceptance criteria, this building would clearly fail to satisfy the Collapse Prevention (CP) requirements.

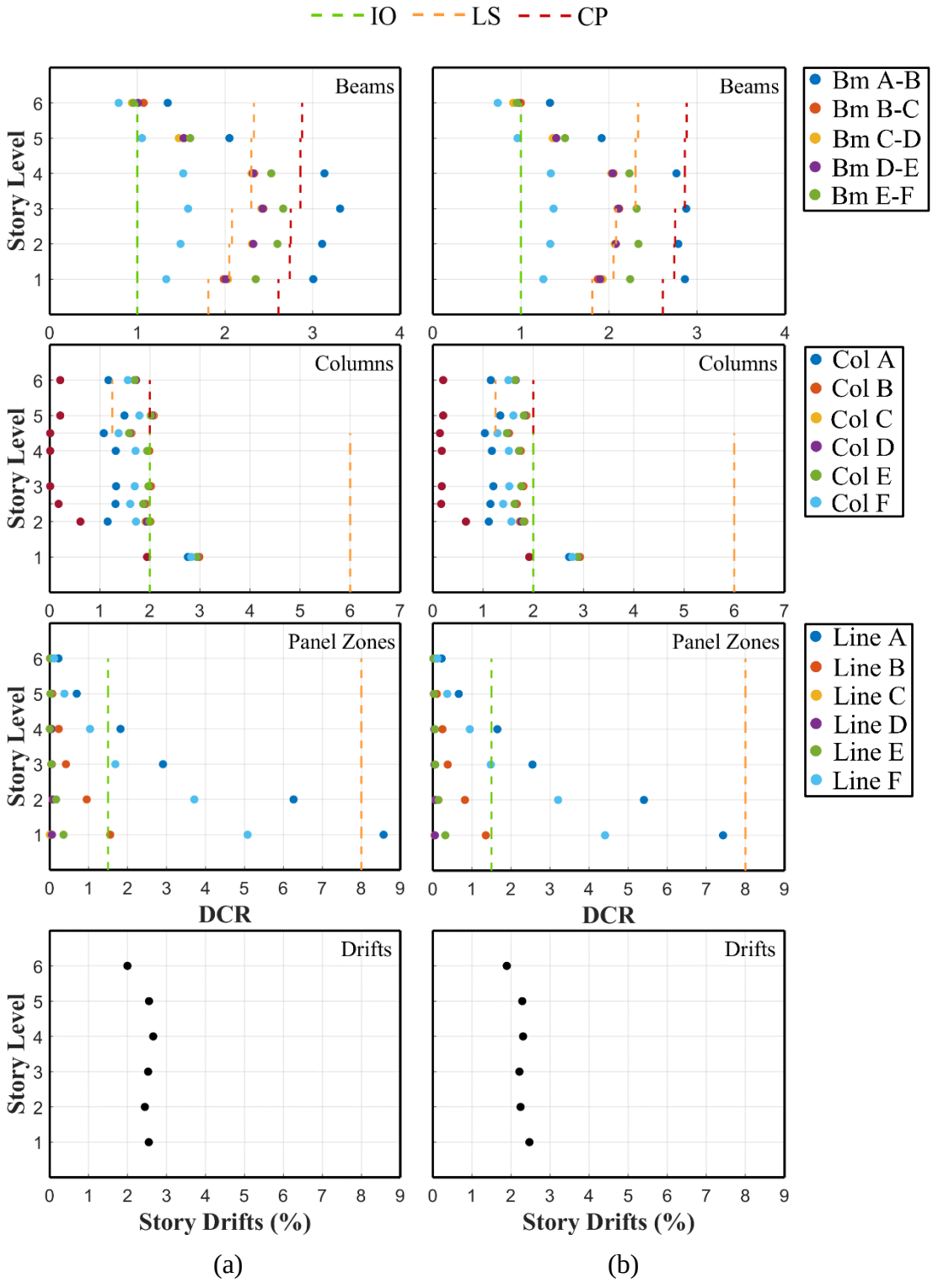

Figure 3-11: Demand-to-capacity ratios for beams/columns/panel zones and interstory drifts from (a) Linear Static Procedure; (b) Linear Dynamic Procedure

3.2.2 Nonlinear Procedures

As in the case of the 3-story frame, nonlinear action in the beams is represented by concentrated springs while columns are modeled using distributed plasticity elements with fiber sections to capture axial force-moment interaction effects. The response of each nonlinear spring is based on the I-M-K model with a backbone envelope developed as shown previously in Figure 3-4.

Nonlinear Static Procedure

For the Nonlinear Static Procedure (NSP), the values used for the modification factors C_0, C_1, and C_2 were 1.42, 1.011, and 1.002 respectively. The computed target displacement was 29.3" (corresponding to a roof drift of 3.0%) and an initial to effective stiffness ratio of 1.43. The model was pushed to the target displacement and component acceptance criteria were assessed. The results, depicted in Figure 3-14a, show that the first story beams and columns exceeded LS and IO, respectively, while the panel zones at the first, second, and third story exceed the LS/CP limit. Note that for the nonlinear procedures, the acceptance limits for both LS and CP were identical for panel zones. The largest drift (~ 3.5%) occurred on the first floor of the frame and peak drifts gradually decreased from the lower to the upper floors.

Nonlinear Dynamic Procedure

A new set of ground motions had to be selected since the site characteristics were different for this building compared to the 3-story building that was assessed in the previous section. Once again, the deaggregation at this site was obtained using the USGS Unified Hazard Tool. The major faults contibuting to the hazard at the site are shown in Table 3-3. Since two different fault types contribute to the hazard, the following search parameters were applied for the selection of the ground motions: (1) fault type: strike slip; magnitude: 6 to 9; distance to rupture: 20 to 50 km, and

(2) fault type: reverse; magnitude: 6.5 to 8.5; distance to rupture: 3 to 15 km. For both sets, the range of the soil shear wave velocity Vs30 was specified as 180 to 360 m/s. Eventually, a total of 11 ground motion pairs were downloaded from the PEER NGA-West2 ground motion database (Ancheta et al. 2013).

Table 3-3: Deaggregation Contributors (USGS, 2017)

Source Set	**rRup**	**M_w**	**%**	**% Sum**
UC33brAvg_FM32 (System)				
San Andreas (Mojave S)	44.52	8.05	8.44	29.21
Hollywood	7.62	7.11	7.00	
Sierra Madre	9.55	7.72	5.24	
Santa Monica alt 2	6.71	7.47	4.35	
Verdugo	3.25	7.52	4.18	
UC33brAvg_FM31 (System)				
San Andreas (Mojave S)	44.52	8.06	8.44	28.68
Hollywood	7.62	7.33	6.80	
Sierra Madre	9.55	7.69	5.34	
Verdugo	3.25	7.55	4.83	
Elysian Park (Upper)	8.29	6.76	3.27	

M_w = moment magnitude, rRup =distance from rupture surface

The 11 ground motion pairs were scaled such that the average maximum direction spectra (RotD100) was at or above 90% of the target response spectrum in the period range $0.2T_1 – 1.5T_1$, as show in Figure 3-12. The ground motions were then rotated to the fault-normal and fault-parallel directions of the Verdugo fault which was the closest fault to the site. Similar to procedure used for the 3-story frame, one of the components from each ground motion set was selected for the 2D frame analysis. A additional scale factor of 1.1 was applied so that the mean spectra of the final

selected ground motion components was above 90% of the target spectrum in the required period range. Figure 3-13 shows the final ground motion spectra and Table 3-4 summarizes essential details of the selected record sets.

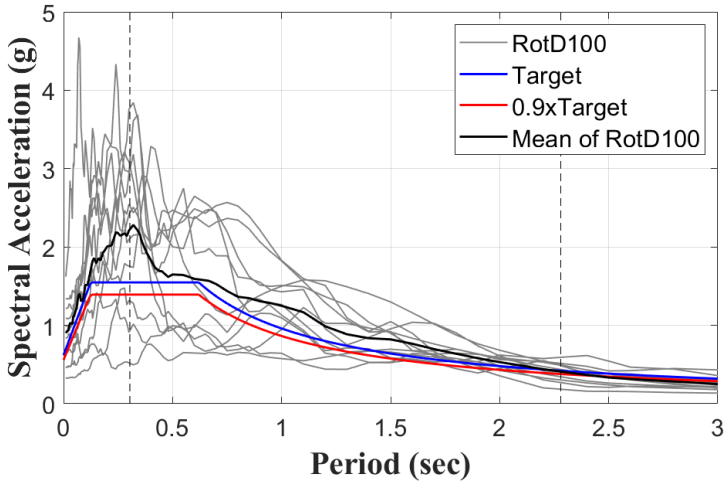

Figure 3-12: Maximum direction spectra of scaled motions and comparison of mean spectrum with target spectrum at site

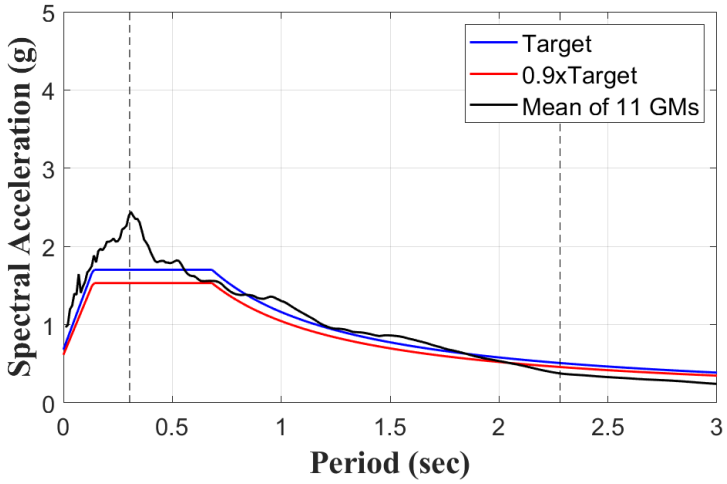

Figure 3-13: Mean spectra of the selected rotated ground motion components and comparison to target spectrum at site

Table 3-4: Selected ground motions

GM #	Record Sequence Number	Earthquake Name	Year	Station Name	Mag	R_{rup} (km)
1	126	Gazli_ USSR	1976	Karakyr	6.80	5.46
2	764	Loma Prieta	1989	Gilroy - Historic Bldg.	6.93	10.97
3	949	Northridge-01	1994	Arleta - Nordhoff Fire Sta	6.69	3.30
4	960	Northridge-01	1994	Canyon Country - W Lost Cany	6.69	11.39
5	1044	Northridge-01	1994	Newhall - Fire Sta	6.69	3.16
6	1491	Chi-Chi_ Taiwan	1999	TCU051	7.62	7.64
7	4210	Niigata_ Japan	2004	NIG020	6.63	7.45
8	4458	Montenegro Yugoslavia	1979	Ulcinj - Hotel Olimpic	7.10	3.97
9	1082	Northridge-01	1994	Sun Valley - Roscoe Blvd	6.69	5.59
10	20	Northern Calif-03	1954	Ferndale City Hall	6.50	27.02
11	850	Landers	1992	Desert Hot Springs	7.28	21.78

For the Nonlinear Dynamic Procedure (NDP), the model was subjected to the eleven ground motions, and the mean values of the component demands were used to assess compliance with the acceptance limits for each performance level. The mean and maximum demands for each component are plotted in Figure 3-14b. The results show that the mean demands for all beams and columns satisfy the Immediate Occupancy (IO) limits. The panel zones fail to satisfy IO, but satisfy the LS/CP performance level. Therefore, the structure can be classified as satisfying Life Safety as per the NDP results. However, when observing the results from the maximum demands at each story level, the panel zones exceed LS/CP limits at the third and higher floors.

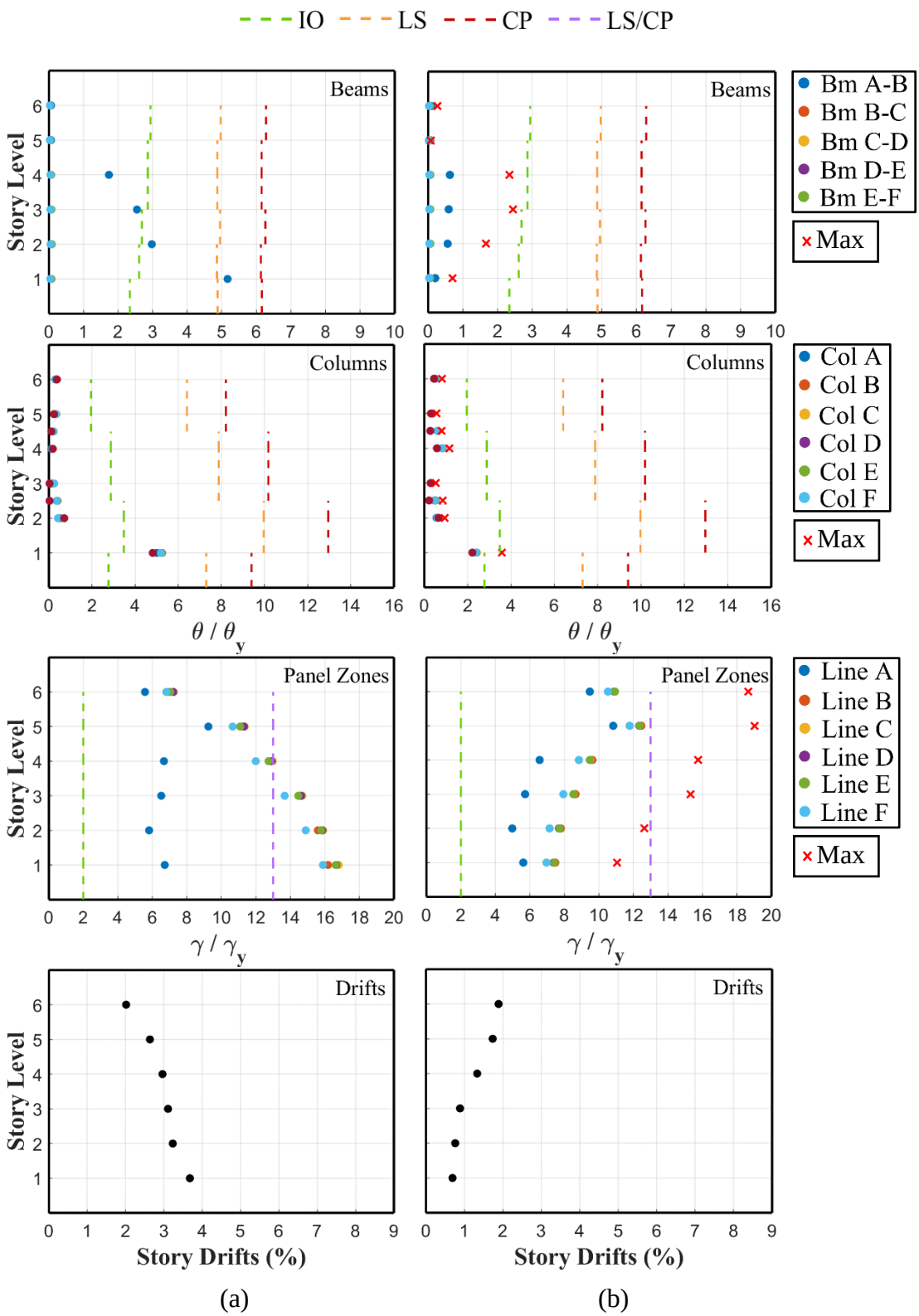

Figure 3-14: Inelastic demands in beams/columns/panel zones and interstory drifts from (a) Nonlinear Static Procedure and (b) Nonlinear Dynamic Procedure

This indicates that GM selection can play a role when using NDP. Finally, when comparing NSP and NDP results, it is evident that NSP seems to be underestimating the demands in the upper stories, as opposed to the 3-story building where the demands were similar for both nonlinear procedures. This finding is also confirmed in the study by Harris and Speicher (2018), where it is reported that higher mode contributions are more significant for taller buildings.

3.3 Assessment of 3-Story Concrete Building

A seismic performance assessment of the building was carried out by analyzing the validated computer model of the 3D building and using both linear and nonlinear analysis procedures prescribed in ASCE 41. Note that in all procedures described hereafter, the lateral load application is preceded by the application of the sustained gravity loads on the building. The seismicity considered in the assessment is based on the BSE-2E hazard level, which represents a 5% probability of occurrence in 50 years. The resulting response spectrum, shown in Figure 3-2, for this site has the following key parameters: S_{XS} = 1.23 g; S_{X1} = 0.873 g; T_O = 0.14 sec and T_S = 0.71 sec.

3.3.1 Linear Procedures

The applicability of linear analysis procedures in ASCE 41, as described previously in Section 3.1.1, for the assessment of the building was first checked and no irreguralities were found to be applicable to this building.

For the linear procedures, the Perform3D model described earlier was used. However, the concrete and rebar steel materials were replaced with linear elastic material behavior. For the

Linear Static Procedure (LSP), an equivalent static load, representative of the seismic hazard, is applied over the height of the building, in each horizontal direction independently. The modification factors are C_1C_2= 1.0 and C_m = 0.8. The effective seismic weight is 5858 kips for the full building. For the Linear Dynamic Procedure (LDP), the assessment was completed by using the Response Spectrum load case type in Perform3D, ensuring that the modes considered captured at least 90% of the participating mass of the building. For both linear procedures, the demands in the components were obtained by applying the 100%-30% and 30%-100% combination rule.

Independently of the LSP and LDP analysis, it was important to accurately obtain the capacity of the walls, particularly because of the L-shape. Therefore the original nonlinear model was pushed in the transverse and longitudinal directions, and the corresponding pushover curves were plotted for each wall to obtain the respective yield capacities. Since both segments of the L-shaped walls act conjointly, the shear and moment capacity was obtained for each L-wall considering both horizontal segments.

Figure 3-15 shows the results from the pushover analyses. Notice that when pushing the structure in one direction, the orientation of the L-wall played a major role. For instance, in the transverse direction, the north walls have a larger capacity because the L-wall is pushed in the strong direction, whereas the south walls are pushed in the weak direction. Therefore, even though the walls are symmetric from a global perspective, the direction of loading will have an impact on which capacity to consider when calculating the demand-to-capacity ratios (DCRs).

The walls have been identified in Figure 3-16. The final results for the linear procedures are listed in Table 3-5, and visually presented in Figure 3-17. Note that the tabular results list the values when the forces are applied in the positive transverse and longitudinal direction only. However, the analysis was repeated in the respective negative directions, and the results were

mirrored. Also note that LDP using a response spectrum only provides the maximum forces in the L-walls, therefore only the walls in the strong direction were compared. The LSP and LDP results are consistent, where all L-shaped walls exceed CP. Additionally, the LSP results produced maximum story drifts of 0.11% (at 2nd story) and 0.07% (at 1st story) in the longitudinal and transverse directions, respectively, and LDP produced 0.19% and 0.14% in the same respective stories and directions.

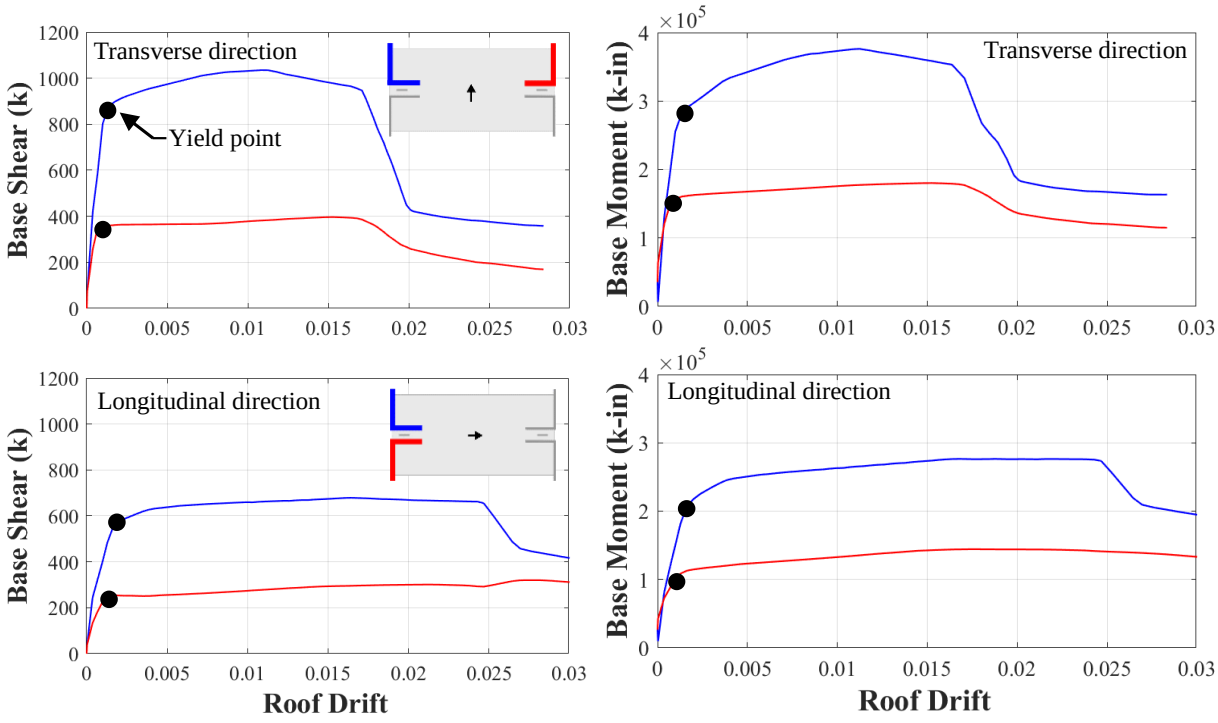

Figure 3-15. Pushover analyses to establish base shear and moment capacities of the L-shaped walls in transverse and longitudinal directions

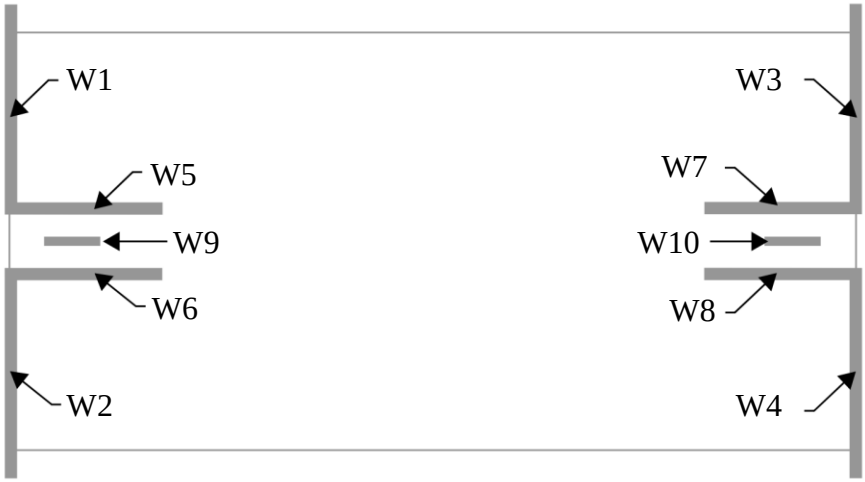

Figure 3-16. Wall identification plan view

Table 3-5: LSP and LDP results

	Wall #	Capacities		LSP			LDP			ASCE -41 m-Factors		
				Demands		Max DCR	Demands		Max DCR	IO	LS	CP
		V (k)	M (k-ft)	V (k)	M (k-ft)		V (k)	M (k-ft)				
Trans	W1_W5	876	282420	1417	641355	2.3	2644	1125433	4.0	2	3	4
	W2_W6	349	147060	1417	717045	4.9				2	3	4
	W3_W7	876	282420	1417	618648	2.2	2644	1125433	4.0	2	3	4
	W4_W8	349	147060	1417	694338	4.7				2	3	4
Long	W1_W5	548	224890	1234	594753	2.6	2187	1030340	4.6	2	3	4
	W2_W6	548	224890	1234	578389	2.6	2187	1030340	4.6	2	3	4
	W3_W7	249	108730	1224	649313	6.0				2	3	4
	W4_W8	249	108730	1224	632949	5.8				2	3	4

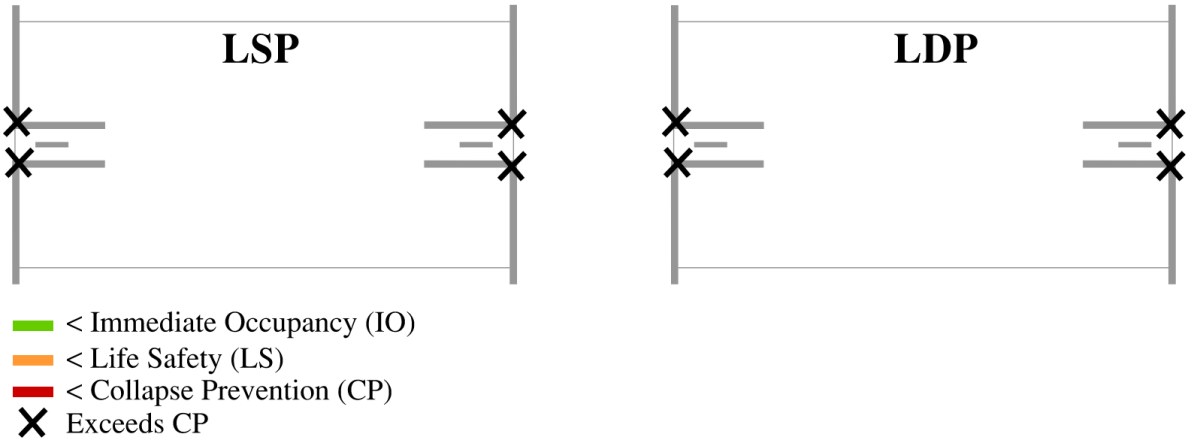

Figure 3-17. LSP and LDP performance level designation

3.3.2 Nonlinear Procedures

For the nonlinear procedures, the original nonlinear model was used in the analyses. For the Nonlinear Static Procedure (NSP), the building was pushed to the target displacements of 7.16 in (0.0124 drift) and 4.10 in (0.0071 drift) in the longitudinal and transverse directions, respectively. The maximum demands between the two directions were used in the assessment.

For the Nonlinear Dynamic Procedure (NDP), the United States Geological Survey (2017) Unified Hazard Tool was utilized for the site deaggregation. The seismic hazard at the site is controlled by the San Andreas fault. A total of 51 ground motions were downloaded from the PEER NGA ground motion database (ngawest2.berkeley.edu) with the following filters: fault type: strike slip; magnitude: 6 to 8; distance to rupture: 5 to 25; and shear wave velocity Vs30: 200 to 400 m/s, based on the controlling seismic hazard at the site. Ground motions with spectral shapes significantly different from the target spectrum were discarded. The final 11 sets of ground motion (pairs) were selected such that the average maximum direction spectra (RotD100) was at or above 90% of the target response spectrum in the period range 0.2T1 – 1.5T1. Even though the site is classified as near-fault, the horizontal components of each selected ground motion were not rotated to the fault-normal and fault-parallel directions of the causative fault. Figure 3-18 shows the selected records spectral accelerations, and Table 3-6 lists the details.

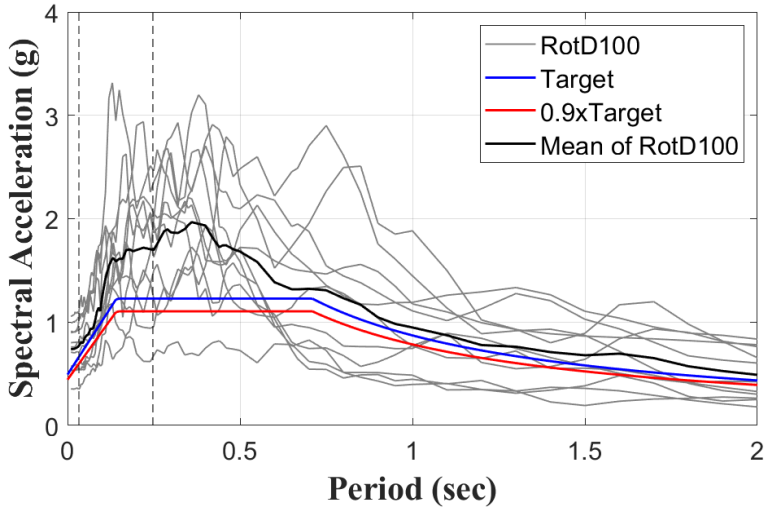

Figure 3-18. Maximum direction spectra of scaled motions, mean spectra, and site target spectrum

Table 3-6: Selected ground motions

GM #	Record Sequence Number	Earthquake Name	Year	Station Name	Magnitude	R_{rup} (km)
1	30	Parkfield	1966	Cholame - Shandon Array #5	6.19	9.58
2	162	Imperial Valley-06	1979	Calexico Fire Station	6.53	10.45
3	169	Imperial Valley-06	1979	Delta	6.53	22.03
4	179	Imperial Valley-06	1979	El Centro Array #4	6.53	7.05
5	184	Imperial Valley-06	1979	El Centro Differential Array	6.53	5.09
6	185	Imperial Valley-06	1979	Holtville Post Office	6.53	7.5
7	558	Chalfant Valley-02	1986	Zack Brothers Ranch	6.19	7.58
8	1101	Kobe_ Japan	1995	Amagasaki	6.9	11.34
9	1107	Kobe_ Japan	1995	Kakogawa	6.9	22.5
10	1158	Kocaeli_ Turkey	1999	Duzce	7.51	15.37
11	1605	Duzce_ Turkey	1999	Duzce	7.14	6.58

For each ground motion set, the horizontal components were applied concurrently to the model, and then again applied but with the directions switched. The maximum demands for each set were calculated and then used in the average demands of the eleven ground motion sets. Table

3-7 lists the results for both nonlinear procedures and Figure 3-19 shows the performance level compliance. The results show that all walls satisfy the LS criteria for NSP, and the IO criteria for NDP. This is significantly different than the performance levels satisfied by the linear procedures. Additionally, the NSP results produced maximum story drifts of 0.72% (at 3rd story) and 1.24% (at 3rd story) in the longitudinal and transverse directions, respectively, and NDP produced 0.70% and 0.53% in the same respective stories and directions.

Table 3-7: NSP and NDP results

Wall #	NSP Max Rotation	NDP Max Rotation	ASCE 41 Acceptable Plastic Hinge Rotation		
			IO	LS	CP
W1	0.0127	0.0037	0.0050	0.0150	0.0150
W2	0.0130	0.0038	0.0050	0.0150	0.0150
W3	0.0127	0.0035	0.0050	0.0150	0.0150
W4	0.0130	0.0035	0.0050	0.0150	0.0150
W5	0.0067	0.0050	0.0050	0.0150	0.0150
W6	0.0067	0.0047	0.0050	0.0150	0.0150
W7	0.0069	0.0050	0.0050	0.0150	0.0150
W8	0.0069	0.0049	0.0050	0.0150	0.0150

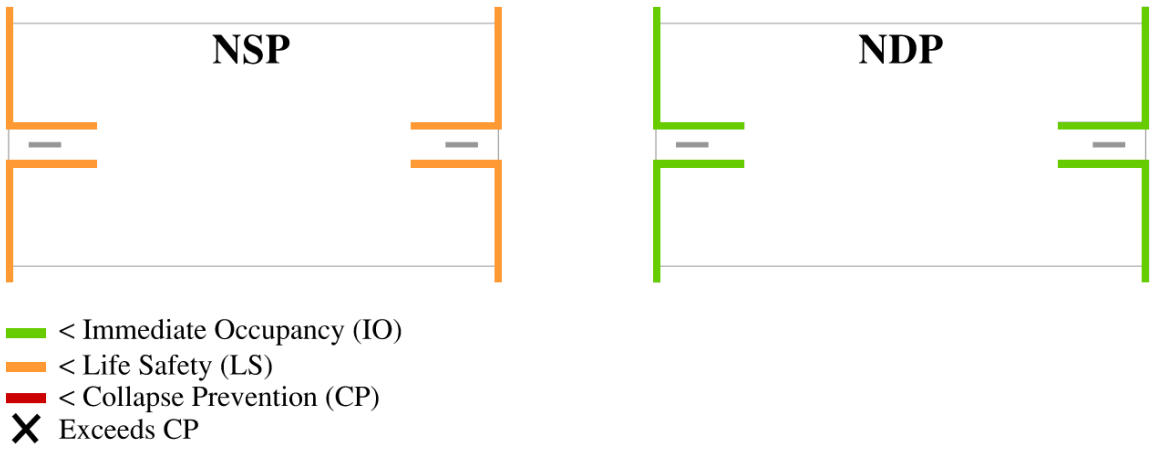

Figure 3-19. NSP and NDP performance level designation

3.4 Assessment of 6-Story Concrete Building

A seismic performance assessment of the building was carried out by analyzing the validated computer model of the 3D building. Both linear and nonlinear analysis procedures prescribed in ASCE 41 will be applied. Note, however, that the west transverse shear wall transfers at the first story, and therefore is considered an in-plane discontinuity irregularity. In conjunction with the high demand-to-capacity ratios (DCRs) in the linear results that will be presented, the linear procedures are not applicable for this building as per ASCE 41. Nevertheless, all analysis results will be presented and compared.

The seismic demands for all procedures will be based on the BSE-2E hazard level, with a 5% probability of occurrence in 50 years. The resulting response spectrum, previously shown in Figure 3-2, has with the following key parameters: S_{XS} = 1.88 g; S_{X1} = 1.198 g; T_O = 0.13 sec and T_S = 0.64 sec.

3.4.1 Linear Procedures

For the linear procedures, the Perform3D nonlinear model described earlier was used to obtain the shear and moment wall capacities in each direction. The model was then updated to reflect the linear elastic relationships for the concrete and steel materials, to be used to obtain the demands for the ASCE 41 assessment.

For the Linear Static Procedure (LSP), an equivalent static load is applied over the height of the building. The modification factors are C_1C_2 = 1.0 and C_m = 0.8. The effective seismic weight is 6989 kips for the full building. For the Linear Dynamic Procedure (LDP), the assessment was completed by using the Response Spectrum load case type. The linear procedures were applied independently in four directions: in the south and west directions (termed *positive direction*) and

in the north and east directions (termed *negative direction*). The demands in the components were then obtained by applying the 100%-30% and 30%-100% combination rule in perpendicular directions.

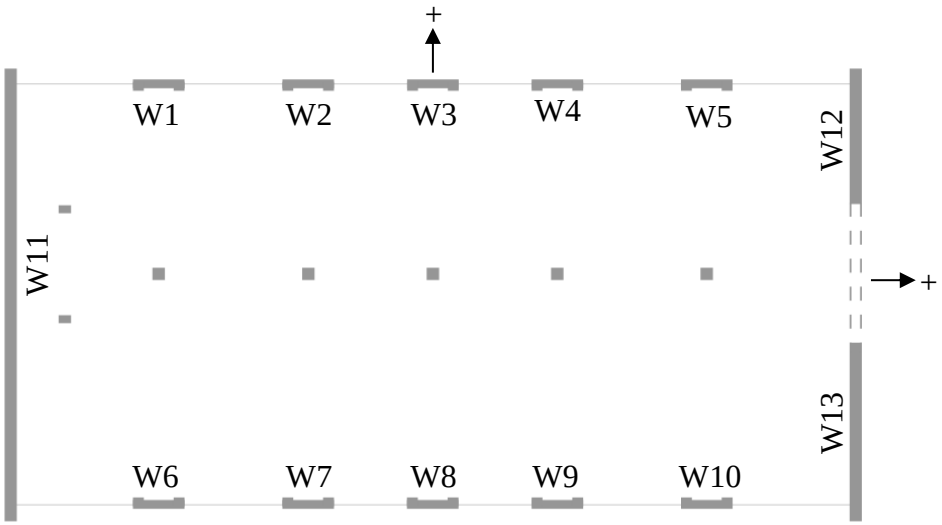

Figure 3-20. Wall identification plan view at ground level

The wall designation is shown in Figure 3-20. The acceptance criteria for the linear procedures is presented in Table 3-8. The final results for the linear procedures are listed in Table 3-9 for LSP, and

Table **3-10** LDP. The demand-to-capacity ratios (DCRs) in all walls exceed the corresponding acceptance criteria for CP, as presented in Figure 3-21. The transverse walls W12 and W13 have especially high DCRs, which can be attributed to the shear wall transfer at the first story. Additionally, the LSP results produced maximum story drifts of 3.28% (at 5th story) and 0.10% (at 2nd story) in the longitudinal and transverse directions, respectively, and LDP produced 2.80% and 0.10% in the same respective stories and directions.

Table 3-8: Acceptance criteria for linear procedures

Wall #	ASCE-41 m-Factors		
	IO	LS	CP
W1 - W13	2	3	4

Table 3-9: LSP capacities, demands, and DCRs

Wall #	Loading in positive direction				Loading in negative direction				Max DCR
	Capacities		Demands		Capacities		Demands		
	V (k)	M (k-in)	V (k)	M (k-in)	V (k)	M (k-in)	V (k)	M (k-in)	
W1	180	75000	751	385539	180	75000	750	385756	5.1
W2	180	75000	750	385556	180	75000	752	385759	5.1
W3	180	75000	751	385549	180	75000	751	385766	5.1
W4	180	75000	751	385549	180	75000	750	385766	5.1
W5	180	75000	751	385549	180	75000	751	385766	5.1
W6	180	75000	749	385072	180	75000	748	385448	5.1
W7	180	75000	748	385052	180	75000	748	385428	5.1
W8	180	75000	748	385052	180	75000	748	385428	5.1
W9	180	75000	748	385052	180	75000	748	385428	5.1
W10	180	75000	748	385072	180	75000	748	385449	5.1
W11	976	586900	5475	3169685	976	586900	5474	3156035	5.6
W12	560	135900	1934	308373	152	33000	1922	308066	12.6
W13	330	57400	3091	602716	770	184000	3102	598519	10.5

Table 3-10: LDP capacities, demands, and DCRs

Wall #	Capacities		Demands		Max DCR
	V (k)	M (k-in)	V (k)	M (k-in)	
W1	180	75000	654	320786	4.3
W2	180	75000	654	320786	4.3
W3	180	75000	654	320796	4.3
W4	180	75000	654	320786	4.3
W5	180	75000	654	320797	4.3
W6	180	75000	653	320658	4.3
W7	180	75000	653	320638	4.3
W8	180	75000	653	320638	4.3
W9	180	75000	653	320638	4.3
W10	180	75000	653	320648	4.3
W11	976	586900	5016	2942734	5.1
W12	152	33000	2155	343563	14.2
W13	330	57400	3455	670145	11.7

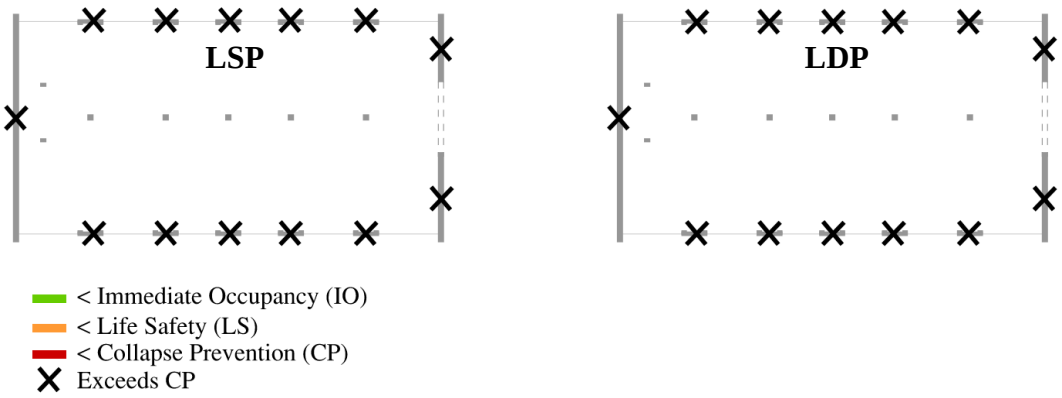

Figure 3-21. LSP and LDP performance level designation

3.4.2 Nonlinear Procedures

For the nonlinear procedures, the nonlinear Perform3D model was used for the analyses. For the Nonlinear Static Procedure (NSP), the building was pushed independently in four directions and the maximum demands in each wall were calculated. The building was pushed to the target displacements of 15.24 in (0.019 drift) and 4.03 in (0.005 drift) in the positive/negative longitudinal and transverse directions, respectively.

For the Nonlinear Dynamic Procedure (NDP), ground motions were downloaded from the United States Geological Survey (2017) Unified Hazard Tool, based on the site deaggregation. Multiple faults contribute to the seismic hazard at the site, but the Rodgers Creek – Healdsburg fault controls the deaggregation. A similar approach as previous case studies was followed to select the ground motions. The following criteria is used to download the initial batch of ground motions: fault type: strike slip; magnitude: 6 to 8; distance to rupture: 0 to 15; and shear wave velocity Vs30: 300 to 400 m/s. The selected ground motions are presented in Table 3-11.

.

Table 3-11: Selected ground motions

GM #	Record Sequence Number	Earthquake Name	Year	Station Name	Magnitude	R_{rup} (km)
1	30	Parkfield	1966	Cholame - Shandon Array #5	6.19	9.58
2	95	Managua_ Nicaragua-01	1972	Managua_ ESSO	6.24	4.06
3	265	Victoria_ Mexico	1980	Cerro Prieto	6.33	14.37
4	448	Morgan Hill	1984	Anderson Dam (Downstream)	6.19	3.26
5	725	Superstition Hills-02	1987	Poe Road (temp)	6.54	11.16
6	727	Superstition Hills-02	1987	Superstition Mtn Camera	6.54	5.61
7	901	Big Bear-01	1992	Big Bear Lake - Civic Center	6.46	8.3
8	3933	Tottori_ Japan	2000	SMN001	6.61	14.42
9	3964	Tottori_ Japan	2000	TTR007	6.61	11.29
10	4098	Parkfield-02_ CA	2004	Parkfield - Cholame 1E	6	3
11	4103	Parkfield-02_ CA	2004	Parkfield - Cholame 4W	6	4.23

This building has significantly different periods in each direction, as presented earlier: 0.86 sec and 0.17 sec in the longitudinal and transverse directions, from here on named T_{max} and T_{min}. It is unclear which period to use for scaling so the following method was applied: the final 11 sets of ground motion (pairs) were selected such that the average maximum direction spectra (RotD100) was at or above 90% of the target response spectrum in the period range $0.2T_{min}$ – $1.5T_{max}$. The final scaled spectra are shown in Figure 3-22. Note however that scaling the long periods to match 90% of the target caused the average spectral acceleration to be significantly higher than the target at short periods. Nevertheless, these final ground motions were used in the NDP analysis procedures. It is worthwhile to now note that if the ground motions had been scaled in the short period range only ($0.2T_{min}$ – $1.5T_{min}$), the NDP rotations would have been 60% of the final rotations presented later for all walls.

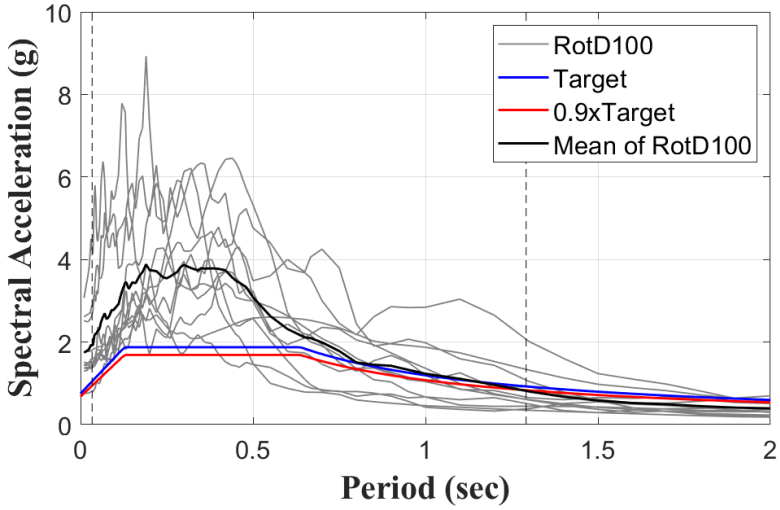

Figure 3-22. Max direction spectra for scaled motions, mean spectra, and site target spectrum

For each ground motion set, the horizontal components were applied concurrently to the model, and then again applied in the respective negative directions. The maximum demands for each set were calculated and then the average of the eleven ground motion sets was calculated. Table 3-12 lists the results for both nonlinear procedures, as well as the acceptance limits for the performance levels. The results show that for the lontigunal walls, for NSP and NDP rotations are in compliance with the corresponding LS criteria. As for the transverse walls, the W11 and W12 walls comply with the IO limits for NSP, and the W11 wall complies with IO for NDP. Figure 3-23 shows a visual representation of these results. Additionally, the NSP results produced maximum story drifts of 1.91% (at 5th story) and 0.50% (at 2nd story) in the longitudinal and transverse directions, respectively, and NDP produced 2.49% (at 5th story) and 0.58% (at 3rd story) in the same respective directions.

Table 3-12: NSP and NDP results, and acceptance criteria

Wall #	NSP Max Rotation	ASCE 41 Acceptable Plastic Hinge Rotation			NDP Max Rotation	ASCE 41 Acceptable Plastic Hinge Rotation		
		IO	LS	CP		IO	LS	CP
W1	0.0132	0.0049	0.0146	0.0146	0.0078	0.0040	0.0100	0.0100
W2	0.0132	0.0050	0.0148	0.0148	0.0078	0.0040	0.0100	0.0100
W3	0.0132	0.0050	0.0148	0.0148	0.0078	0.0040	0.0100	0.0100
W4	0.0132	0.0050	0.0148	0.0148	0.0078	0.0040	0.0100	0.0100
W5	0.0132	0.0050	0.0149	0.0149	0.0078	0.0040	0.0100	0.0100
W6	0.0132	0.0049	0.0144	0.0144	0.0077	0.0040	0.0100	0.0100
W7	0.0132	0.0050	0.0148	0.0148	0.0077	0.0040	0.0100	0.0100
W8	0.0132	0.0050	0.0148	0.0148	0.0077	0.0040	0.0100	0.0100
W9	0.0132	0.0050	0.0148	0.0148	0.0077	0.0040	0.0100	0.0100
W10	0.0132	0.0050	0.0150	0.0150	0.0077	0.0040	0.0100	0.0100
W11	0.0044	0.0050	0.0150	0.0150	0.0029	0.0048	0.0138	0.0138
W12	0.0021	0.0044	0.0121	0.0121	0.0059	0.0041	0.0105	0.0105
W13	0.0054	0.0050	0.0150	0.0150	0.0057	0.0044	0.0119	0.0119

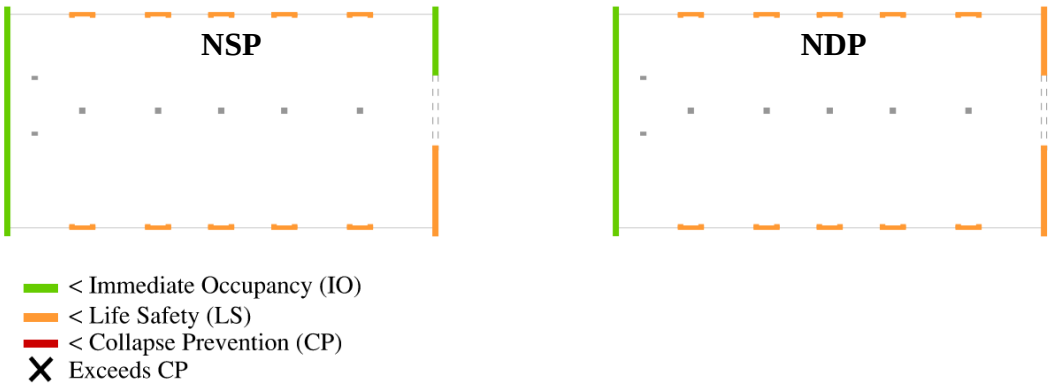

Figure 3-23. NSP and NDP performance level designation

3.5 Discussion

This chapter presented the evaluation of the consistency between the four different analysis methods permitted in ASCE 41, for two steel moment frame and two reinforced concrete shear wall buildings. This section summarizes and discusses the major findings.

Steel buildings

The calibrated models of the 3-story and 6-story steel moment frame buildings were used in a complete ASCE 41 evaluation, for all linear and nonlinear procedures. For the 3-story frame, both linear procedures resulted in consistent findings where several beams exceeded Life Safety (LS) performance level at the lower two levels, a few columns just exceeded Immediate Occupany (IO) limits at the first floor level and panel zones exceeded IO performance level at the first story level. Likewise the two nonlinear procedures also produced consistent findings – all beams and columns satisfied IO criertia while most panel zones failed the IO limit but satisfied LS limits. However, if the maximum demand from any of the ground motions is considered during NDP, beams and panel zones exceed the Collapse Prevention (CP) limit, while the columns exceed the IO limit.

Two observations arise from these findings: first, the assessment using linear procedures resulted in a more conservative assessment of the building performance since both linear methods concluded that the system would fail Life Safety limits whereas both nonlinear procedures indicate that the building will satisfy acceptance criteria for this limit state; and secondly, the drift profiles are different for the two nonlinear methods – the static procedure indicates maximum demands at the 2^{nd} story level whereas the dynamic procedure results in peak demands at the 3^{rd} story level.

In the case of the 6-story building, similar to the findings for the 3-story building, both linear procedures produced similar DCR values as well as interstory drifts. Several beams on the lower floors exceeded Collapse Prevention (CP) limits with LSP resulting in a slightly more

conservative assessment than the LDP procedure. In the case of panel zones, LSP indicates that LS limits are exceeded on the first floor whereas LDP results are less conservative with panel zones passing LS limits.

When using NSP, the first story beams and columns exceeded LS and IO, respectively, while the panel zones at the first, second, and third story exceed the LS/CP limit. However, when NDP is used, the mean demands for all beams and columns satisfy IO limits and panel zones fail to satisfy IO, but satisfy the LS/CP performance level. Therefore, the structure can be classified as satisfying Life Safety as per the NDP results. Hence, when comparing NSP and NDP results, it is evident that NSP seems to be underestimating the demands in the upper stories, as opposed to the 3-story building where the demands were similar for both nonlinear procedures.

It is of importance to note that since the publication of ASCE 41-17, there have been recommended updates to the equations used to calculate concentrated hinge component model parameters, essentially modifying the A-E points shown in Figure 3-4. New modeling parameters for beams are suggested in a NIST report (NIST GCR 17-917-45 2017) and further recommendations are presented for columns in an ASCE paper (Lignos et al. 2019). For columns specifically, there is a new suggested ultimate rotation of 0.15. The model parameters were updated for beams and columns to follow these recommendations and the ASCE 41 analysis and evaluation were repeated. The results were essentially the same as shown previously, primarily because the ground motions did not cause large enough component rotations to cause significant changes due to the updated parameters. Therefore the observations above for the nonlinear analyses are valid even after considering the recommended modeling parameters based on the latest research.

As a final remark, for both steel moment frame buildings, the panel zones were modeled with a set of elastic beam-column elements, with a trilinear-equivalent rotational spring, as

explained in Section 2.1.1. However, this degree of model refinement is not always applied in research or practice. Therefore, an indepth study was conducted using the 6-story frame model to determine the effect of panel zone modeling on an ASCE 41 performance-based assessment. This study is summarized in Appendix A.3 of this dissertation and highlights the importance of modeling the flexibility and shear-distortion behavior of his critical zone.

Concrete buildings

The existing 3-story and 6-story reinforced concrete shear wall models calibrated in Chapter 2 were used in an ASCE 41 assessment following the four linear and nonlinear procedures. For the 3-story building, the results show that LSP and LDP produced demands exceeding the acceptance criteria for the CP performance level for all L-shaped walls. However, the NSP and NDP demands satisfied LS and IO, respectively, for all walls. For the 6-story building, both LSP and LDP resulted in failure to meet the acceptance criteria for Collapse Prevention, whereas NSP and NDP satisfied the Life Safety performance level. However, recall that this building actually does not comply with the requisites to apply the linear procedures since there is a vertical irregularity in the transferred transverse shear wall. Similar to the steel buildings, these findings highlight inconsistency in performance level designation between linear and nonlinear procedures, and between the nonlinear static and nonlinear dynamic procedures.

4 Review of Dynamic Analysis Procedures and Component-Based Acceptance Criteria in ASCE 41

The assessment of the two steel moment frame and two reinforced concrete shear wall buildings presented in the previous chapter highlighted the inconsistency between the different procedures recommended in ASCE 41, as it relates to designating performance levels based on the corresponding acceptance criteria. In this chapter, additional studies are carried out to examine the dynamic analysis procedures on the following topics: (a) differences in using time histories for the linear assessment as opposed to a response spectrum analysis; (b) effect of ground motion selection; (c) margin of safety against collapse that is implicit in the ASCE 41 assessment, and (d) the correlation between a system based measure and component-based performance levels.

4.1 Linear Dynamic Procedure (LDP): Response Spectrum versus Time History Analysis

Four buildings were previously analyzed using the ASCE 41 response spectrum when conducting an LDP-based assessment. To examine the consistency in the methodology when using a linear dynamic procedure, the steel moment frame models were re-analyzed using the ground motions selected in the previous chapter for the nonlinear dynamic procedure (GM details are listed in Table 3-2 and Table 3-4, respectively).

Results are presented in Figure 4-1 for the 3-story steel frame building. It is seen that though the interstory drift demands are similar for both methods, the moment demands in the

beams using time histories are larger than the corresponding demands using a response spectrum. In fact, a few beams fail the acceptance criteria for Collapse Prevention (CP) at the 1st and 2nd story levels when the average demands from 11 GMs are considered whereas all beams satisfy CP limits when using a response spectrum analysis.

Next, the results of the assessment of the 6-story steel frame are presented in Figure 4-2. Here, the drift profiles are reasonably similar for both approaches though the maximum demands occur in the response spectrum analysis. However, demands in the beams using actual ground motion histories are higher than those produced by the response spectrum analysis. Note that the demands are based on the average of eleven ground motions. Additionally, a panel zone on the first floor exceeds Life Safety criteria whereas all panel zones satisfy LS limits when the assessment is based on a response spectrum analysis.

Hence it can be concluded that the linear dynamic procedure in ASCE 41 using time histories is more conservative than using a response spectrum. Since there are inherent uncertainties associated with GM selection, this conclusion needs further verification using alternate ground motion sets.

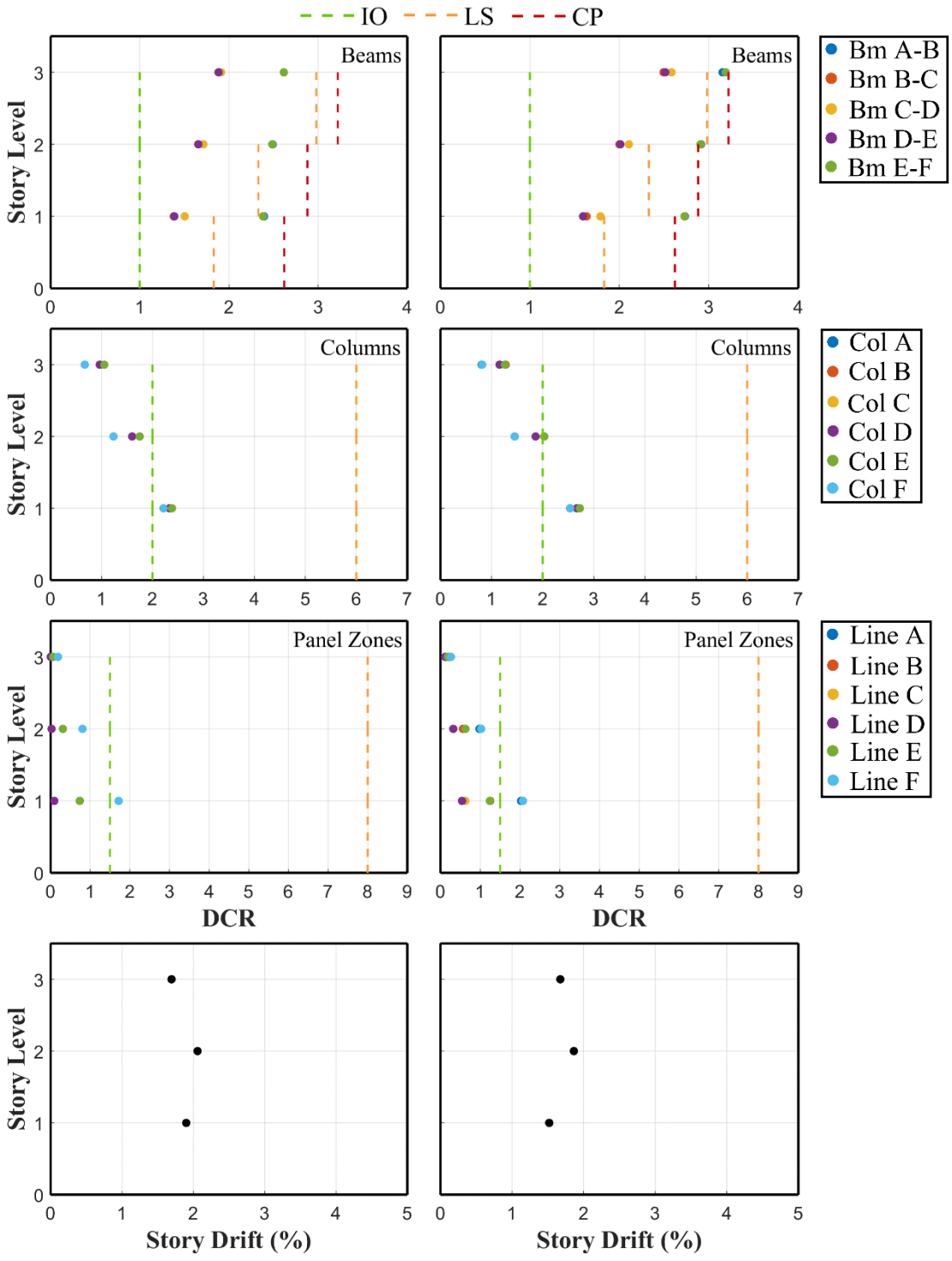

(a) (b)

Figure 4-1: Demand-to-capacity ratios and interstory drifts for 3-story frame using LDP (a) Response Spectrum (b) Time History Analysis

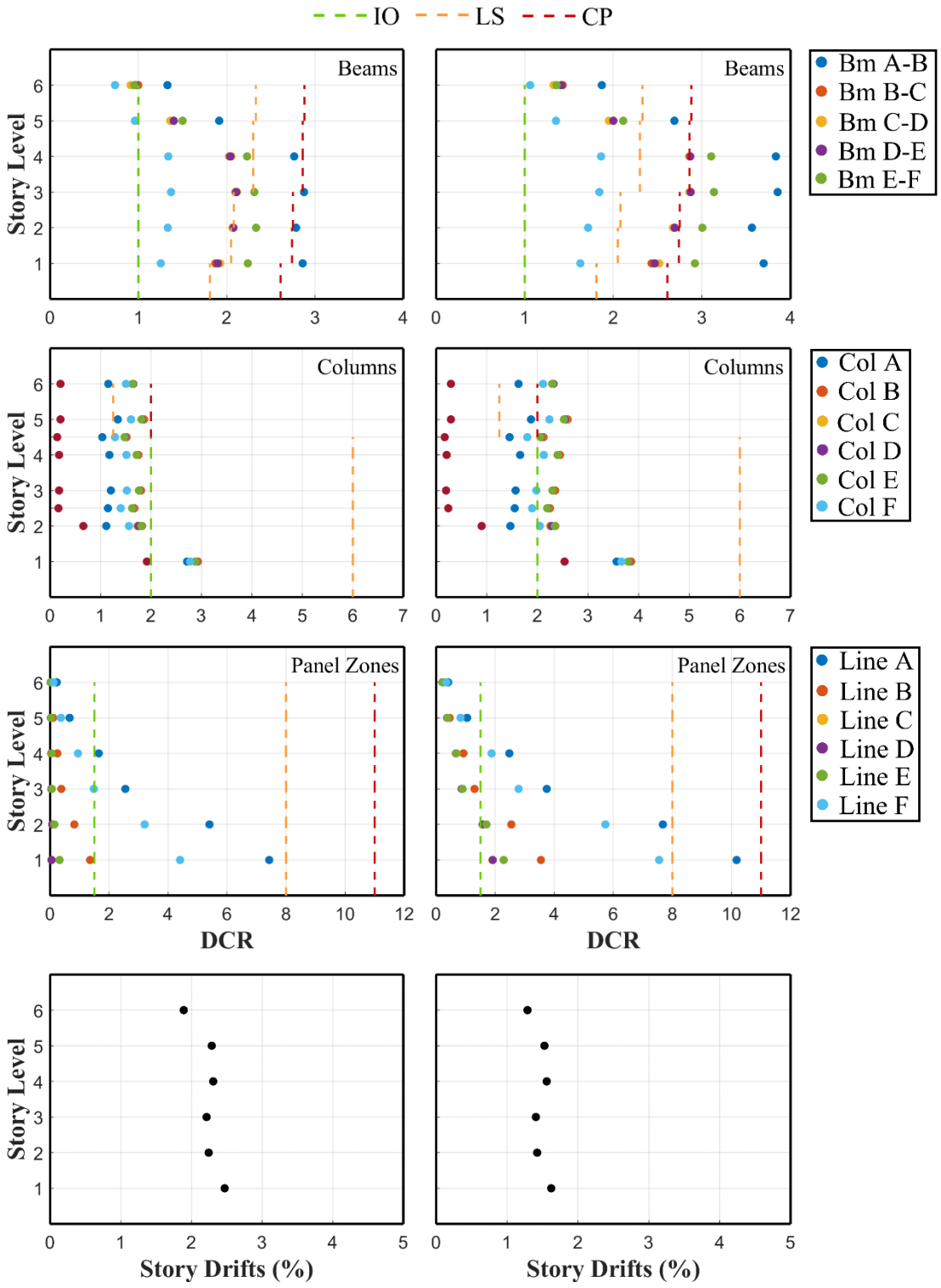

Figure 4-2: Demand-to-capacity ratios and interstory drifts for 6-story frame using LDP (a) Response Spectrum (b) Time History Analysis

4.2 Effect of Ground Motion Selection

A notable concern raised in the previous section was that an LDP assessment can result in different outcomes depending on whether the assessment was based on a response spectrum analysis or a series of time history analyses. This implies that the GM selection process itself can be a contributor to the assessment. Hence, in this section, different ground motion sets that meet the site hazard criteria are utilized in the assessment process.

Using the same selection criteria outlined in Sections 3.1.2 and 3.2.2, new sets of 11 ground motions were selected for the steel moment frame buildings. In the case of the 3-story frame, two new sets were selected resulting in a total of three GM suites. For the 6-story frame, only one additional GM set was developed. In each case, as required in ASCE 41, the 11 ground motion pairs were scaled such that the average maximum direction spectra (RotD100) was at or above 90% of the target response spectrum in the period range $0.2T_1 – 1.5T_1$. The mean spectra for each set for both buildings is displayed in Figure 4-3.

The assessment in this case is carried out using NDP. Results comapring the demands for the different GM sets for the 3-story model are presented in Figure 4-4 and the results for the 6-story model are shown in Figure 4-5.

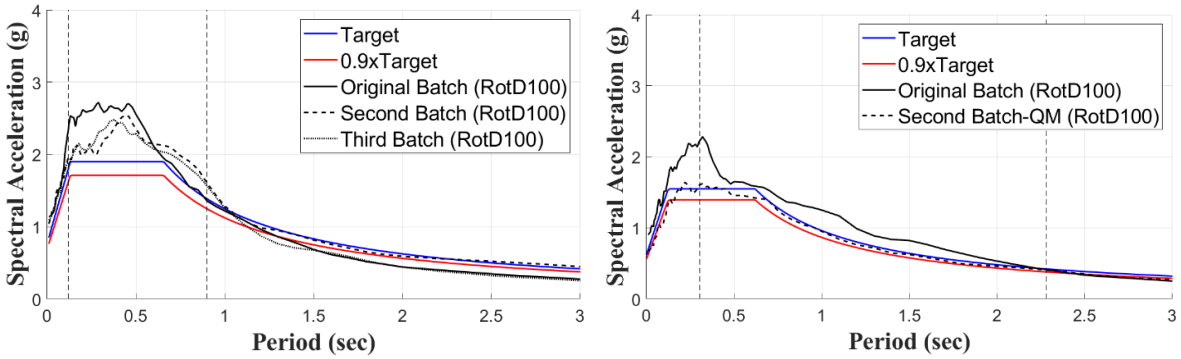

(a) (b)

Figure 4-3: Mean spectra for different ground motion sets:
(a) 3 GM sets for the 3-story building; (b) 2 GM sets for the 6-story building

As evident from Figure 4-4, the mean demands in the components are generally similar for all three GM sets for the 3-story building though the peak interstory drifts vary and do not occur at the same level. The 2nd and 3rd GM sets suggests that the peak drift occurs at the 1st story level whereas the 1st GM set highlight the possibility of higher mode contributions with the result that the peak drift occurs in the top floor.

In the case of the 6-story building (Figure 4-5), both the interstory drift pattern and the maximum deformation demands in the beams, columns and panel zones are similar for both ground motion sets. For this building, the effects of variability in the GM selection was not significant.

In both buildings, there was some variation in the maximum demands, notably in the beam demands, and was more prominent for the 3-story frame. Since the spectral demands at longer periods tend to flatten out, it is reasonable to expect larger variations for short period buildings and buildings with significant high mode contribution. This also brings into question the validity of using mean demand estimates in performance assessment since damage to a building is often the consequence of a particular ground motion at a particular site.

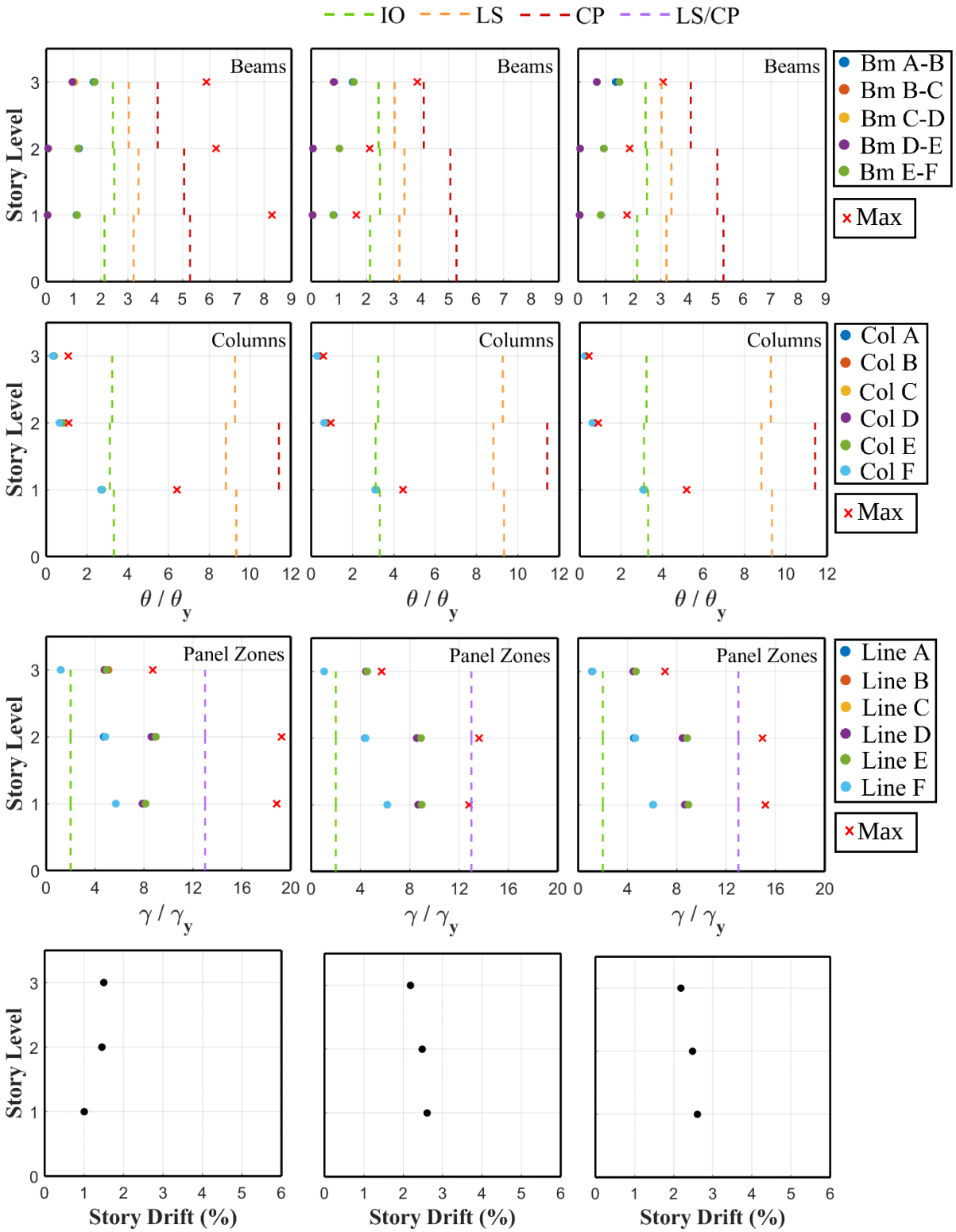

(a) (b) (c)

Figure 4-4: NDP assessment of 3-story building:
(a) Original GM Set (b) 2nd GM Set (c) 3rd GM Set

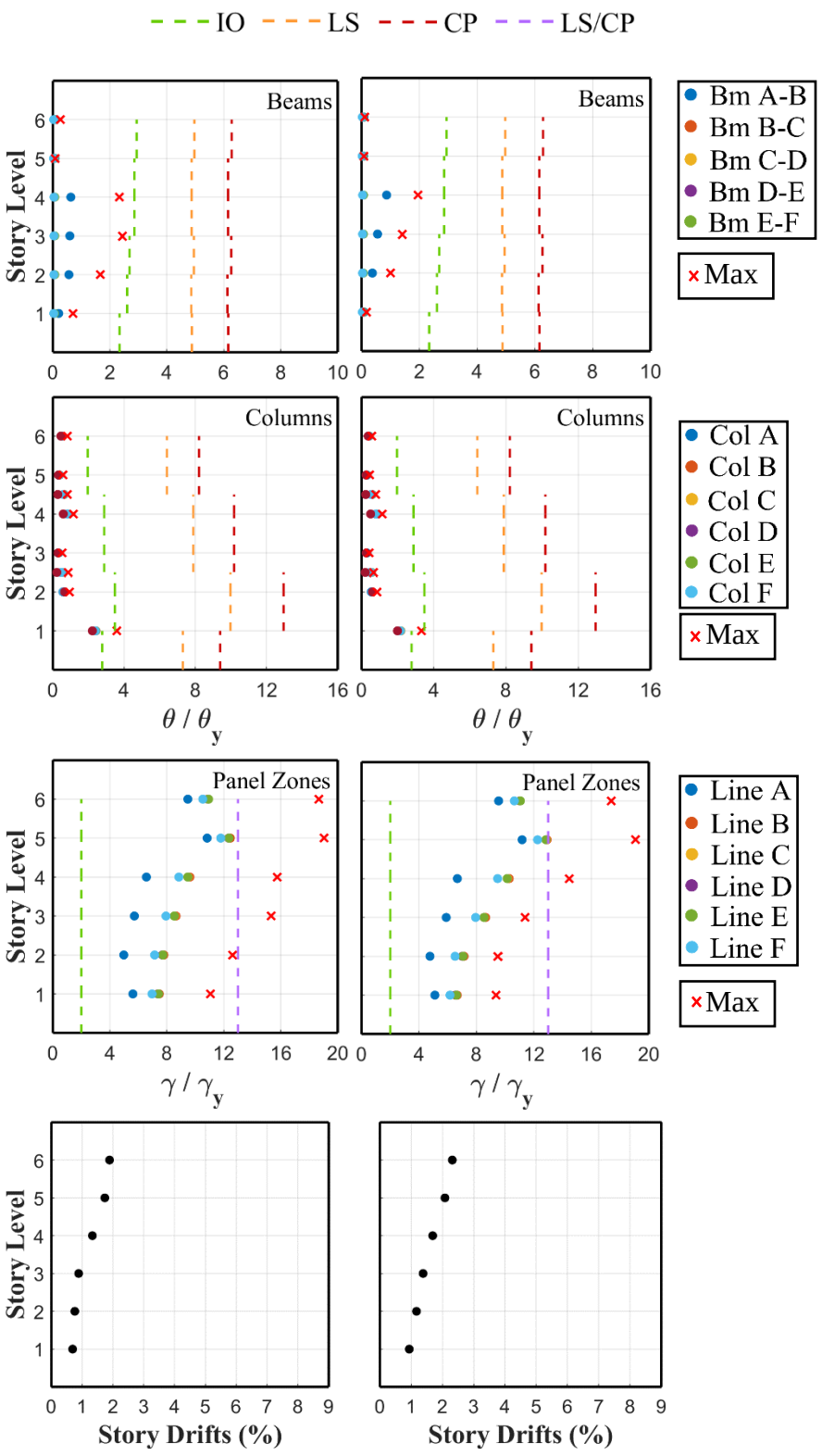

(a) (b)

Figure 4-5: NDP assessment of 6-story building: (a) Original GM Set (b) 2nd GM Set

4.3 Margin of Safety against Collapse

A major focus of this dissertation was on global issues related to the overall assessment of buildings. One of the issues that was raised at the outset was the basic premise of the ASCE 41 assessment which implies that a building is deemed not to meet a performance objective if even a single component fails to meet the corresponding acceptance criteria. To further examine the implications of the ASCE 41 component-based acceptance criteria, a comprehensive FEMA P-695 (FEMA 2009) based evaluation was carried out on each building so that the median probability of collapse could be established and compare the demands and intensity measures so obtained with ASCE 41 based criteria.

An incremental dynamic analysis (IDA) was completed with the recommended near-field ground motions in FEMA P-695, consisting of 14 pairs (two orthogonal components) of pulse records, and 14 pairs of non-pulse records, totalling 56 acceleration histories. The records were normalized as suggested in the P-695 methodology to remove some variability from the event magnitude, distance to source, source type and site conditions, while preserving the necessary variability to predict the collapse fragility. This set of ground motions was used in the analyses described in the next sections.

4.3.1 Steel Buildings

Each of the steel moment frame 2D nonlinear model in OpenSees was subjected to the near-field P-695 ground motions. The ground motions were succesively scaled until half of the records caused collapse. Collapse, in the present study, was defined as reaching or exceeding either 6% story drift, or 2% residual story drift. When this target was reached, the median spectral acceleration values from the 56 ground motions, termed S_{CT}, was recorded, as shown in Table 2-1.

The spectral accelerations at the fundamental periods of the 3-story and 6-story buildings, used in the ASCE 41 assessments, are 1.90 g and 0.60 g, respectively.

Table 4-1: Spectral intensity representing median collapse probability, S_{CT}

Collapse Definition	*3-Story*	*6-Story*
>= 6% story drift	3.52 g	1.18 g
>= 2% residual drift	3.09 g	1.35 g

In addition to the P-695 methodology to determine S_{CT}, a comprehensive set of Incremental Dynamic Analyses (IDAs) was also conducted using the same 56 ground motions with the objective of establishing collapse fragility curves that accounts for the dispersion in the complete data set. Note that the collapse fragilities were eventually developed using the 6% story drift criterion though the 2% residual drift resulted in almost identical fragility curves.

Figure 4-6 shows the results of the IDA study on the 3-story frame. Superimposed on the IDA curves (Figure 4-6 a) are the ASCE 41 acceptance criteria (independent of component type – meaning that 'x' can be a beam, column or panel zone). LS criteria is exceeded at a drift of approximately 3% and CP is exceeded almost immediately after. Figure 4-6 b plots the collapse fragility based on the P-695 motions and conditioned on $S_a(T_1)$. The marker corresponding to ASCE 41 is the mean spectral acceleration at the fundamental period of the building based on the BSE 2-E hazard level selected ground motions. The markers corresponding to LS and CP refer to the spectral demands at which the first component exceeds the corresponding acceptance criterion.

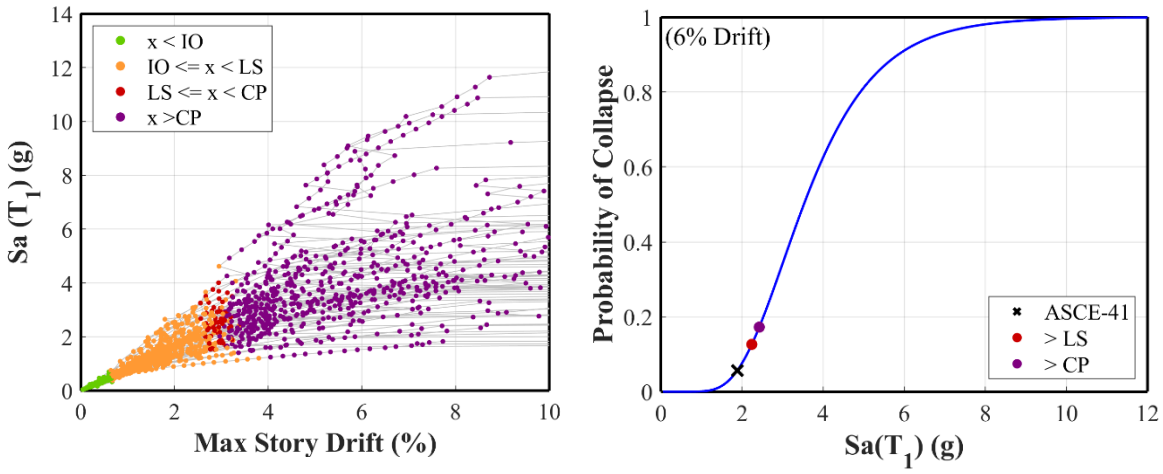

(a) (b)

Figure 4-6: Collapse assessment of 3-story frame:
(a) IDA curves incorporating ASCE 41 acceptance criteria; (b) collapse fragility

The findings reported here are based on assuming collapse to occur at a peak interstory drift of 6%. If a different threshold drift for collapse was used, the median collapse probability can shift towards a less conservative or more conservative value depending on whether the collapse drift is set a higher or lower value, respectively. The results presented in Figure 4-6 are very informative - it is seen that the probability of collapse corresponding to the ASCE 41 target spectrum for this building is approximately 5%. The spectral demand corresponding to the median collapse probability is ~3.5 g whereas CP limits based on the ASCE 41 assessment are exceeded at a spectral value of about 2.6 g. The difference in the spectral demand between LS and CP is almost negligible (2.5 g vs. 2.6 g) indicating that the ASCE 41 acceptance criterion for LS as a function of CP is highly conservative.

Finally, the sequence and number of components failing LS and CP limits are examined in Figure 4-7. The color scheme used in the plots are the same as in previous figures with the red dots signifying exceedance of the LS limit and the purple dots representing CP criteria being exceeded. The first set of components to exceed LS are beam and the first set of component to exceed CP are

panel zones. Column acceptance criteria for LS are exceeded at significantly higher drifts consistent with strong-column weak beam behavior. At a peak interstory drift of 4%, approximately 35% of the beams have exceeded LS or CP and approximately 60% of the panel zones exceed the LS/CP. Note again that the acceptance criteria for LS and CP are identical for nonlinear procedures.

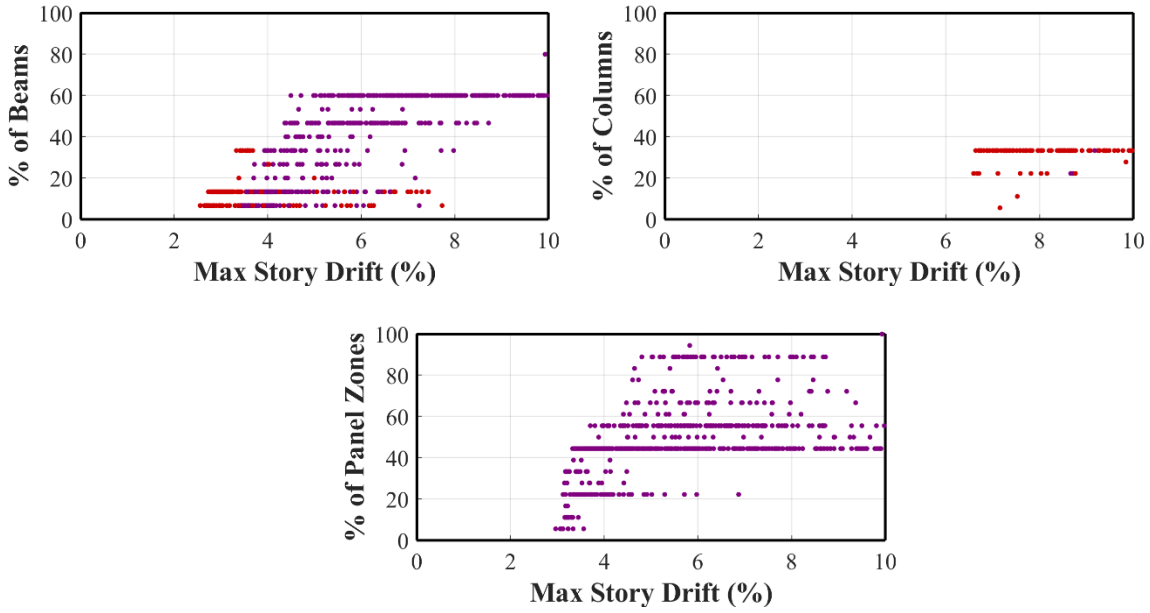

Figure 4-7: Cumulative count of components exceeding LS & CP as a function of drift (3-story frame)

The above process is repeated for the 6-story frame and results are presented in Figure 4-8 and Figure 4-9. The building response is controlled by weak panel zones with all panel zones failing CP limits at a drift of approximately 4%. Consequently, the spectral demand at CP is lower than the target ASCE 41 spectral acceleration at T_1. Since both LS and CP limits for panel zones are identical, both limit states are exceeded at a spectral value significantly lower than the value corresponding to the median collapse probability of the building. This once again highlights the fact that the ASCE 41 assessment is highly conservative.

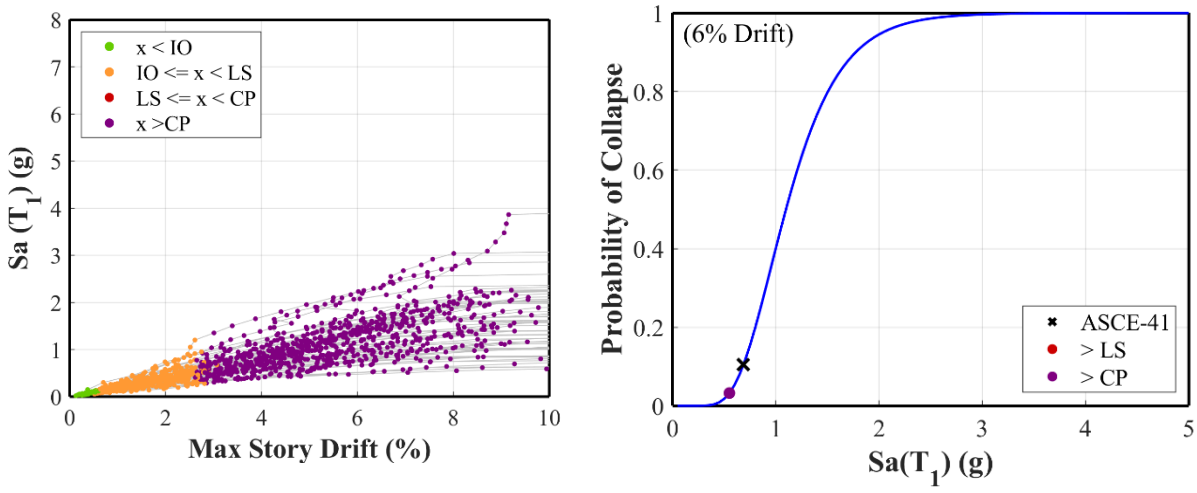

(a) (b)

Figure 4-8: Collapse assessment of 6-story frame:
(a) IDA curves incorporating ASCE 41 acceptance criteria; (b) collapse fragility

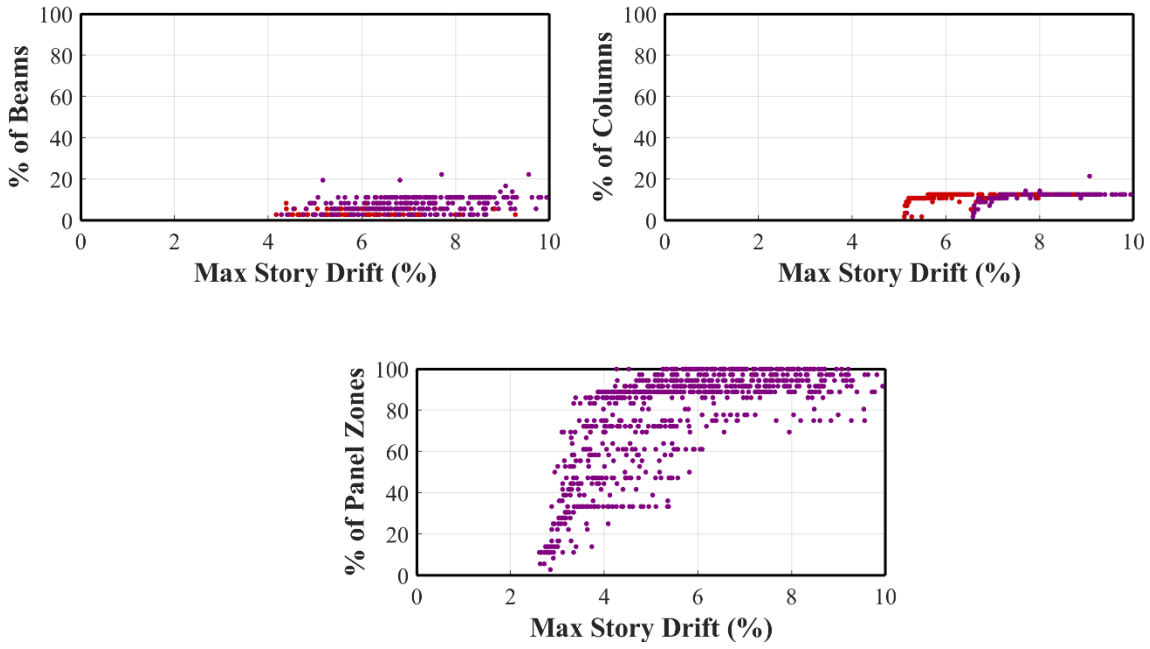

Figure 4-9: Cumulative count of components exceeding LS and CP as a function of drift (6-story frame)

Finally, the fragility curves for both buildings obtained from the analyses using the P-695 ground motions was used to establish Intensity Measures corresponding to 10% and 50% collapse probabilities. The spectral acceleration corresponding to the median collapse probability can be considered to represent the CP limit and the spectral value corresponding to 10% probability of exceedance is proposed as the threshold for the LS limit. Table 4-2 summarizes the spectral quantities for the different probabilities for both buildings considering two definitions of collapse. The residual drift criterion is more conservative for the 3-story building whereas the interstory drift is more conservative for the 6-story building.

Table 4-2: $S_a(T_1)$ based on collapse fragility

Collapse Definition	**3-Story Building**		**6-Story Building**	
	10% Collapse Probability	*Median Collapse Probability*	*10% Collapse Probability*	*Median Collapse Probability*
6% story drift	2.16 g	3.60 g	0.68 g	1.11 g
2% residual drift	1.68 g	3.03 g	0.77 g	1.44 g

4.3.2 Concrete Buildings

Each of the 3D nonlinear concrete building models in Perform3D was subjected to the near-field P-695 ground motions, with the horizontal components being applied concurrently for the 28 earthquakes. Through an incremental dynamic analysis (IDA), the ground motions were successively scaled until target story drifts were reached. The following sections present the results for both concrete buildings.

Three-Story Concrete Building

For the 3-story building, the Perform3D model was subjected to the 28 ground motion sets, although four ground motions were excluded from the set since the seismic demands corresponding to these seemed to be outliers, skewing the trend. The results are presented in Figure 4-10 for both directions. In the longitudinal direction, the relationship between the maximum longitudinal story drift is plotted against the spectral acceleration at the 1st mode period of the structure $S_a(T_1)$, where T_1 is 0.194 sec. In the transverse direction, the relationship between the maximum transverse story drift is plotted against the spectral acceleration at the 2nd mode period (which is the period in the transverse direction) of the structure $S_a(T_2)$ where T_2 is 0.143 sec. Also superimposed on the plots are the ASCE 41 performance levels based on the demands on all the walls in this building. For example, an orange marker on either Figure 4-10 a, or Figure 4-10 b, signifies that at least one longitudinal or transverse shear wall exceeded the IO criteria.

The fragility curve representing the probability of collapse in the longitudinal and transverse directions is presented in Figure 4-11, conditioned on $S_a(T_1)$ and $S_a(T_2)$ respectively. Collapse is defined at a peak story drift equalling or exceeding 6%.

The marker corresponding to ASCE 41 is the mean spectral acceleration at the fundamental period of the building based on the BSE 2-E hazard level selected ground motions. The markers corresponding to >LS and >CP refer to the spectral demands at which the first component exceeds the corresponding acceptance criterion. In the longitudinal direction, the following observations can be made: the $S_a(T_1)$ values are 3.0 g for the median probability of collapse, 1.23 g at a 14.3% collapse probability corresponding to the ASCE 41 ground motions selected for the BSE 2-E hazard level, 1.18 g at a 13.1% collapse probability corresponding to the mean of the spectral demands at which the first component exceeds the LS criteria in the IDA runs, and 1.46 g at a

19.5% collapse probability corresponding to when the first component exceeds the CP criteria in the IDA runs.

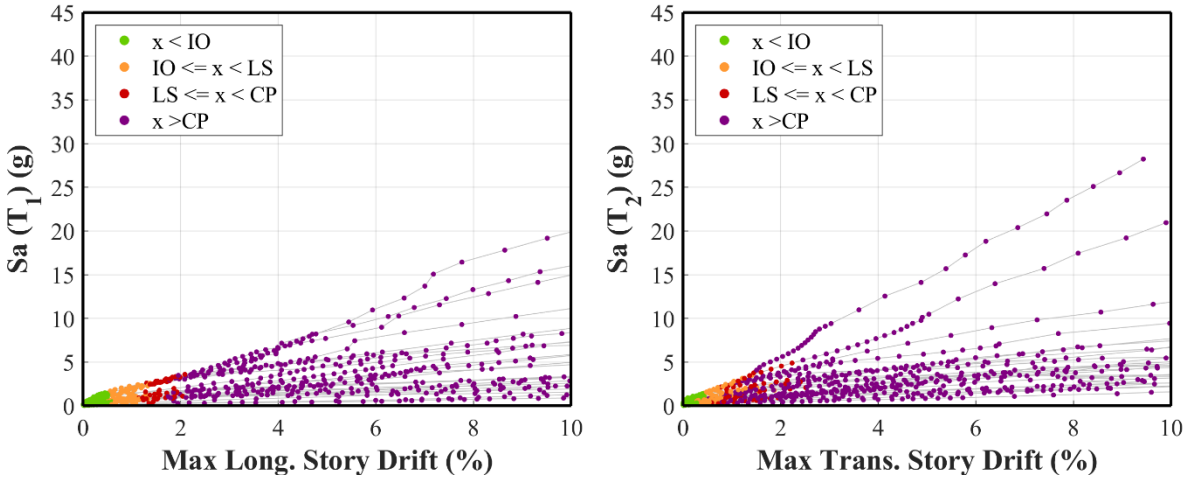

(a) (b)

Figure 4-10. IDA results: maximum story drift in each direction vs corresponding spectral acceleration at the governing period (a) Longitudinal; (b) Transverse direction

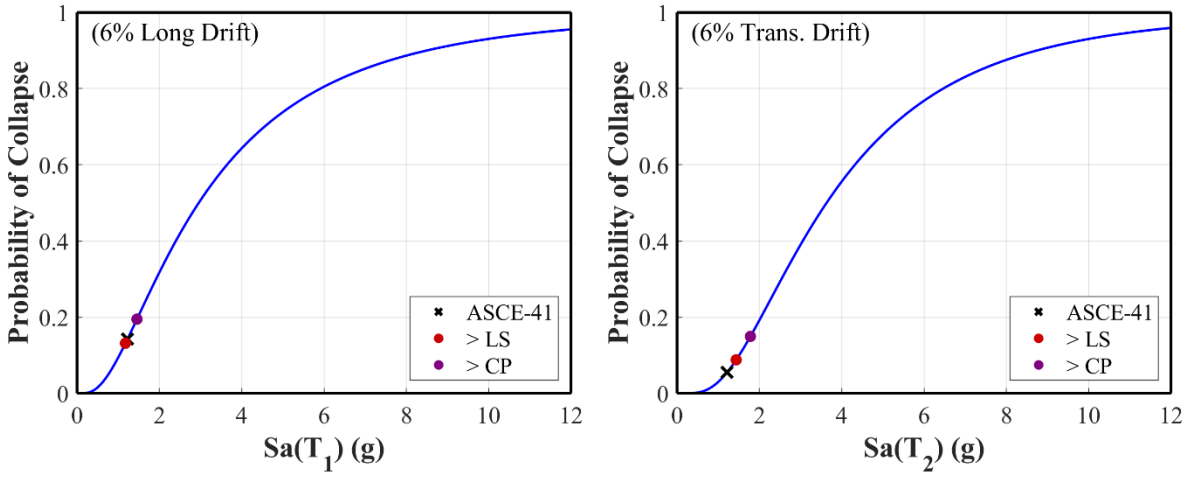

Figure 4-11. Collapse fragility: (a) Longitudinal; (b) Transverse direction

Six-Story Concrete Building

For the 6-story building, the Perform3D model was subjected to the 28 ground motion sets, although three ground motions were excluded from the set for reasons cited previously for the three-story building. The results are presented in Figure 4-12 both directions. In the longitudinal direction, the relationship between the maximum longitudinal story drift is plotted against the spectral acceleration at the 1st mode period of the structure $S_a(T_1)$, where T_1 is 0.86 sec. In the transverse direction, the relationship between the maximum transverse story drift is plotted against the spectral acceleration at the 2nd mode period of the structure $S_a(T_2)$ where T_2 is 0.168 sec. Superimposed on the plots are the ASCE 41 performance levels based on the demands on all the thirteen walls in this building.

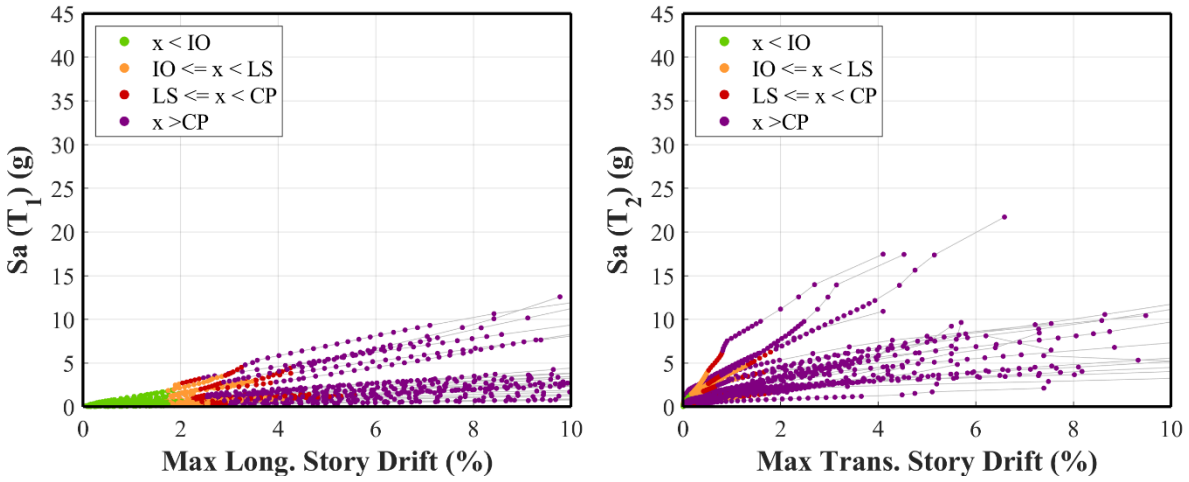

(a) (b)

Figure 4-12. IDA results: maximum story drift in each direction vs corresponding spectral acceleration at the governing period (a) Longitudinal; (b) Transverse direction

As evident from the IDA curves, for each run, the longitudinal story drift governs. In fact, for every run, the maximum story drift as well as the maximum wall rotations corresponds to the walls in the longitudinal direction. For the largest scale factor applied on the concurrent ground

motions, all peak longitudinal story drifts exceeded 10%, whereas for some ground motions, the peak transverse story drift remained below 6%. Further reviewing the results, the following observations can be made: (1) the immediate occupancy performance level designation seems to correspond to a maximum story drift of less than 2%; (2) all runs fail to satisfy collapse prevention at a maximum story drift of 6%.

The fragility curve representing the probability of collapse in the longitudinal and transverse directions is presented in Figure 4-13, conditioned on $S_a(T_1)$ and $S_a(T_2)$, respectively. In the longitudinal direction, collapse is defined at a maximum longitudinal story drift of 6%, which for this building consistently represents the maximum story drift in any direction. In the transverse direction, since maximum story drifts did not exceed 6%, a collapse condition at 4% transverse story drift was assumed.

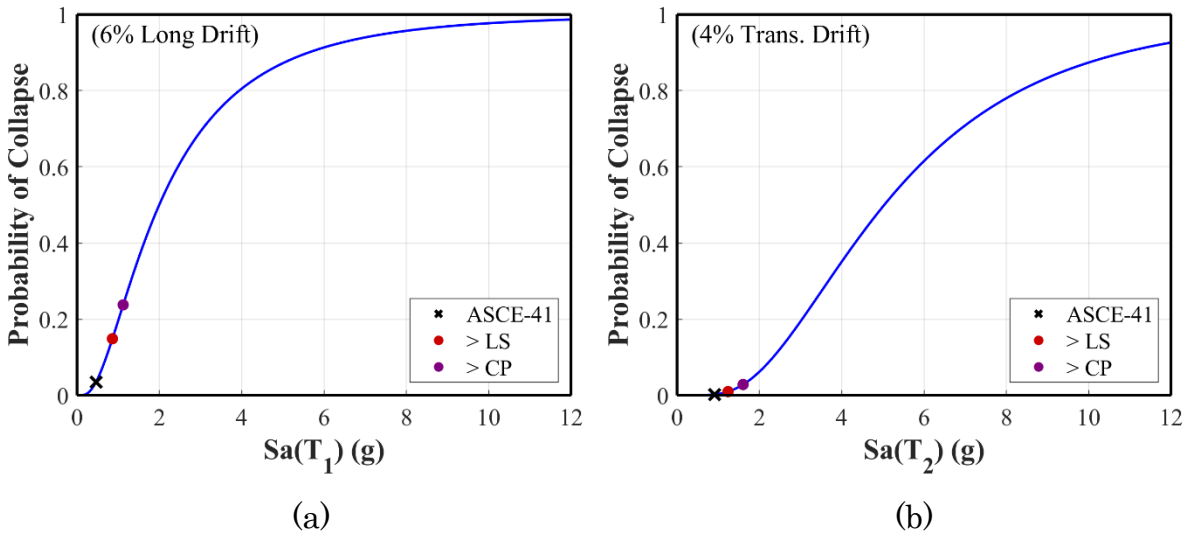

Figure 4-13. Collapse fragility: (a) Longitudinal; (b) Transverse direction

Focusing on the longitudinal direction which experienced the maximum drift and corresponds to the fundamental vibration mode of the structure, the following findings are evident: the $S_a(T_1)$ values are 2.0 g for the median probability of collapse, 0.46 g at a 3.5% collapse

probability corresponding to the ASCE 41 ground motions selected for the BSE 2-E hazard level, 0.85 g at a 14.5% collapse probability corresponding to the mean of the spectral demands at which the first component exceeds the LS criteria in the IDA runs, and 1.10 g at a 23.0% collapse probability corresponding to when the first component exceeds the CP criteria in the IDA runs.

Assessment of Performance Levels in Independent Directions

Previously for the 6-story building, Figure 4-12, the IDA was shown for the maximum longitudinal and transverse drifts, and the corresponding performance level designation for the entire building was superimposed. However, the results can also be presented in each direction independently, for the same model with concurrent ground motions applied. In Figure 4-14a and Figure 4-14b , the IDA is shown with the performance level assessed for the longitudinal walls only, and then considering the transverse walls only. The corresponding collapse fragility curves are presented in Figure 4-15.

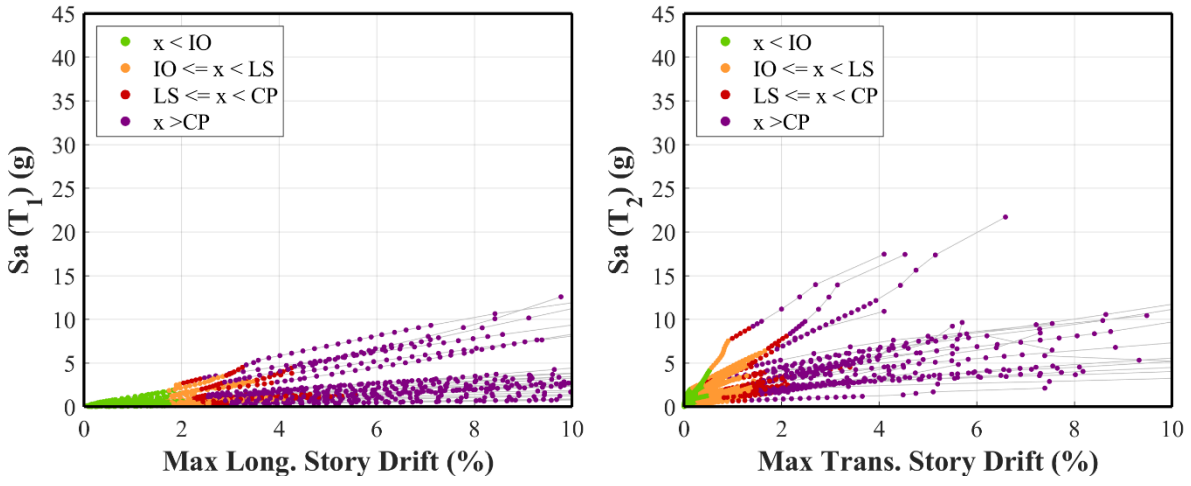

(a) (b)

Figure 4-14. IDA results: maximum story drift in each direction vs corresponding spectral acceleration at the governing period: (a) Longitudinal; (b) Transverse direction

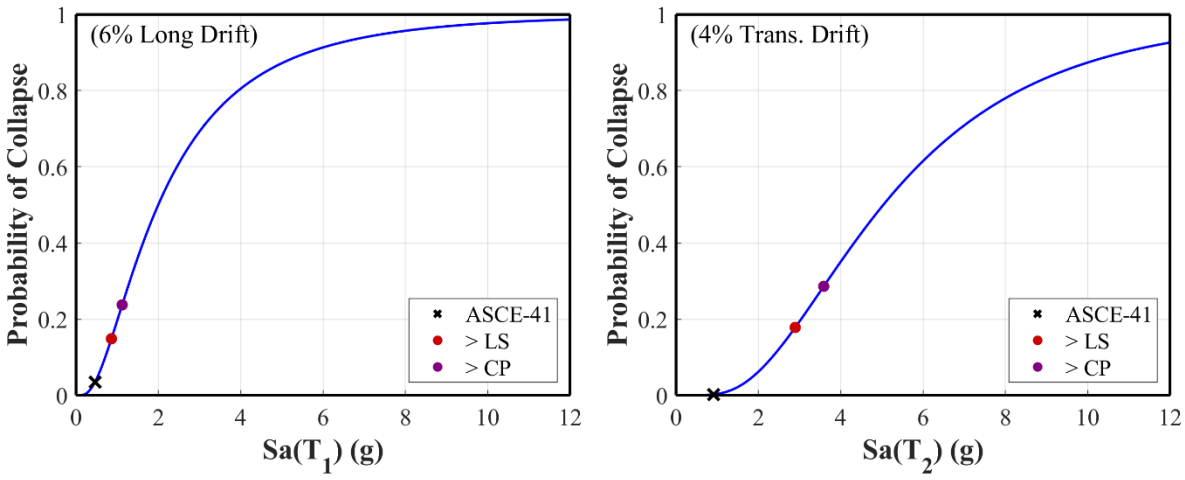

(a) (b)

Figure 4-15. Collapse fragility
(a) Longitudinal; (b) Transverse direction

Since the demands in the longitudinal walls govern for all runs, the results remain unchanged in the longitudinal direction. However, in the transverse direction, the required transverse drifts are much higher to attain the same performance level (compare Fig. 4-15 b versus Fig. 4-13b). This is also evident in Figure 4-16, where the points corresponding to IO, LS, and CP have been grouped separately, and are presented as empirical cumulative distributions. The dashed lines correspond to the performance level based on all walls, whereas the solid lines represent the performance level for the transverse walls. It is clear that when only including the transverse walls, the performance levels shift to larger maximum transverse drifts.

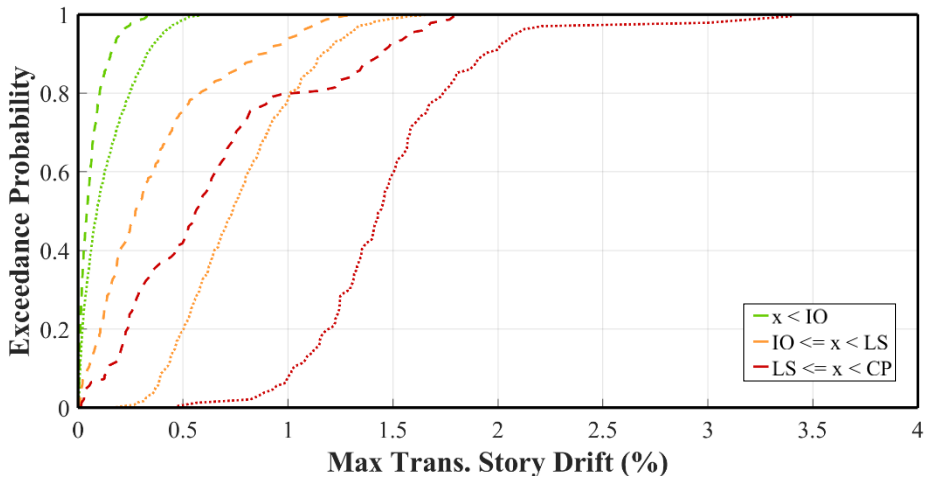

Figure 4-16. Empirical cumulative distributions from IDA using 2D models: any wall has exceeded corresponding Performance Level (dashed) vs only transverse walls have exceeded the Performance Level (solid)

2D vs 3D Incremental Dynamic Analyses

The FEMA P-695 methodology typically is applied a two-dimensional model of a building, with the objective of quantifying seismic performance factors for a lateral force resisting system. Therefore, it was of interest to compare the FEMA P-695 based incremental dynamic analysis on a 2D versus a 3D model. Therefore, the three-dimensional Perform3D model of the 6-story concrete building was reduced to a 2D model comprising the east transverse wall only. First, the relative roof displacement was compared with the original 3D model, and the results showed a satisfactory calibration against the recorded data at the site. Next, the same FEMA P-695 recordings that were applied to the 3D model in the transverse direction were applied to the 2D model. The final IDA results are presented in Figure 4-17, with the corresponding collapse fragility, also based on a collapse condition at 4% story drift.

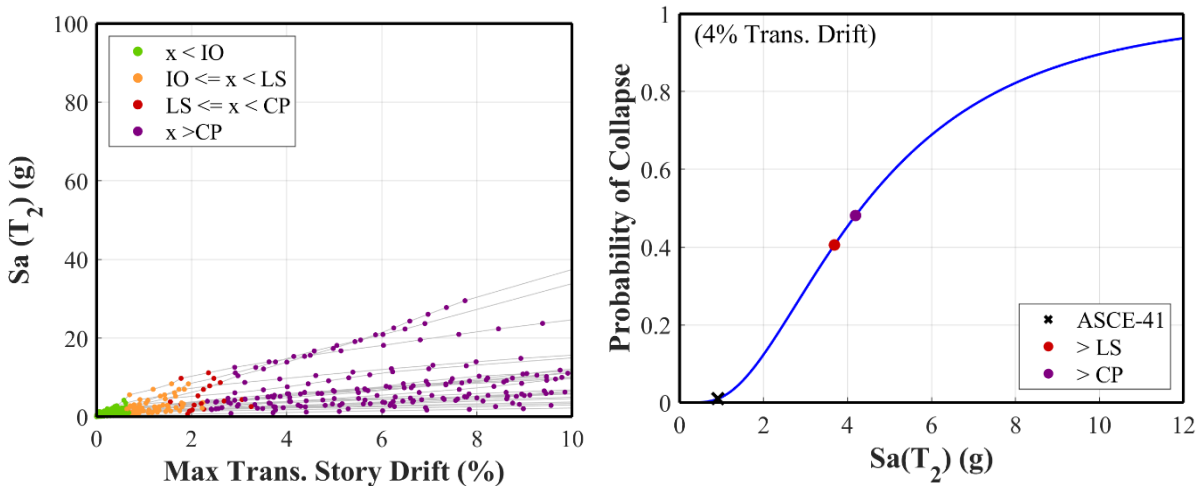

(a) (b)

Figure 4-17. IDA results for 2D model of 6-story frame: (a) maximum transverse story drift vs $S_a(T_2)$; (b) Collapse fragility in transverse direction

A comparison between the 2D and 3D IDA results was carried out, with a focus on transverse story drift at the different performance levels. The IDA results from Figure 4-12b and Figure 4-17a were synthesized, and an empirical cumulative distribution plotted for all points that satisfied either the IO, LS, or CP performance levels. Figure 4-18 shows the comparison of results. The solid lines are the results of the 2D analysis, and the dashed lines are the results of the 3D analysis with the performance level assigned based on all walls (longitudinal included). These results show that the transverse story drifts for the 2D model are much higher than for the 3D model for certain performance levels. The 2D model fails to capture the interaction between the longitudinal and transverse directions. In the 3D model, the structure is much more flexible in the longitudinal direction than the transverse, and therefore the rotations in the walls are much larger, leading to larger longitudinal story drifts. The structure is unable to achieve large transverse drifts, since the response is controlled by the rotation capacity of the longitudinal walls.

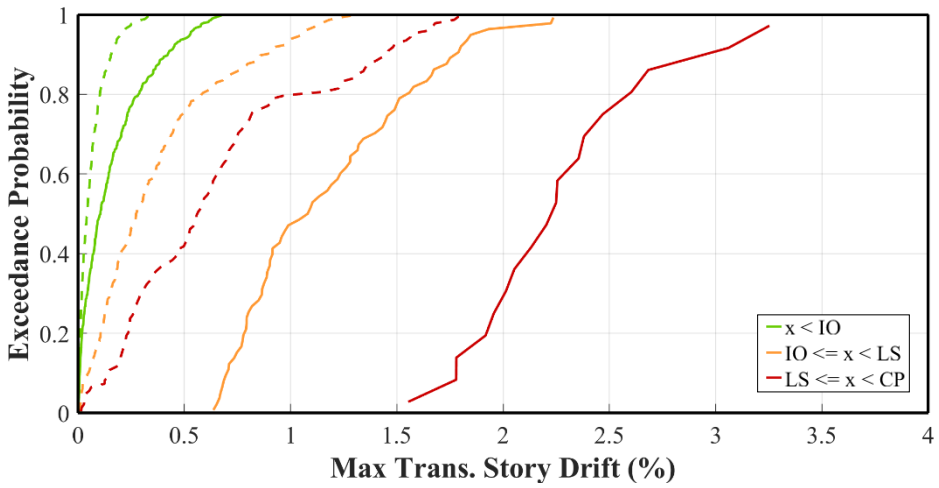

Figure 4-18. Comparing empirical cumulative distribution from IDA results: 2D (solid) vs 3D (dashed)

4.4 Correlation between System Based Measure and Component-Based Performance Levels

The previous section summarized the incremental dynamic analyses and the focus on the collapse probability of the structure and the relation to the Collapse Prevention performance level being exceeded. However, it is also important to deduce a correlation between the system-based story drift, to when the Immediate Occupance, Life Safety, and Collapse Prevention performance levels are exceeded. Therefore, using the IDA results, the runs were grouped in terms of performance levels (IO, LS, or CP), and the corresponding maximum story drift in any direction was recorded. No results are presented for points that exceeded CP. The results are discussed with the objective of quantifying a relationship between the three component-based performance levels and a system-based measure such as story drift.

4.4.1 Steel Buildings

The IDA results are presented in Figure 4-19a and Figure 4-19b, for the 3-story and 6-story steel buildings. The system-based measures are the maximum total and residual story drifts, separately.

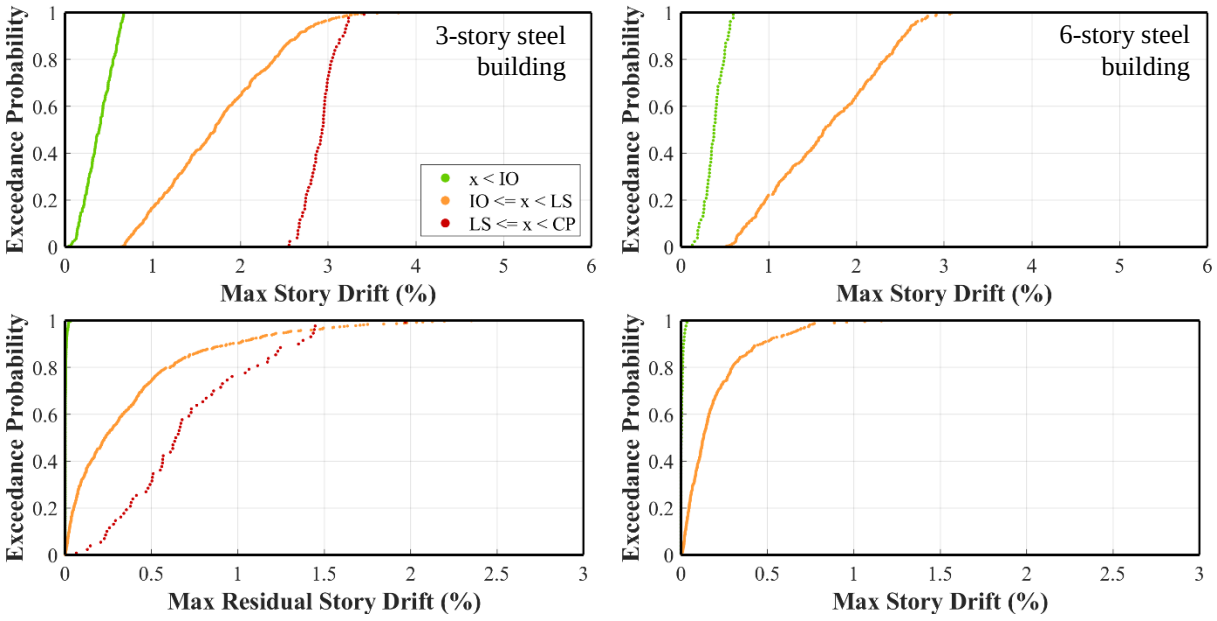

(a) (b)

Figure 4-19: Exceedance probability of maximum total and residual story drifts corresponding to IO, LS, and CP; (a) 3-story steel building; (b) 6-story steel building

For the 3-story building, the IO, LS, and CP performance levels are satisfied corresponding to median story drift demands of 0.39%, 1.71%, and 2.93%, respectively, or to median residual story drifts of 0.002% (negligible), 0.23%, and 0.64%, respectively. For the 6-story building, the IO and LS performance levels are satisfied corresponding to median story drift demands of 0.38%, 1.63%, or to median residual story drifts of 0.002% (negligible), and 0.13%. Note that the CP performance levels for the 6-story building are not shown because the critical components were the (weak) panel zones, which have the same acceptance limit for LS and CP levels, therefore once life safety is exceeded, the panel zone also fails to meet collapse prevention criterion.

4.4.2 Concrete Buildings

The IDA results are presented in Figure 4-20a and Figure 4-20b, for the 3-story and 5-story concrete buildings, respectively, in terms of the exceedance probability of maximum story drifts. For the 3-story building, the IO, LS, and CP performance levels correspond to median story drifts of 0.21%, 0.89%, and 1.58%, respectively. For the 6-story building, the IO, LS, and CP levels correspond to median story drifts of 0.85%, 2.22%, and 2.95%, respectively.

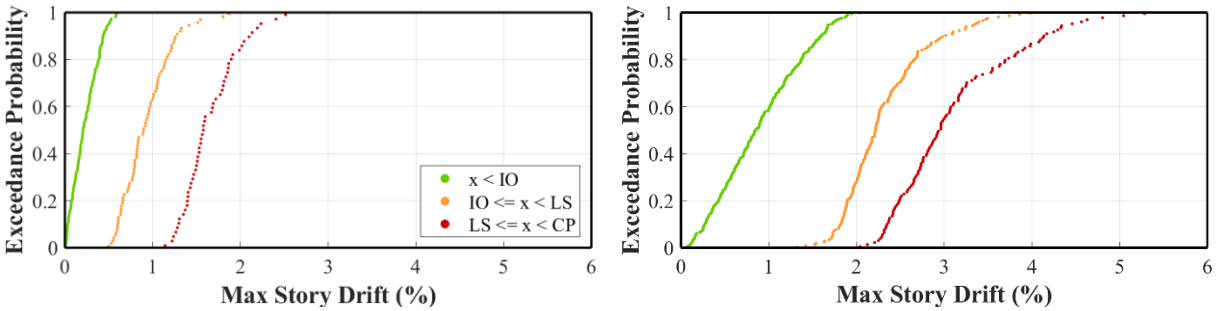

(a) (b)

Figure 4-20: Exceedance probability of maximum total story drifts corresponding to IO, LS, and CP; (a) 3-story concrete building; (b) 5-story concrete building

4.5 Discussion

Additional studies were also completed to investigate other uncertain guidelines in ASCE 41. First, the linear dynamic procedure was applied to the steel buildings using both the response spectrum and suites of scaled ground motions. The results showed that using the time histories produced more conservative results. However, since there are numerous uncertainties with ground motion selection, this observation needs further investigation with other ground motion sets, as well as additional case studies with other building configurations.

A second minor study was carried out using both steel buildings to determine the effect of using different ground motion sets that satisfy the same hazard criteria when performing an ASCE 41 assessment based on the nonlinear dynamic procedure. The results for both steel buildings indicated that the effects of the ground motion variability on the performance levels was not significant. However, further studies are needed to confirm the validity of using mean demand estimates of the eleven ground motions, since damage to a building is often a consequence of one specific ground motion at a site.

A major study was completed to assess the current component-based criteria in ASCE 41 when assessing a performance level. Incremental dynamic analyses were completed for each building, and the demands experienced were transformed into plots showing the relationship between the seismic hazard (spectral acceleration at 1^{st} mode periods in each horizontal direction), story drifts, and performance levels. Table 4-3 shows a summary of the results for all buildings, where the spectral acceleration at T_1 and the corresponding probability of collapse for different measures are presented. Compared to the median collapse probability, which as per FEMA P695 should represent the collapse probability of the system, the following observations are made.

Table 4-3: Collapse probability and corresponding intensity measure $S_a(T_1)$ obtained from IDA results for all buildings

Measures	3-Story Steel Building		6-Story Steel Building		3-Story Concrete Building		5-Story Concrete Building	
	$S_a(T_1)$ (g)	Prob. of Collapse (%)	$S_a(T_1)$ (g)	Prob. of Collapse (%)	$S_a(T_1)$ (g)	Prob. of Collapse (%)	$S_a(T_1)$ (g)	Prob. of Collapse (%)
Collapse Fragility: median based on collapse condition at 6% story drift	3.53 g	50%	1.1 g	50%	3.0 g	50%	2.0 g	50%
ASCE 41 BSE-2E Hazard: Mean of 11 selected ground motions for NDP	1.89 g	5.7%	0.69 g	10.5%	1.23 g	14.3%	0.46 g	3.5%
IDA Analysis: mean of 56 ground motions, when first component exceeds LS	2.24 g	12.6%	NA	NA	1.18 g	13.1%	0.85 g	14.5%
IDA Analysis: mean of 56 ground motions, when first component exceeds CP	2.43 g	17.2%	0.55 g	3.2%	1.46 g	19.5%	1.10 g	23.0%

For the steel buildings, the point representing when Collapse Prevention is first exceeded has collapse probabilities of 17.2% for the 3-story building, and 3.2% for the 6-story building, much lower than the median value. Both values show that the component-based CP criteria is conservative when compared to the system-based measure (assuming a collapse condition at 6% story drift). Furthermore, for the 6-story building, since the acceptance criteria for panel zones has the same values for life safety and collapse prevention, once the panel zone exceeds the life safety limit, it also fails the collapse prevention limit. This results in a collapse probability of 3.2%, much lower than the 3-story building, and is overly conservative.

Excluding the 6-story steel building for the above reasons, the probability of collapse at the point when LS is first exceeded is 12.6%, 13.1%, and 14.5% for the 3-story steel, 3-story concrete, and 5-story concrete buildings, respectively. The probability at the point when CP is first exceeded is 17.2%, 19.5%, and 23% for the same respective buildings. These results indicate that the probability of collapse are fairly consistent when LS and CP are exceeded for the three buildings. The probability of collapse at an intensity corresponding to the $S_a(T_1)$ from the ASCE 41 BSE-2E hazard is 5.7%, 10.5%, 14.3%, and 3.5%, for the steel and concrete buildings respectively. This shows the inherent conservatism in ASCE 41.

It is however important to mention that while it was demonstrated that the component-based criteria is conservative for all buildings, such a margin of safety may be justified, especially for the concrete shear wall buildings, where all walls are load-bearing elements and are critical to the seismic resistance of the building.

Another major study stemmed from the incremental dynamic analyses. The results from the IDA were grouped into the runs that satisfied immediate occupancy, life safety, and collapse prevention, for all buildings separately. Table 4-4 summarizes the results from the empirical cumulative distributions for the maximum story drift. The results correlate the system-based drift measure to the three different performance levels for each run. For the steel buildings, IO correlates to median story drifts of 0.39% and 0.38%, and LS to median story drifts of 1.71% and 1.63%, for the 3 and 6-story buildings, respectively. This shows consistency in the observed median drifts for these buildings. The results for the concrete shear wall buildings are more inconsistent, with IO correlating to median story drifts of 0.21% and 0.85%, LS to median story drifts of 0.89% and 2.22%, and CP to median story drifts of 1.58% and 2.95%, for the 3 and 5-story buildings, respectively. The difference in the drifts between the concrete buildings can be attributed to the

extreme difference in periods in the longitudinal and transverse directions for the 5-story concrete buildings. The maximum drifts were consistently observed in the walls in the longitudinal direction and controlled the performance of the building. Therefore for this study, the 3-story results might provide a better correlation between drift and performance levels for the concrete buildings.

Table 4-4: Median story drifts corresponding to IO, LS, and CP

Performance Level	3-Story Steel Building	6-Story Steel Building	3-Story Concrete Building	5-Story Concrete Building
Immediate Occupancy (IO)	0.39%	0.38%	0.21%	0.85%
Life Safety (LS)	1.71%	1.63%	0.89%	2.22%
Collapse Prevention (CP)	2.93%	NA	1.58%	2.95%

5 Conclusions and Unresolved Issues

The scope of work carried out in this dissertation focused on two main objectives: to evaluate the consistency between different analysis methods permitted in ASCE 41 and to investigate the validity of the current component-based acceptance criteria corresponding to the three performance levels. The research also embarked upon multiple smaller studies as the work progressed, and other minor uncertain issues in ASCE 41 were discovered.

The research work was organized into three phases: (1) In the first phase, two steel moment frame and two reinforced concrete shear wall buildings were identified from the CSMIP database and computer models were developed for each of the target structures from structural drawings and available material property information. The models were validated through comparisons of time-history traces of displacement and acceleration at recorded floor levels; (2) The calibrated models were then analyzed using the four procedures allowed in ASCE 41 and the results of the simulations were examined to determine consistency in the predicted assessment of the target buildings; (3) Finally, a comprehensive collapse assessment of each of the four buildings were carried out using the FEMA P-695 methodology. This enabled to establish the margin of safety against collapse using the ASCE 41 approach and provide a basis for developing a system level performance assessment. The results of the assessment were also used to establish a correlation between a system-based measure and the component-based performance levels for the four buildings.

5.1 Primary Findings

This section presents a summary of the main research findings in this dissertation. More detailed findings and summaries are located in the *Discussion* section of each chapter.

Modeling

The steel chapter in ASCE 41-17 generally has adequate guidance for the modeling of beam connections and columns, although more commentary is needed for differentiating weak and strong panel zone behavior and modeling. One of the studies in this dissertation highlighted the importance of modeling the flexibility and shear-distortion behavior of the panel zone, which is currently not a requirement in ASCE 41. Likewise, the concrete chapter in ASCE 41 does not provide specific guidelines on modeling a shear wall element, specifically to differentiate between flexure and shear-controlled modeling and behavior. Guidance is particularly needed on how to model the nonlinear shear properties in walls.

Linear and Nonlinear Analysis Procedures

The building case studies presented in this research work demonstrate that there are inconsistencies in the analysis procedures in the current ASCE 41 guidelines. The linear static and linear dynamic procedures produce similar component demands, drifts, and performance levels, and are demonstrated to be conservative compared to the nonlinear procedures. The nonlinear static and nonlinear dynamic procedures differ significantly in component-demands and drift patterns, and the nonlinear static procedure seems to underestimate the demands in the upper stories of the six-story steel building.

Component-Based Performance Level Acceptance Criteria

Based on the incremental dynamic analyses completed for all four buildings, the Life Safety and Collapse Prevention component-based acceptance criteria is conservative compared to the system collapse probability based on a collapse condition defined at 6% story drift. The first component to exceed Life Safety and Collapse Prevention performance levels correlate to no more than 15% and 23% probability of collapse, respectively, for the four buildings, which is significantly lower that the median.

The correlation between attaining (not exceeding) a performance level and the corresponding maximum story drift in any direction shows the following: Immediate Occupancy, Life Safety, and Collapse Prevention, corresponds to a story drift of no more than 0.4%, 1.7 %, and 3.0%, respectively, for the steel buildings, and 0.9%, 2.3%, and 3.0% for the concrete buildings.

5.2 Unresolved Issues

This section presents recommendations for future work in developing a system-based measure to augment to the current component-based acceptance criteria for the different performance levels. Also, while focusing on the main objectives of this dissertation work, various issues were discovered in the current performance-based methodology and guidelines for selecting intensity measures (for hazard modeling) and engineering demand parameters (for simulation modeling). While the author investigated these during the analysis of case studies presented in this dissertation, they need further examination. This section also presents recommendations for further work in these additional areas.

5.2.1 System-Based Criteria to Augment to Component-Based Criteria

The incremental dynamic analyses of the four steel and concrete buildings showed that the current component-based criteria is overly conservative. Currently, if one component fails to meet the acceptance criteria for a performance level, the entire building fails to meet the criteria. In order to augment the current criteria using a system-based measure, it is recommended that maximum story drifts are established for each performance level. Such future work can be guided by the following recommendations, as inferred from the work presented in this dissertation.

1. For steel moment frame and reinforced concrete shear wall buildings, the acceptance criteria should be augmented with required drift limits. Specifically, there should be a maximum drift check that corresponds to the exceedance of each of the three performance levels: Immediate Occupancy, Life Safety, and Collapse Prevention. Findings from this research indicate that the current component-based criteria corresponds to a maximum story drift of no more than 0.9%, 2.3%, and 3.0% for each respective performance level. Future work should focus on determining if these drift limits are justified, or if larger limits can be allowed for each performance level.
2. For the steel moment frame buildings, the current component criteria should include a check on which and how many components exceeded the target performance level. For collapse prevention, if the component is load-bearing and critical to the overall stability of the system, the *one-component* criteria should remain. However, if the element is a beam connection, or a panel zone, that exceeded the acceptance criteria by a small percentage, further investigation by the engineer is suggested, to determine whether the demands in that component are critical, and if the acceptance criterion in ASCE 41 is reasonable. As for the concrete buildings, given that shear walls are critical load-bearing components, one

component exceeding the Collapse Prevention performance level may be a valid assessment.

3. For the other performance levels, Immediate Occupancy and Life Safety, the acceptance criteria should include an exception to the current one-component exceeding the criteria rule. For example, if only two components slightly exceeded the demands for Life Safety, but the rest of the components have significantly smaller demand-to-capacity ratios than the LS criteria, it should be allowed to designate the building as satisfying Life Safety. This should be accompanied by a drift check. In future work, the details on how many components to allow to pass or fail criteria, as well as what is the maximum story drift for each performance level, should be established based on more extensive studies of different types of buildings.
4. In future work relating to establishing drift limits, it is important to identify special cases, such as the 6-story concrete building in this study, where the first mode periods in the two orthogonal directions are substantially different. This can skew the results when correlating the drift to a performance level. Attention should also be directed to steel moment frame buildings with weak panel zones, since the panel zones have the same acceptance criteria for LS and CP, and therefore can affect the correlation of story drift for each performance level.

5.2.2 Hazard Modeling

The current ASCE 41-17 guidelines have prescriptive requirements for the determination of the parameters representing a seismic hazard at a site. These primarily reference the procedures in ASCE 7-16 (2017) with some minor adjustments. However, there were some specific cases for ground motion scaling for 2D and 3D models that need further clarification in the guidelines.

Scaling ground motions for 2D analysis

The ASCE 41 and ASCE 7 guidelines currently include procedures for ground motion scaling to be used in three-dimensional models. Section 2.4.1.7 in ASCE 41-17 and Section 16.2 in ASCE 7-16 provide procedures for developing a target response spectrum for a site, which is then used as a reference to scale a suite of eleven ground motion pairs. A maximum direction spectrum (RotD100) is developed for each ground motion using both horizontal components. Each ground motion pair is then scaled such that the average of the RotD100 spectra from all ground motions does not exceed 90% of the target response spectrum for any point within the specified period range. The scaled horizontal components are then applied concurrently to a 3D model. However, for a 2D model, there is no guidance on which ground motion component to apply. It is left to the judgement of the engineer to decide which horizontal component to select. Furthermore, given that the two components of a ground motion are not used in the analysis, the concept of the maximum direction spectra becomes less relevant. Further clarification in ASCE 7 and ASCE 41 is needed for 2D analyses.

Note that for the 2D analysis completed in this research project, the following procedure was assumed, as mentioned in earlier chapters: for each ground motion set, the base motions and their spectra in each direction were compared; the horizontal component motion with a larger evident pulse in the time history or a larger spectral value within the target period range was selected. A additional scale factor of 1.1 was necessary to ensure that the actually applied ground motions had a mean spectra that was equal to or above 90% of the target spectrum in the required period range.

Scaling ground motions for 3D analysis

As previously mentioned, ground motions are scaled within a period range. ASCE 41-17 Section 2.4.3 provides the following guidance on this range: the lower-bound period should not exceed T_{min} and the upper-bound period should not exceed $1.5T_{max}$, where T_{min} and T_{max} are the smallest and largest first-mode period for the two principal horizontal directions of response. For the case of the 6-story concrete building, the controlling periods were 0.86 sec and 0.17 sec in the longitudinal and transverse directions, respectively. When scaling the ground motions, the scale factors were controlled by the longer period region. Therefore, the mean spectra of the eleven ground motions was more than twice the target spectra from approximately 0.1 to 0.5 sec, as shown in Figure 3-22. The ground motion component then applied to the transverse direction may likely represent an overestimation of the seismic hazard at the site for the corresponding controlling period in that direction. More work should be completed for this case scenario where the periods in the horizontal directions are significantly different.

5.2.3 Simulation Modeling

There are other issues that affect the simulation modeling in the current performance-based methodology. This section discusses some of these issues and provides recommendations for future work.

Modeling of Shear-Controlled Walls

Currently, ASCE 41-17 does not provide guidelines on modeling shear walls. Furthermore, there is no clarity on how flexure-controlled versus shear-controlled walls should differentiate in terms of modeling, as well as expected response. In Section 2.3.1 of this dissertation, four different numerical models in OpenSees were validated using experimental tests of two specimens. The

results showed evidence that most models are able to capture the behavior of flexure-walls wells, but most models fail to capture the shear response of shear-controlled response. Currently, the best models out of the ones examined was the two-dimensional OpenSees SFI-MVLEM model. However, more work and validation needs to be dedicated to the three-dimensional SFI-MVLEM model, which was recently published (Kolozvari et al. 2021).

ASCE 41 needs further guidelines on which procedures and models are recommended when modeling shear walls, and the limitations and assumptions that are inherent in some tools currently available. Specifically, there is not sufficient published work on which parameters to use when modeling the nonlinear shear response of concrete. Therefore, it is left to the engineer, as was the case for this project, to calibrate the nonlinear parameters against experimental data. Realistically, many engineering firms do not have the resources to do this, and might be making inaccurate assumptions in the modeling process. Therefore, additional research and modeling guidelines is needed for shear-controlled walls as well as the corresponding validation of commonly used nonlinear software such as Perform3D.

References

American Concrete Institute (ACI) (2014). Building Code Requirements for Structural Concrete. ACI 318-14.

American Society of Civil Engineers (ASCE) (2017). Minimum design loads for buildings and other structures. ASCE/SEI 7-16. Reston, VA.

American Society of Civil Engineers (ASCE) (2017) Seismic evaluation and retrofit of existing buildings. ASCE/SEI 41-17. Reston, VA.

Ancheta, T.D., Darragh, R.B., Stewart, J.P. et al. (2013) PEER NGA-West2 Database. PEER Report No. 2013/03. Pacific Earthquake Engineering Research Center. University of California, Berkeley, CA. Available at http://ngawest2.berkeley.edu (last accessed August 2021).

Applied Technology Council (ATC) (2017) Recommended modeling parameters and acceptance criteria for nonlinear analysis in support of seismic evaluation, retrofit, and design. Report No. NIST GCR 17-917-45. National Institute of Standards and Technology (NIST), U.S. Department of Commerce. Gaithersburg, MD. DOI: 10.6028/NIST.GCR.17-917-45

Applied Technology Council (ATC) (2022) Benchmarking Evaluation Methodologies for Existing Reinforced Concrete Buildings. Report No. NIST GCR 22-917-50. National Institute of Standards and Technology (NIST), U.S. Department of Commerce. Gaithersburg, MD. DOI: 10.6028/NIST.GCR.22-917-50

Birely, A.C., Lowes, L.N., and Lehman, D.E. (2014). Evaluation of ASCE 41 Modeling Parameters for Slender Reinforced Concrete Structural Walls. ACI Special Publication, 297, pp. 1-18.

CSI (2021). Perform-3D: Performance-Based Design of 3D Structures. Computers and Structures Inc., Walnut Creek, CA.

Falborski, T., Hassan, A.S., Kanvinde, A.M (2020) Column base fixity in steel moment frames: Observations from instrumented buildings. *Journal of Constructional Steel Research*, 168. 105993. DOI: 10.1016/j.jcsr.2020.105993.

Federal Emergency Management Agency (FEMA) (2009) Quantification of building seismic performance factors. Report No. FEMA P-695. Washington, D.C.

Foutch, D. and Yun, S. (2002) Modeling of steel moment frames for seismic loads. *Journal of Constructional Steel Research*, 58:529-564.

Goel, Rakesh. (2008). Mode-based procedure to interpolate strong motion records of instrumented buildings. *ISET Journal of Earthquake Technology*. 45.

Han, X., Chen, B., Ji, J., Xie, S., and Lu, H. (2019) Deformation limits of L-shaped reinforced concrete shear walls: Experiment and evaluation. Structural Design of Tall and Special Buildings. 28:e1627. DOI: 10.1002/tal.1627

Harris, J. and Speicher, M. (2018) Assessment of performance-based seismic design methods in ASCE 41 for new steel buildings: Special moment frames. *Earthquake Spectra*, 34 (3), pp. 977-999. DOI: 10.1193/050117EQS079EP.

Hartloper, A.R., de Castro e Sousa, A., and Lignos, D.G. (2021) Constitutive modeling of structural steels: Nonlinear isotropic/kinematic hardening material model and its calibration. *Journal of Structural Engineering*, 147 (4). DOI: 10.1061/(ASCE)ST.1943-541X.0002964.

Ibarra L.F., Medina R. A., and Krawinkler H. (2005) Hysteretic models that incorporate strength and stiffness deterioration. *Earthquake Engineering and Structural Dynamics*, 34 (12), 1489-1511.

Kabeyasawa, T., Shiohara, H., Otani, S. and Aoyama H. (1983). Analysis of the full-scale seven-story reinforced concrete test structure.J. Fac. Eng..University of Tokyo.XXXVII:2,432–78.

Kolozvari K., Orakcal K., and Wallace J. W. (2015). Modeling of Cyclic Shear-Flexure Interaction in Reinforced Concrete Structural Walls. I: Theory, *ASCE Journal of Structural Engineering*, 141(5).

Kolozvari K., Kalbasi, K., Orakcal, K., and Wallace J. W. (2021). Three-dimensional shear-flexure interaction model for analysis of non-planar reinforced concrete walls, *Journal of Building Engineering*, 44, 102946.

Krawinkler, H. and Mohasseb, S. (1987) Effect of panel zone deformations on seismic response. *Journal of Constructional Steel Research*, 8:233-50.

Kutter, B.L., Moore, M., Hakhamaneshi, M. et al. (2016). Rationale for shallow foundation rocking provisions in ASCE 41-13. *Earthquake Spectra*, 32 (2), 1097-1119. DOI: 10.1193/121914eqs215m

Lagaros, N., and Fragiadakis, M. (2011). Evaluation of ASCE-41, ATC-40 and N2 static pushover methods based on optimally designed buildings. *Soil Dynamics & Earthquake Engineering*, 31 (1), 77-90. DOI: 10.1016/j.soildyn.2010.08.007.

Lignos, D., Hartloper, A.R., Elkady, A. et al. (2019). Proposed updates to the ASCE 41 nonlinear modeling parameters for wide-flange steel columns in support of performance-based seismic engineering. *Journal of Structural Engineering*, 145, 04019083. DOI: 10.1061/(ASCE)ST.1943-541X.0002353.

Lowes, L., Lehman D., and Baker, C. (2018). Recommendations for modeling the nonlinear response of slender reinforced concrete walls using PERFORM-3D, 2016 SEAOC Convention Proceedings, 2016.

Maison, B.F., Kasai, K., and Deierlein, G. (2009) ASCE-41 and FEMA-351 Evaluation of E-Defense Collapse Test. *Earthquake Spectra*, 25 (4), 927-953. DOI: 10.1193/1.3224159

Massone, L.M., Orakcal, K. and Wallace J.W. (2006). Shear–flexure interaction for structural walls.ACI special publication—Deformation capacity and shear strength of reinforced concrete members under cyclic loading. ACI-SP236-07, 127–150.

McKenna, F., Fenves, G., and Scott, M. (2021) OpenSees: Open System for Earthquake Engineering Simulation. Pacific Earthquake Engineering Research Center. University of California, Berkeley, CA. Available at: http://opensees.berkeley.edu (version 3.2.2, last accessed August 2021).

Orakcal, K., Wallace, J.W., and Conte, J.P. (2004).Flexural modeling of reinforced concrete walls—model attributes. *ACI Structural Journal.*101:5,688–98.

Thomsen, J. H., IV, and Wallace, J. W. (1995) Displacement-based design of reinforced concrete structural walls: Experimental studies of walls with rectangular and T-shaped cross sections. Rep. No. CU/CEE-95/06, Department of Civil and Environmental Engineering, Clarkson University, Potsdam, NY.

Tran T.A. and Wallace J.W. (2012). Experimental study of nonlinear flexural and shear deformations of reinforced concrete structural walls, Proceedings, 15th World Conference on Earthquake Engineering, Lisbon, Portugal.

U.S. Geological Survey (USGS) (2017). Unified Hazard Tool, accessed in September, 2020 at URL https://earthquake.usgs.gov/hazards/interactive/

Appendix A

This appendix contains several studies that extended from the main research work presented in this dissertation.

A1. Calibration of Damping

In Section 2.1.1, the proposed methodology by Falborski et al. (2020) was implemented for the 3-story steel building in order to estimate the nonstructural stiffness of the steel moment frame. A similar procedure can be followed to estimate the damping constant C_k at each story, with the objective of finding the Rayleigh damping coefficients α_o and α_1. The main difference to the method explained earlier is that, for each story, the time instants at which the interstory drifts are zero are instead considered, in order to neglect the stiffness terms in the equation of motion. Therefore, the total damping force at the time instants will be equal to the summation of *mass* x *acceleration* at the floors above the story, eliminating the need to do the static analysis. The following are the regression plots obtained from this analysis for the San Bernardino ground motions only for reference.

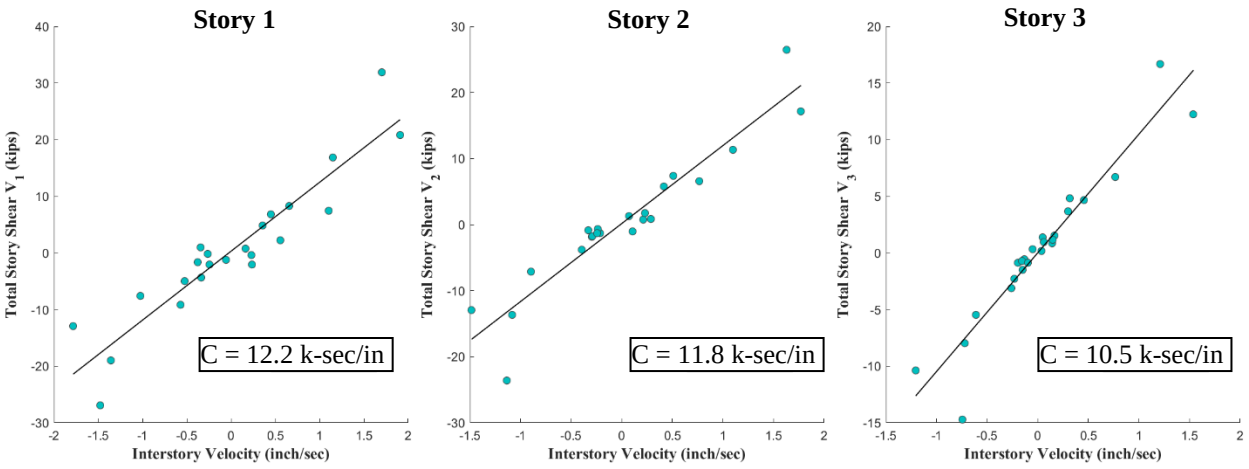

Figure A-1. Example of damping coefficient regression (San Bernardino ground motion)

Moving forward with the calibration, shear building idealization is applied, where only the lateral degrees of freedom are considered. Using this generalization, the damping and stiffness matrices can be written as follows. Note that the K values shown represent the total story stiffness values from Table 2-2, and the m values are the lumped massed at each story.

$$[C] = \begin{bmatrix} C_1 + C_2 & -C_2 & 0 \\ -C_2 & C_2 + C_3 & -C_3 \\ 0 & -C_3 & C_3 \end{bmatrix} \quad \text{and} \quad [K] = \begin{bmatrix} K_1 + K_2 & -K_2 & 0 \\ -K_2 & K_2 + K_3 & -K_3 \\ 0 & -K_3 & K_3 \end{bmatrix}$$

The damping matrix can then be divided into the mass and stiffness proportional terms, following the Rayleigh damping formulation.

$$\begin{bmatrix} C_1 + C_2 & -C_2 & 0 \\ -C_2 & C_2 + C_3 & -C_3 \\ 0 & -C_3 & C_3 \end{bmatrix} = \alpha_0 \begin{bmatrix} m_1 & 0 & 0 \\ 0 & m_2 & 0 \\ 0 & 0 & m_3 \end{bmatrix} + \alpha_1 \begin{bmatrix} K_1 + K_2 & -K_2 & 0 \\ -K_2 & K_2 + K_3 & -K_3 \\ 0 & -K_3 & K_3 \end{bmatrix}$$

This can be condensed to the following system of equations where there are 2 unknowns and 5 equations.

$$\begin{Bmatrix} C_1 + C_2 \\ -C_2 \\ C_2 + C_3 \\ -C_3 \\ C_3 \end{Bmatrix} = \alpha_0 \begin{Bmatrix} m_1 \\ 0 \\ m_2 \\ 0 \\ m_3 \end{Bmatrix} + \alpha_1 \begin{Bmatrix} K_1 + K_2 \\ -K_2 \\ K_2 + K_3 \\ -K_3 \\ K_3 \end{Bmatrix}$$

Due to the nature of the overdetermined system where the α terms need to be positive, non-negative least squares is used to find the best coefficients that satisfy this system of equations. The damping constants from the regression as well as the corresponding Rayleigh damping coefficients are shown below for each of the ground motions considered.

Table A-1. Damping constants and corresponding Rayleigh coefficients

Damping Constants C (k-sec/in)				
GMs:	Landers	San Bernardino	Chino	All 3 Ground Motions
Story 1	14.6	12.2	6.7	14.0
Story 2	11.8	11.8	8.2	11.7
Story 3	11.7	10.5	9.3	11.5
Rayleigh Damping Coefficients				
α_o	1.5271	0.7218	1.3431	1.4226
α_1	0.0217	0.0207	0.0143	0.0213
Damping Ratio for Mode 1				
ξ_{mode1}	0.192	0.151	0.141	0.185

Also presented in the table above is the equivalent damping ratio for the first mode corresponding to the pairs of Rayleigh coefficients based on the following formula. The frequency at mode 1 is denoted as w_1.

$$\xi_1 = \frac{a_o}{2\, w_1} + \frac{a_o\, w_1}{2}$$

Note from the tabulated results that the more intense the ground motion, the higher the equivalent damping ratio. This confirms the earlier observation that the Landers ground motion requires a higher damping ratio for the model to have a better match with the recorded time histories. The final Rayleigh coefficients were not used for the calibrated model since the ASCE 41 assessment succeeding the calibration will be based on a hazard level with a 5% probability of occurrence in 50 years, and therefore the ground motions selected will be much more intense than

those presented in Table A-1. Therefore, the damping ratio is expected to decrease during the stronger ground motions.

A2. Incremental Dynamic Analysis (IDA) on Linear Models

In Section 4.3, incremental dynamic analyses were completed on the nonlinear models, for all buildings. However, it is important to highlight the response of the linear models when subjected to the set of 56 ground motions from P-695. The models for the steel moment frame buildings were subjected to these ground motions. However, instead of increasing the scale factor until a certain drift was surpassed, the following criteria was implemented: using a scale factor such that the average of the spectral accelerations of the P-695 ground motions was the same as the average of the ASCE 41 based ground motions that are derived from scaling at the period of the structure at the target site spectra. The results for both buildings are presented in Figure A-2. Note that only maximum story drifts are shown, since the linear models should provide negligible residual drifts.

As observed from the plots, for the 3-story steel building, at the target ground motion intensity, the structure mainly satisfies immediate occupancy, with some points being classified as life safety. However, for the 6-story steel building, most points are in life safety, with a few points being in the collapse prevention performance level. It is clear that the linear models have higher story drifts that would need to be scaled down using a factor with a similar purpose to the deflection amplification factor to fairly make a comparison to a collapse drift limit.

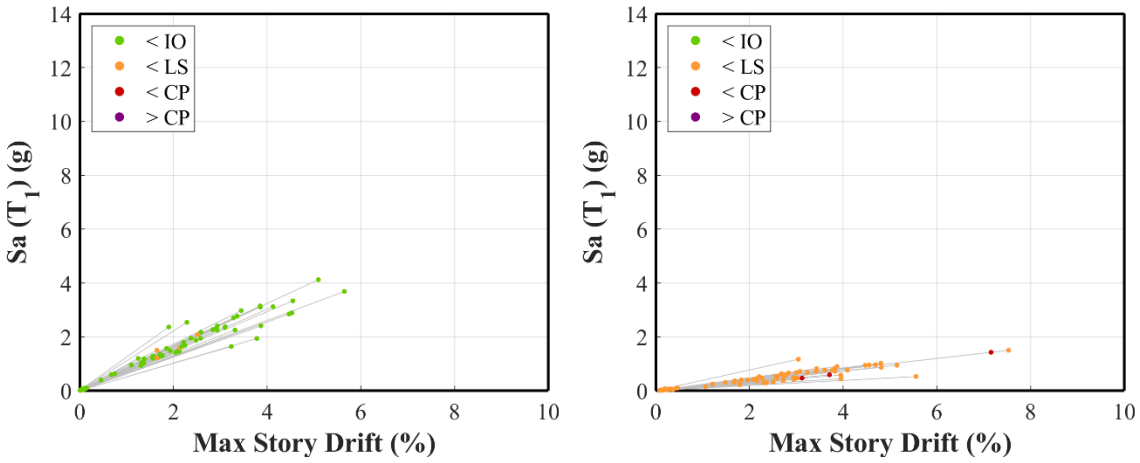

Figure A-2. Ground motion intensity vs maximum story drift in linear models (a) 3-story steel building, (b) 6-story steel building

A3. Effect of Panel Zone Modeling in Steel Moment Frames

For the steel moment frame buildings, all frame models have been created with explicit panel zone connections incorporated in both the linear and nonlinear models. An indepth study was conducted on the 6-story steel building to determine the effect of panel zone modeling as it pertains to a performance-based assessment. The content of the study was presented and published in the 12th National Conference on Earthquake Engineering. The text that follows is the full script included in the paper.

Publication

Hernández-Bassal L., Kunnath S. (2022). Performance-Based Assessment of Steel Moment Frames with and without Panel Zones. Proceedings of the 12th National Conference on Earthquake Engineering, Salt Lake City, Utah.

Abstract

Modeling assumptions have been demonstrated to have a significant impact on the response of systems for both high-fidelity finite element and macro-element analysis. In performance-based assessment, the degree of model refinement is typically left to the judgement of the engineer. For steel moment frames, an element that is often not explicitly modeled, due to time constraints or project goals, is the panel zone at the moment connections. This study highlights the importance of modeling the flexibility and shear-distortion behavior of this critical zone. The results from the assessment of a six-story moment frame building indicate that for linear models, the impact is minor, while for nonlinear analyses, modeling the panel zones significantly affects the computed demands at the component and system level. It is therefore recommended that panel zones be explicitly modeled, particularly in nonlinear analyses used for performance-based assessment.

Introduction

The perusal of literature in the past decade reveals that there exists some inconsistency in the way panel zones are modeled by both researchers and practicing engineers. Krawinkler and Mohasseb (1987) were among the first to investigate the importance of panel zones and recommended that the joint shear strength and stiffness be included in inelastic models, particularly for frames with weak joints. Another study by Foutch and Yun (2002) presented results and observations for two mid-rise buildings, recommending clear span dimensions and panel zone models for accuracy. However, there continue to be new building designs or research studies based on models where the importance of the joint is overlooked. This current study revisits this topic with a focus on performance-based structural assessment.

As part of a larger project evaluating ASCE 41 (2017) based seismic assessment of buildings, an existing six-story steel moment frame building in California designed in 1976 was analyzed and evaluated. The structure, instrumented by the California Strong Motion Instrumentation Program, has steel moment frames along its perimeter that serve as the main lateral force resisting system in both directions. The gravity system is composed of concrete on metal deck spanning in the east-west direction. This building was selected as a case study so that the computer model could be appropriately validated and calibrated against instrumented data from past earthquakes, providing more reliable analysis results. A detailed description of the structure and its geometry can be found in Chapter 2. The objective of this study is to utilize the validated model to determine the effect of explicitly modeling panel zones at the beam-column moment frame connections in performance-based seismic assessment.

Nonlinear System Model

Two-dimensional models using Opensees (McKenna et al. 2021) are created to analyze the exterior frame in one direction. Beams are modeled using elastic beam-column elements, and inelastic springs (constructed with zero-length elements) are added at the ends. All inelastic action is lumped into these concentrated springs in which the cyclic response is represented using the Modified Ibarra-Medina-Krawinkler deterioration model (Ibarra et al. 2005) In order to capture the axial load-moment interaction, columns are modeled as force-based elements with five Lobatto integration points and the Voce-Chaboche material model is used to represent the inelastic cyclic behavior of steel (Hartloper et al. 2021). An additional leaning column is attached to the moment frame using rigid links with pinned connections at each end to account for P-Delta effects and contributing gravity loads from the interior frames are applied at each level. Two versions of this model are considered: In *Model A*, center-line dimensions are used for beams and columns to indirectly account for the flexibility of the panel zones. In *Model B*, the panel zones are explicitly modeled at the moment connections with a set of elastic beam-column elements, with a trilinear equivalent rotational spring on the top right corner that captures the shear distortion through the use of the Hysteretic material model. The modeling choices are shown in Figure A-3. For the linear analyses, the beam springs are removed, the columns are modeled using elastic beam-column elements, and the panel zone rotational spring follows linear material behavior.

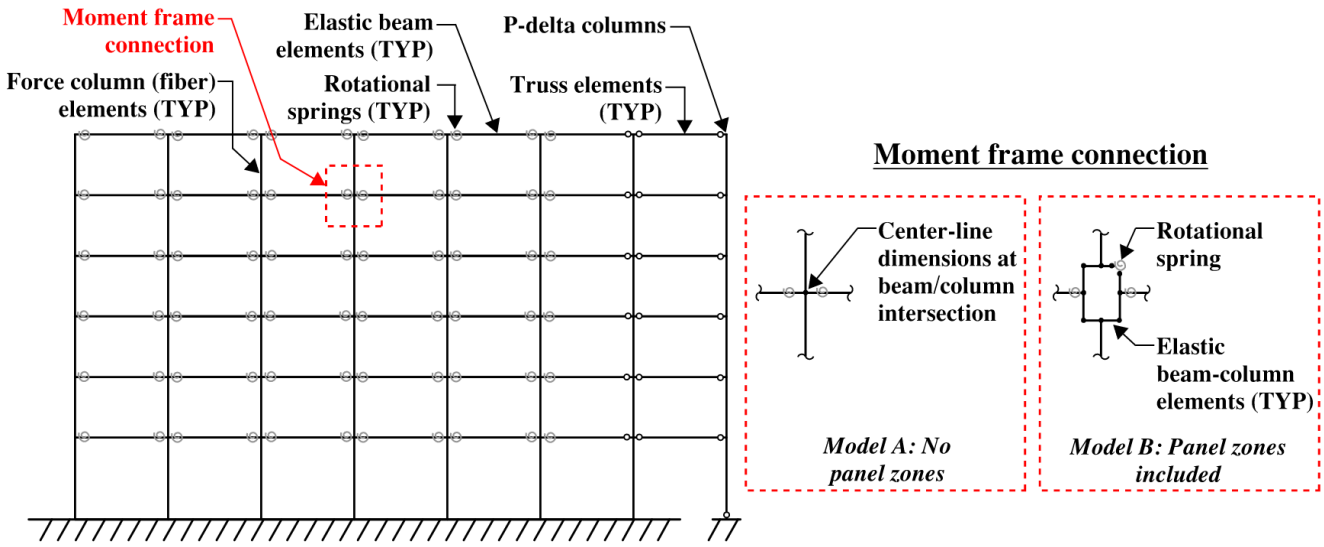

Figure A-3. Elevation view of OpenSees nonlinear model with panel zone modeling options

Analysis and Results

A seismic performance assessment of the building was carried out by analyzing Model A and Model B using the four analysis procedures prescribed in ASCE 41: Linear Static (LSP), Linear Dynamic (LDP), Nonlinear Static (NSP), and Nonlinear Dynamic (NDP). The resulting demands of the primary components are shown in Figure A-4, with respect to the acceptance criteria for three performance levels: Immediate Occupancy (IO), Life Safety (LS), and Collapse Prevention (CP). Note that the panel zone demands for Model A are not shown since these components are not explicitly modeled. The interstory drifts, which can serve as a parameter for measuring system-level response, are also presented. The addition of the panel zones shifted the fundamental period of the structure from 1.50 sec to 1.59 sec for the linear model and from 1.52 sec to 1.60 sec for the nonlinear model.

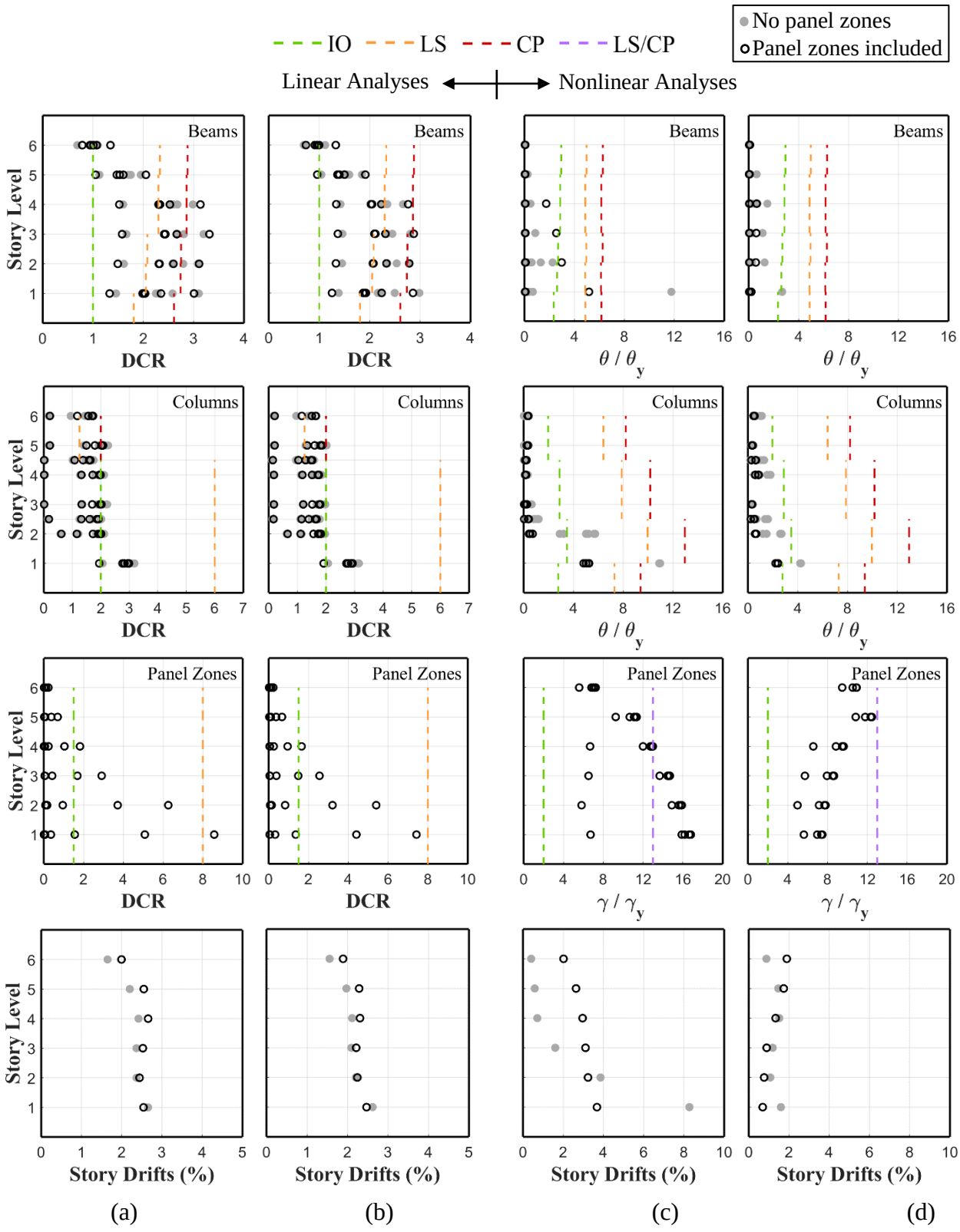

Figure A-4. Demand-to-capacity ratios for primary components and interstory drifts from (a) Linear Static; (b) Linear Dynamic; (c) Nonlinear Static; (d) Nonlinear Dynamic

Results from both linear procedures shown in Figure A-4a and Figure A-4b indicate that the beam and column demands did not vary significantly between Models A and B. The panel zones presented for Model B, show demands that slightly exceed the LS acceptance criteria. However, since the beams are the controlling components causing exceedance of the CP limits, the performance level rating is the same for both models. Finally, the drifts presented are also clearly similar in pattern and magnitude.

For the Nonlinear Static Procedure (NSP) as shown in Figure A-4c there was evident variation in the normalized rotation demands between the models. It is important to note that during this analysis, Model A (no panel zones) actually did not converge at the target displacement of 29.3” at the top floor (the run terminated at 26.3”). When the panel zones were added in Model B, the building was successfully pushed to the total target displacement. Nevertheless, when adding panel zones, there is a significant decrease in beam and column demands, which can be attributed to the large panel zone deformations seen in Model B. In Model A, the beams and columns in the first story exceeded CP limits; however, in Model B, these components satisfied the CP limit, while the panel zones exceeded it.

The Nonlinear Dynamic Procedure (NDP) results in Figure A-4d also show a decrease in beam and column demands, albeit to a smaller degree. This shift can also be attributed to the deformations concentrated in the panel zones. Both models show results that satisfy the LS limits; the panel zones in Model B however, are very close to failing the corresponding LS/CP criteria.

When comparing NSP and NDP results, it is clear from the drift profile that NSP underestimates the demands in the upper stories. This was also observed in the study by Harris and Speicher (2018) where it was noted that the possibility of higher mode contributions cannot be captured in static procedures.

Conclusion

Performance-based seismic assessment of a six-story steel moment frame was completed using two distinct modeling assumptions: (a) using center-line dimensions at beam/column moment frame intersections and (b) explicitly modeling panel zones to account for the corresponding strength and shear distortion behavior. An ASCE 41 evaluation was carried out using LSP, LDP, NSP and NDP. For the linear procedures, the results show insignificant changes in beam, column, and drift demands. For the nonlinear procedures, it was shown that the deformation concentrated in the panel zones cannot be captured by Model A, and therefore the rotational demands for beams and columns are much greater for the model without panel zones. It is also important to note that Model B provides a more accurate representation of behavior of the beam-column connection. This study serves to highlight the importance of modeling panel zones when using nonlinear procedures.